

Thermo-poromechanical modeling of saturated clay soils considering bound water dehydration.

Mohammadhossein Sojoudi

A Thesis
In the Department
Of

Building, Civil and Environmental Engineering

Presented in Partial Fulfillment of the Requirements
for the Degree of
Doctor of Philosophy (Civil Engineering) at
Concordia University
Montréal, Québec, Canada

December 2023

© Mohammadhossein Sojoudi, 2023

CONCORDIA UNIVERSITY
SCHOOL OF GRADUATE STUDIES

This is to certify that the thesis prepared

By: Mohammadhossein Sojoudi

Entitled: Thermo-poromechanical modeling of saturated clay soils considering bound water dehydration

and submitted in partial fulfillment of the requirements for the degree of

Doctor of Philosophy (Civil Engineering)

complies with the regulations of the University and meets the accepted standards with respect to originality and quality.

Signed by the final examining committee:

| | |
|----------------------|-----------------------|
| _____ | Chair |
| Dr. Pragasen Pillay. | |
| _____ | External Examiner |
| Dr. Mohamed Meguid. | |
| _____ | Arm's Length Examiner |
| Dr. Liangzhu Wang. | |
| _____ | Examiner |
| Dr. Adel Hanna | |
| _____ | Examiner |
| Dr. Ayhan Ince. | |
| _____ | Thesis Supervisor |
| Dr. Biao Li. | |

Approved by

Chair of Department or Graduate Program Director

Date of Defence

Dean

Abstract

Thermo-poromechanical modeling of saturated clay soils considering bound water dehydration.

Mohammadhossein Sojoudi, Ph.D.

Concordia University, 2023

The non-isothermal deformation of clay soils is a critical concern in energy and environmental-related geotechnics, given the complex microstructure and mineral composition of clay-related geomaterials. Investigating their thermo-mechanical behaviors poses significant challenges that previous studies have often overlooked. Specifically, distinguishing between thermal plastic strain and clay dehydration strain has received little attention.

To address these gaps, a novel constitutive model is proposed for describing the thermo-elastoplastic behaviors of water-saturated clayey soils. The model incorporates the effects of temperature variation and mechanical loading on elastoplastic strains and dehydration behavior. The thermo-mechanical behavior is quantified using thermodynamics laws and unconventional plasticity principles. Additionally, a finite element method (FEM) model is employed to simulate the thermo-hydro-mechanical (THM) responses of water-saturated clay soils. This FEM model accounts for temperature variation effects on bound water dehydration and corresponding thermo-poromechanical strains. By incorporating unconventional plasticity, the elasto-plastic behavior is more accurately described. The validation process for this FEM model involves laboratory results on various clay soils with different geological origins, demonstrating a reasonable agreement between the model's predictions and experimental data. Notably, the numerical results highlight the impact of bound water dehydration on the generation of excess pore pressure in clay soils during heating.

Expanding beyond the realm of theoretical models, a research project is underway to assess the geomechanical performance of a potential borehole thermal energy storage system (BTES) in a Canadian subarctic region. To quantify the poromechanical impact, a two-dimensional finite element model (FEM) is created to simulate a BTES system, encompassing the borehole and the surrounding soil formation. The model aims to analyze the effects of cyclic temperature variations and bound water dehydration on the short-term ground response and pore water pressure development. Our results indicate the importance of considering bound water dehydration in

characterizing the ground heave process during the short-term BTES operation in an overconsolidated formation. The simulated ground expansion behavior is due to the high excess pore pressure generated during thermal storage, which is accompanied by the release of in-situ effective stresses. The neglect of bound water dehydration will underestimate the magnitude of ground heave during a short-term BTES operation.

Keywords: Thermo-hydro-mechanical (THM) coupling, Subloading yield surface, Clay-bound water dehydration, Finite element method (FEM), Borehole thermal energy storage (BTES) systems.

Acknowledgments

I would like to express my heartfelt gratitude to my dedicated supervisor, Dr. Biao Li, whose unwavering guidance, wisdom, and support was instrumental in the successful completion of this Ph.D. journey. Your expertise, patience, and continuous encouragement have been invaluable, shaping not only my academic growth but also my personal development. I am truly fortunate to have had the privilege of working under your mentorship.

My deepest appreciation also goes to my loving wife, Tahereh, and my two sons, Arman and Radman, whose unwavering love, understanding, and sacrifice sustained me throughout this challenging academic endeavor. Your patience during the long hours and your belief in me were constant sources of motivation. I am indebted to my parents for their endless encouragement and for instilling in me the values of determination and perseverance. Lastly, I extend my thanks to my colleagues and friends, especially Emad Norouzi, who have shared their knowledge, provided valuable insights, and offered their support during this research journey. Your camaraderie made the academic road less daunting, and I am grateful for the collaborative spirit that defined our work together.

I also would like to acknowledge the fund provided by NSERC Discovery Grant Canada (NO. RGPIN-2017-05169).

Dedication

To my beloved Tahereh, my two shining stars, Arman and Radman, and my unwavering pillars of support—my father and my mother.

List of Publications

Refereed journal papers:

- Sojoudi, M. and Li, B., 2023. A thermodynamic-based model for modeling thermo-elastoplastic behaviors of saturated clayey soils considering bound water dehydration. *Journal of Rock Mechanics and Geotechnical Engineering*. v. 15, p. 1535–1546.
- Sojoudi, M, Li, B., and Norouzi, E., 2023. Finite element modeling of thermal-hydro-mechanical coupled processes in clay soils considering bound water dehydration. Submitted to the journal of *Acta Geotechnica*. Manuscript # AGEO-D-23-00544.
- Sojoudi, M, Li, B., and Norouzi, E., 2023. Numerical study of the performance of a borehole geothermal energy storage well in a Canadian subarctic region. Submitted to the journal of *Renewable energy*. Manuscript # RENE-D-23-05783.

Conference proceedings papers and presentation:

- Sojoudi, M, and Li, Biao. Numerical study of the performance of a borehole geothermal energy storage well in a Canadian subarctic region. *People international conference*, 7-11 Aug. 2023
- Sojoudi, M, and Li, Biao. Numerical Implementation of an Equilibrium Thermodynamics-based Thermo-Viscoplastic model for clay soils. *GeoCalgary2022, the 75th Canadian Geotechnical Conference*, 2-5 Oct. 2022.
- Sojoudi, M. and Li, Biao. Modeling temperature and rate dependent behaviors of clay soils using the thermodynamic-based hyper-viscoplasticity framework. *GeoNiagara2021, the 74th Canadian Geotechnical Conference*, 26-29 Sep. 2021.
- Sojoudi, M. and Li, Biao. Thermodynamic-based model for the thermo-poro-elastoplastic behavior of saturated clay, *The 73rd Canadian Geotechnical Conference*, 13-16 Sep. 2020.

Contribution of Authors

The sections encompassing this thesis showcase the author's distinctive contributions. The candidate independently embarked upon tasks involving model formulation, Finite Element Method (FEM) implementation, and developmental enhancements. Throughout these undertakings, close guidance and supervision were provided by Dr. Biao Li.

Additionally, it should be noted that in chapters 4 and 5, Emad Norouzi, a member of our research group, contributed to the poroelastic coding of the FEM model.

All authors reviewed the final manuscript and approved of the contents.

Table of Contents

| | |
|---|------|
| List of Figures | xiii |
| List of Tables | xvii |
| Chapter 1 | 1 |
| 1 Introduction | 1 |
| 1.1 Context and Inspiration for the Study | 1 |
| 1.2 Objectives and scope | 3 |
| 1.3 Original contribution | 3 |
| 1.4 Thesis organization | 5 |
| Chapter 2 | 6 |
| 2 Literature review | 6 |
| 2.1 Introduction | 6 |
| 2.2 Multiphysics simulation of clay soils. | 6 |
| 2.2.1 Plasticity-based approach | 7 |
| 2.2.2 Thermodynamic-based approach | 9 |
| 2.2.3 Bound water dehydration | 10 |
| 2.3 Implementation in Finite Element Method (FEM) | 12 |
| 2.4 Advancements in Modeling Thermo-Hydro-Mechanical Behaviors | 14 |
| Preface to Chapter 3 | 17 |
| Chapter 3 | 18 |
| 3 A thermodynamic-based model for modeling thermo-elastoplastic behaviors of saturated clayey soils considering bound water dehydration | 18 |
| 3.1 Abstract | 18 |
| 3.2 Introduction | 19 |

| | | |
|-------|--|----|
| 3.3 | Thermodynamic bases for constitutive model | 20 |
| 3.4 | A new thermo-elastoplastic model..... | 24 |
| 3.4.1 | Thermo-elastic strain and thermo-plastic strain..... | 25 |
| 3.4.2 | Dehydration strain..... | 27 |
| 3.5 | Model validations..... | 30 |
| 3.5.1 | Thermally induced volumetric strain | 31 |
| 3.5.2 | Temperature-controlled triaxial compression behavior | 37 |
| 3.6 | Discussion..... | 42 |
| 3.6.1 | On clay-bound water..... | 42 |
| 3.6.2 | Dehydration-induced strain..... | 43 |
| 3.7 | Conclusions..... | 45 |
| 3.8 | List of symbols..... | 45 |
| | Preface to Chapter 4..... | 49 |
| | Chapter 4..... | 50 |
| 4 | Finite element modeling of thermal-hydro-mechanical coupled processes in clay soils considering bound water dehydration. | 50 |
| 4.1 | Abstract..... | 50 |
| 4.2 | Introduction..... | 51 |
| 4.3 | Bound water dehydration..... | 52 |
| 4.4 | Governing equations | 54 |
| 4.4.1 | THM coupled equations..... | 54 |
| 4.5 | Thermo-Plasticity..... | 59 |
| 4.6 | Finite-element solution | 62 |
| 4.6.1 | Initial and boundary conditions | 62 |
| 4.6.2 | Variational formulation..... | 63 |
| 4.6.3 | Numerical implementation..... | 65 |

| | | |
|-------|--|-----|
| 4.7 | Model validations..... | 66 |
| 4.7.1 | Description of material parameters..... | 66 |
| 4.7.2 | High temperature triaxial tests..... | 68 |
| 4.7.3 | High temperature oedometer tests..... | 71 |
| 4.8 | Discussions..... | 74 |
| 4.8.1 | Impact of bound water on deformation behavior..... | 74 |
| 4.8.2 | Impact of bound water on pore pressure development..... | 75 |
| 4.9 | Conclusion..... | 77 |
| 4.10 | List of symbols..... | 78 |
| | Preface to Chapter 5..... | 82 |
| | Chapter 5..... | 83 |
| 5 | Thermal-hydro-mechanical modeling of short-term ground responses due to the borehole thermal energy storage operations in a Canadian subarctic region..... | 83 |
| 5.1 | Abstract..... | 83 |
| 5.2 | Introduction..... | 84 |
| 5.3 | Governing equations..... | 86 |
| 5.4 | Simulation of BTES systems in a Canadian subarctic region..... | 89 |
| 5.4.1 | Material properties..... | 90 |
| 5.4.2 | FEM modeling..... | 91 |
| 5.4.3 | Results and analysis..... | 94 |
| 5.5 | Discussions..... | 99 |
| 5.5.1 | Impact of bound water dehydration on displacement and pore water pressure..... | 99 |
| 5.5.2 | Effective stress path analysis and the role of plastic strain..... | 101 |
| 5.6 | Conclusions..... | 103 |
| | Chapter 6..... | 105 |
| 6 | Conclusions, limitations, and recommendations for future work..... | 105 |

| | |
|---|-----|
| 6.1 Conclusion | 105 |
| 6.2 Limitations | 107 |
| 6.3 Recommendations for future work | 108 |
| Bibliography | 109 |

List of Figures

| | |
|---|----|
| Figure 1-1 Borehole stability issues related to a thermal energy storage project in a clay soil formation. (Background image is from www.img2go.com .)..... | 2 |
| Figure 1-2 Flow chart showing the contribution of the thesis. | 4 |
| Figure 2-1 Volumetric strain caused by real stress and equivalent stress [9](θ is temperature). ... | 8 |
| Figure 2-2 Normal yield and subloading yield surfaces [29]. | 9 |
| Figure 2-3 Illustration depicting free water and bound water in clay-water composites..... | 11 |
| Figure 3-1 Sketch showing normal yield and subloading yield surfaces of the modified Cam-Clay model in p - q plane..... | 25 |
| Figure 3-2 Sketch showing free water and bound water in clay-water composites..... | 28 |
| Figure 3-3 Experimental details for the high temperature oedometer test: (a) Schematic of setup; and (b) Insulated consolidation cell under a loading frame. | 32 |
| Figure 3-4 Monitored position changes of soil samples' top surface during heating tests..... | 33 |
| Figure 3-5 Monitored position evolution curve of the top surface of sample SQ2. | 34 |
| Figure 3-6 Measured and modeled thermal deformation behaviors of smectite-quartz mixtures. | 36 |
| Figure 3-7 The modeled results and measured data for the thermal volumetric behavior of Boom Clay (adopted from Del Olmo et al., 1996 [35])..... | 37 |
| Figure 3-8 Modeled results and measured data of drained triaxial compression tests on normally consolidated (NC) Bangkok Clay at different temperatures: (a) Stress-strain curves; and (b) Axial strain-volumetric strain curves ($P_0' = 300$ kPa, measured data is from Abuel-Naga, 2006 [94]). | 38 |

| | |
|---|----|
| Figure 3-9 The modeled and measured results of drained triaxial compression tests on NC and OC Bangkok clay at $T = 70^{\circ}\text{C}$: (a) Stress-strain and (b) Axial strain - volumetric strain (measured data is from Abuel-Naga, 2006 [94]). | 39 |
| Figure 3-10 Plots of modeled results and experimental data of drained triaxial compression tests on NC and OC Kaolin clay: (a) NC; (b) $OCR = 2$ and (c) $OCR = 3$ (measured data is from Cekerevac and Laloui, 2004 [6]) | 41 |
| Figure 3-11 Measured relationship between thermal plastic strain and OCR of geomaterials with different geological origins (modified after Li and Wong, 2017 [12]). | 44 |
| Figure 4-1 Sketch showing free water and bound water in clay-water composites. | 53 |
| Figure 4-2 Sketch showing normal yield and subloading yield surfaces in a temperature hardening situation, modified after [104]. | 59 |
| Figure 4-3 Bound water content versus temperature for different value of α_{bf} . | 67 |
| Figure 4-4 Axisymmetric finite element mesh and boundary conditions of numerical tests on Boom Clay soils. | 70 |
| Figure 4-5 Comparison of simulated and measured data for the thermo-mechanical behavior of Boom Clay soils. | 70 |
| Figure 4-6 Plots showing (a) the experimental setup, and (b) axisymmetric finite element mesh and boundary conditions for the numerical test. | 72 |
| Figure 4-7 Simulated and measured nonlinear thermo-mechanical behaviors of highly compacted smectite-quartz mixture (SQ1, clay fraction = 0.2; SQ2, clay fraction = 0.45), the positive sign is treated as expansion herein. | 73 |
| Figure 4-8 Curves showing the variation of degree of saturation of bound water (S_b) with time for samples SQ1 and SQ2 at the monitoring point (P1). | 74 |
| Figure 4-9 Comparison of model simulation with and without bound water for (a) SQ1, and (b) SQ2. | 75 |

| | |
|---|-----|
| Figure 4-10 Simulated pore pressure generation in monitoring point of SQ2 under different heating rates. | 76 |
| Figure 5-1 Sketch showing the thermal disturbance in soils surrounding a Borehole Thermal Energy Storage (BTES) system. | 85 |
| Figure 5-2 Sketch showing the geometry of the modeled BTES well and the applied temperature cycles..... | 92 |
| Figure 5-3 Boundary conditions and meshes used for the THM coupled FEM analysis. | 93 |
| Figure 5-4 Selected six key monitoring points for analyzing the simulation results..... | 94 |
| Figure 5-5 Simulated temperature development at different monitoring points: (a) P1 and P2, (b) P4 and P6. | 95 |
| Figure 5-6 Simulated temperature (unit of °C) distribution profiles by the end of 3.5 years: a) Maximum $T = 60^{\circ}\text{C}$, b) Maximum $T = 30^{\circ}\text{C}$ | 96 |
| Figure 5-7 Simulated vertical displacements (positive indicates expansion) at the top surface of the soil (monitoring points P1 and P2) under two different temperature ranges (1°C to 60°C and 1°C to 30°C)..... | 97 |
| Figure 5-8 Curves showing simulated displacements at P5 for two different temperature ranges. | 97 |
| Figure 5-9 Simulated pore pressure development at different monitoring points: (a) P3 and P4, (b) P5 and P6..... | 99 |
| Figure 5-10 Comparison of simulated vertical displacement at P1 for cases with and without considering bound water dehydration, maximum $T = 60^{\circ}\text{C}$ | 100 |
| Figure 5-11 Comparison of simulated pore water pressures for cases with and without considering bound water dehydration, maximum $T = 60^{\circ}\text{C}$: (a) at point P3, (b) at point P5. | 101 |

Figure 5-12 Curves showing the effective stress paths at key monitoring points, *CLS* = critical state line. 102

Figure 5-13 Simulated vertical displacements at P1 for cases with and without considering plasticity..... 103

List of Tables

| | |
|---|----|
| Table 3-1 Parameters involved in proposed model..... | 35 |
| Table 4-1 THM material properties of clay soils..... | 68 |
| Table 5-1 Related THM properties of the studying soil formation for numerical modeling..... | 90 |

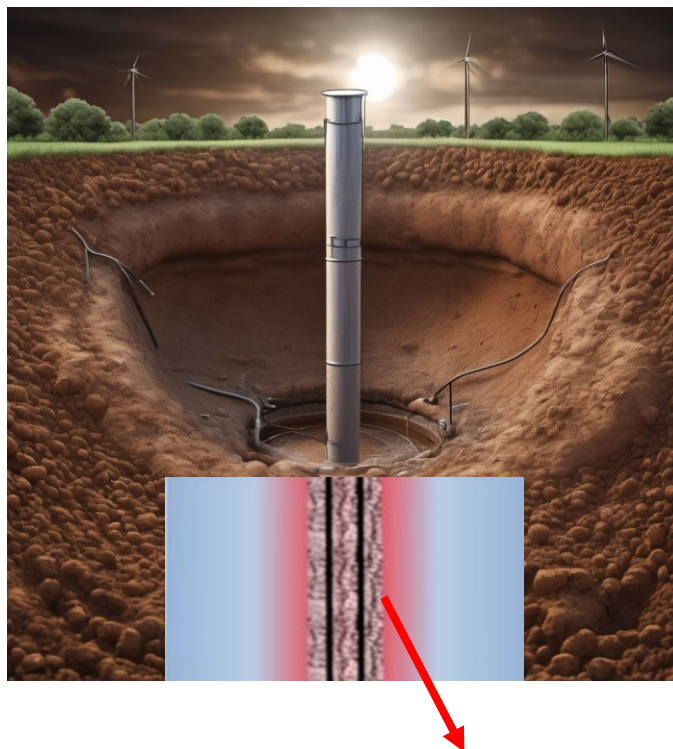
Chapter 1

1 Introduction

1.1 Context and Inspiration for the Study

Clay soils play a crucial role in the realm of energy storage systems and environmental geotechnics. Clay soils exhibit a complex microstructure and mineral composition, which pose significant challenges when studying their thermo-mechanical behaviors. While previous studies have shed light on this intricate thermo-poromechanical behavior. However, many studies have overlooked the crucial differentiation between thermal plastic strain and the strain resulting from clay bound water dehydration. Describing the complicated thermo-elastoplastic behaviors of clayey soils under non-isothermal conditions requires a groundbreaking research endeavor.

A noteworthy application of a comprehensive grasp of the thermo-mechanical characteristics of clay soils lies in Thermal Energy Storage (TES) systems. Such system garnered significant attention in today's energy systems, aligning with the global shift towards sustainability and renewable energy sources [1, 2]. In some subarctic regions of Canada, villages heavily rely on fossil fuels for both electricity and heat production, resulting in substantially higher production costs compared to southern areas. To address this challenge, the concept of using seasonal borehole thermal energy storage (BTES) has emerged as a strategic solution to enhance energy and food security in off-grid communities located in circum-arctic countries, particularly when the winter season's solar energy is insufficient to meet local demands [3, 4]. BTES projects aim to store heat in low-permeability layers rich in clay soils to minimize heat loss. However, the thermo-hydro-mechanical (THM) behaviors of clay soils are pivotal factors in the design and stability of these BTES projects. Figure 1-1 shows the schematic view of borehole stability problems in a BTES project in a clay soils.



Risk of borehole failure because of thermo-hydro-mechanical behavior of clay soils.

Figure 1-1 Borehole stability issues related to a thermal energy storage project in a clay soil formation. (Background image is from www.img2go.com.)

The poromechanical behaviors of clay soils are intricately tied to their saturation state, and even for water-saturated clay soils, the interplay between clay minerals and water introduces complexity in temperature dependence. A comprehensive understanding and accurate modeling of this THM behavior necessitates a multidisciplinary approach. Past experimental data has revealed that heating often leads to irreversible contraction deformation in clay soils, especially in unconsolidated geomaterials [5–7]. Over time, several thermo-mechanical coupled constitutive models have been developed to predict the non-isothermal poro-mechanical behaviors of clayey soils, typically grounded in the fundamental laws of thermodynamics [8–11]. Nevertheless, limited attention has been paid to accounting for the impact of clay-bound water dehydration, which should be treated as a distinct deformation mechanism [12, 13]. The increase in temperature within a water-saturated clay-rich geomaterial can lead to the transformation of clay-bound water into free water, resulting in dehydration-induced pore changes and deformations [14–16].

The intricacies of these behaviors have introduced significant complexity into the precise modeling of clay soils. Nevertheless, it is imperative to develop suitable descriptions of these behaviors to ensure their accurate incorporation in thermal energy storage projects and other non-isothermal initiatives.

1.2 Objectives and scope

The primary goal of this thesis is to propose a constitutive model capable of explaining the thermo-hydro-mechanical responses of clay material under thermo-mechanical stress, while accounting for the influence of bound water dehydration. To achieve this goal, the subsequent tasks have been addressed:

- 1- Developing and assembling the codebase for the proposed numerical model.
- 2-Verifying the model's simulations through comparison with existing experimental data.
- 3-Investigating the impact of bound water dehydration on the alterations in stress and strain within the soil.

The second aim of this thesis involves implementing the proposed numerical model into the couple THM finite element method to account for the geometry, formulating and compiling the finite element code, verifying the model outcomes using experimental test data, and assessing the influence of bound water dehydration on soil behavior.

The third goal of this thesis aims to offer practical perspectives on numerically simulating boreholes within BTES systems. This objective was realized by integrating our suggested FEM model to examine how the cyclic temperature fluctuations impact the stability of boreholes in the subarctic region of northern Canada,

1.3 Original contribution

This thesis contains original contributions in three main areas: 1- Development of a constitutive model based on the fundamentals of thermodynamics. 2- Integration of the model into the FEM. 3- Exploration of the model's applicability in the subarctic region of Canada. The following are

the notable achievements presented in this work (In Figure 1-2, the schematic flowchart illustrating the contributions of the thesis is presented):

- 1- Proposing a constitutive model that accounts for the impact of bound water dehydration on the thermo-elastoplastic behavior of clay soils.
- 2-Incorporation of the proposed model into FEM using the Galerkin discretization method.
- 3-Verification and validation of the model through comparison with experimental data in simulation.
- 4-Examining the geomechanical performance of a potential BTES system in a Canadian subarctic region.

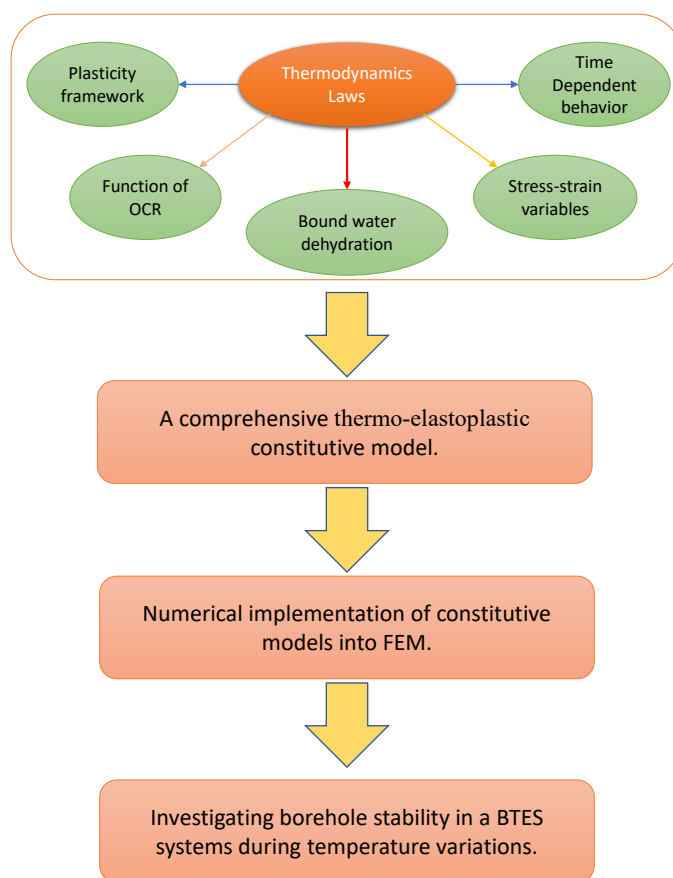


Figure 1-2 Flow chart showing the contribution of the thesis.

1.4 Thesis organization

This thesis follows a manuscript-based format, with three of the six chapters comprising journal article manuscripts that have either been published or under review, as detailed in the list of publications. With the exclusion of this particular chapter, the thesis is structured in the subsequent manner:

Chapter 2 offers an extensive review of existing literature, elucidating the specific issues at hand and outlining the suggested analytical and numerical resolution.

Chapter 3 focuses on presenting the relationships and numerical validations of the proposed thermo-poro-elastoplastic constitutive model for clay soils. This model is based on the principles of thermodynamics and incorporates unconventional plasticity principles. Within the model, the capture of irreversible strain is achieved through the utilization of the subloading surface plasticity framework.

Chapter 4 of the thesis focuses on the implementation of the proposed constitutive model into the finite element method (FEM) and its validation through high temperature triaxial tests and high temperature oedometer tests. The details of this implementation and verification process are discussed in this chapter.

Moving on to chapter 5, it delves into the application of the presented FEM framework for simulating the behavior of borehole thermal energy storage (BTES) in northern Quebec. The simulation covers a period of 3.5 years and considers the effects of temperature variations. The findings and insights obtained from this investigation are presented in this chapter.

Chapter 6 is dedicated to the conclusion and recommendations for future work. It provides a summary of the research findings and suggests potential areas of further exploration and development.

Chapter 2

2 Literature review

2.1 Introduction

In this chapter, we provide a concise overview of earlier research efforts focused on modeling and characterizing the THM properties of clay soils. This overview is organized into three distinct sections. Firstly, we examine the methodologies for describing the geomechanical behavior of clay soils and the significance of considering bound-water dehydration. Secondly, we delve into prior studies that explored the implementation of constitutive models in FEM simulations. Finally, we scrutinize BTES project simulations, designs, specifications, and their practical applications in subarctic regions.

2.2 Multiphysics simulation of clay soils.

Over the past few decades, numerous experiments have demonstrated the significant impact of temperature variations on the mechanical behavior of clay soils [17, 18]. Changes in temperature have multiple effects on the mechanical and hydraulic characteristics of water-saturated clay soils, which represent major concerns in geotechnical engineering. The Thermo-Hydro-Mechanical (THM) behaviors of clay soils play a pivotal role in various engineering projects, such as nuclear waste disposal [19] and underground geothermal utilization and storage [20].

Previous experimental findings indicate that the THM behavior of clay soil correlates with the Over-Consolidation Ratio (OCR). When clay soil is heated, its particles expand. However, an increase in temperature reduces the strength of adsorbed layers, leading to a decrease in the distance between clay particles. Under normally consolidated conditions, this behavior alters the equilibrium between Van der Waals attractive forces and electrostatic repulsive forces, resulting in grain rearrangement and shrinkage. Conversely, in highly over-consolidated clay soil heated conditions, it primarily undergoes reversible thermal expansion. Studies by [6, 21] suggest that the inclination of the soil toward dilation and contraction, as well as the intensity of the

reversible/irreversible parts of the deformation during heating and cooling cycles, relate to clayey material types, OCR, and plasticity.

Despite extensive research, the precise thermo-poro-mechanical behavior of clayey materials remains a subject of ongoing debate, without a comprehensive consensus. On one hand, numerous experimental and numerical studies suggest that increasing temperature may reduce the strength of clayey materials, with some cases even reporting thermal failure [18, 22]. On the other hand, research by Zhang et al. (2012) [1], Laloui and Cekerevac (2008) [8], and Kuntiwattanakul et al. (1995) [9], indicates that increasing temperature can enhance the shear strength of clay soils. Understanding and simulating this complex behavior of clayey soil has garnered significant attention over the past few decades.

The Plasticity-based approach and the thermodynamic-based approach are two prominent methods widely used in modeling and characterizing the THM behavior of clay soils. In the Plasticity-based approach, the focus lies on capturing clay's mechanical response through plasticity theories, enabling the simulation of deformation, shear strength, and stress-strain behavior. On the other hand, the Thermodynamic-based approach takes a more holistic perspective by considering the thermodynamic principles governing clay behavior, incorporating concepts such as energy dissipation and entropy production. These approaches are not mutually exclusive but rather complementary, offering researchers and practitioners valuable tools for analyzing and predicting the behavior of clay soils in a wide range of geotechnical and environmental contexts.

Furthermore, it is essential to emphasize the critical importance of considering bound-water dehydration in clay material simulation. Bound-water molecules play a fundamental role in clay's behavior, influencing its volume change, stiffness, and strength properties. Thus, incorporating the effects of bound-water dehydration into simulations is essential for achieving an accurate and reliable description of clay material behaviors.

2.2.1 Plasticity-based approach

The plasticity-based method, as its name suggests, is founded on the principles of plasticity and continuum mechanics. Within this framework, the THM (Thermo-Hydro-Mechanical) characteristics of geomaterials heavily hinge on factors such as yield surfaces and hardening laws.

Precisely and suitably accounting for temperature fluctuations, stress-strain rates, and the development of yield surfaces constitute the pivotal elements of this approach. Over the last few decades, numerous scholars have employed this approach to elucidate the thermo-mechanical properties of geomaterials [22, 24–27].

Zhang et al. (2012) [9], introduced an innovative constitutive model rooted in the plasticity framework to characterize the intricate thermo-mechanical responses of clay soils. Within this model, they introduced a straightforward notion called "equivalent stress" to account for the impact of temperature fluctuations on soil hardening. In this concept, they posited that the volumetric strain induced by temperature variation is equivalent to the volumetric strain resulting from an increment in equivalent stress. This concept is shown in Figure 2-1.

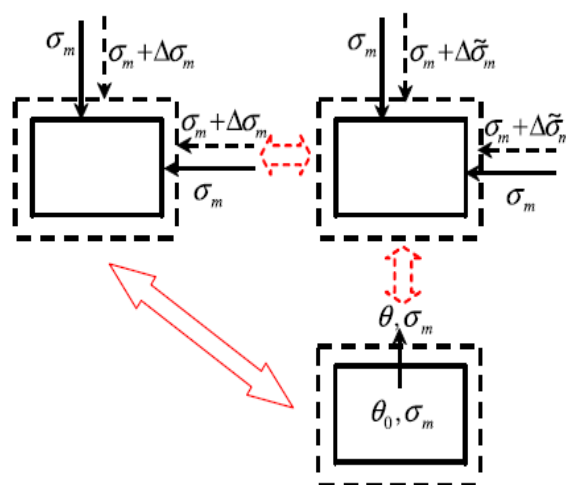


Figure 2-1 Volumetric strain caused by real stress and equivalent stress [9](θ is temperature).

In 1989 Hashiguchi [28], introduced an innovative plasticity concept, departing from traditional approaches, to better capture the mechanical properties of geomaterials. Unlike conventional plasticity, this framework incorporates the elastoplastic domain within the interior of the yield surface. Consequently, this model can describe elastoplastic behavior starting from the soil's initial stress conditions. To achieve this, Hashiguchi proposed the concept of a surface, referred to as the "subloading yield surface," which maintains a similar shape to the normal yield surface and always passes through the current stress points. In Figure 2-2 the subloading surface and normal yield surface is presented.

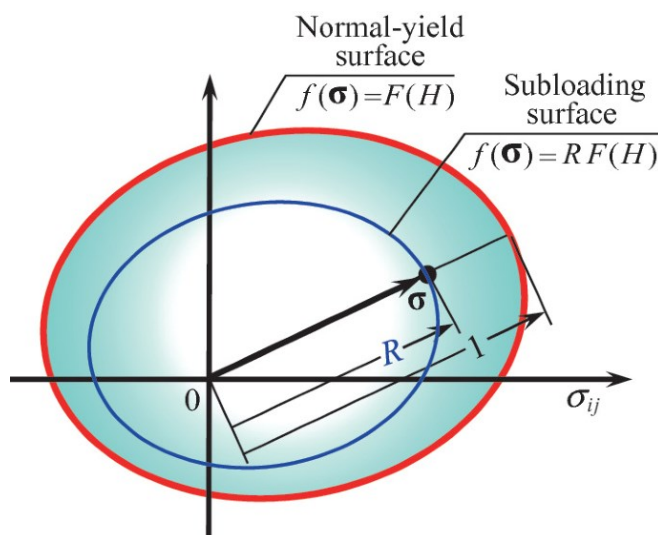


Figure 2-2 Normal yield and subloading yield surfaces [29].

Although the plasticity-based model and the innovations applied to it have provided a strong platform for numerically modeling the behavior of clay soils, the primary drawback of this approach is its inability to adhere to all the fundamental laws of thermodynamics. Constitutive models that violate the laws of thermodynamics cannot effectively simulate THM behavior in most cases, they can only describe THM behavior under certain predefined conditions [30].

2.2.2 Thermodynamic-based approach

Describing the soil behavior based on the thermodynamic theory and fundamental laws of thermodynamics is an approach that is widely used by researchers. In this approach, the thermo-mechanical behavior of the geomaterials is described based on the concepts of elastic potential energy, free energy, physical conservation laws, first and second principles of thermodynamics, and entropy balance equations.

Furthermore, both laboratory and field measurements have demonstrated the significant influence of temperature fluctuations on clay soil properties [31]. It has been observed that thermal disturbances can result in lasting deformations within these soils [6, 32–36]. Substantial experimental evidence indicates that heating can induce irreversible deformations along drained stress paths, especially in loosely consolidated clayey soils [37].

To predict the non-isothermal poro-mechanical behaviors of clayey soils, several thermo-mechanical coupled constitutive models have been developed. These models typically incorporate temperature-dependent yield surfaces to describe the thermo-mechanical response [5, 7, 21, 32, 38, 39]. A comprehensive review of these advanced thermo-mechanical models for saturated clays is provided by Hong et al. 2013 [40].

In addition to the thermo-mechanical models, there are other thermo-elastoplastic models that incorporate thermodynamic principles [8, 9]. These models apply a series of thermodynamic constraints on constitutive model variables, such as stress, strain states, and strain evolution laws [10]. The overall framework of most thermodynamic-based models is similar to classical phenomenon-based elastoplastic models [11]. An advantage of using phenomenon-based elastoplastic models is that many of the model parameters can be determined through temperature-controlled triaxial tests.

However, one limitation of these models is the inadequate consideration of dehydration-induced strain (conversion of clay-bound water to free water). The constitutive modeling of dehydration-induced strain in clayey soils has been specifically addressed by Hueckel in 1992 [41] and Hueckel in 2002 [42]. The study of dehydration in saturated clayey soils has gained recent attention [12, 13, 43, 44]. Researchers have focused on understanding the effects of bound water dehydration on the mechanical behavior of clayey soils.

2.2.3 Bound water dehydration

The liquid phase in water-saturated clay soil is divided into the free and bound water forms. This division happened because of the electrochemical interaction between clay particles and water [45, 46]. Free water is the amount of water that fills the clay pores and is known as bulk water in soil skeleton; bound water is another form that is absorbed by the clay minerals and plays an important role in the THM behavior of clayey materials. These two water forms are illustrated in Figure 2-3.

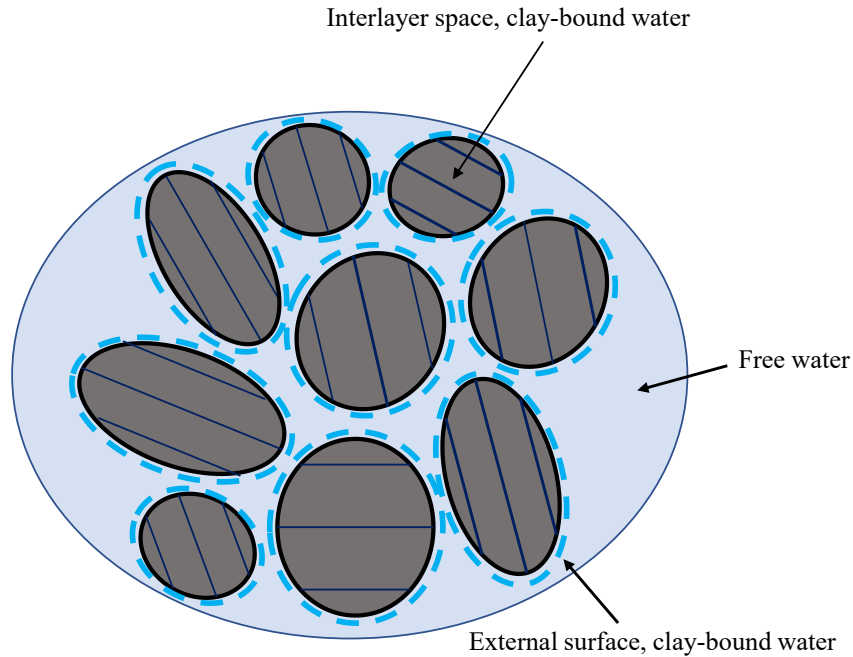


Figure 2-3 Illustration depicting free water and bound water in clay-water composites.

When clay soil is heated, the bonding between water and the clay minerals is weakened and some amount of bound water can transfer to free water. This transformation behavior creates a deformation in the soil which is named as dehydration strain. [12, 16, 47, 48].

The development of this strain at the microscopic level presents challenges in gaining a comprehensive understanding of dehydration behavior. Furthermore, quantifying dehydration strain poses another significant challenge.

Li and Wong in 2017 [12] proposed an explanation for the thermally induced strain observed in soft mudrocks. They suggested that this strain arises from the expansion of solid minerals, the release of interlayer bound water, and thermal plastic strain. However, implementing their mechanistic model in constitutive modeling tools such as phenomenon-based elastoplastic models is not straightforward.

To address this challenge, Zhang and Cheng in 2017 [43] introduced the Tsinghua ThermoSoil model, which offers a new approach to simulate the coupled thermo-mechanical behavior of clayey soils. This model incorporates a double-entropy concept that captures the effects of energy

dissipation at the microscopic level on continuum behavior. It also considers the exchange between bound and free water. However, compared to phenomenon-based elastoplastic models, the Tsinghua ThermoSoil model requires a more complex procedure to determine the relevant parameters for numerical modeling.

In light of these considerations, it becomes clear that there is a compelling need to introduce a novel constitutive model. This model should effectively describe the THM behavior of clay soils by incorporating the principles of thermodynamics. Furthermore, it should possess the capability to consider the impact of bound water dehydration strain while being founded upon unconventional plasticity principles.

2.3 Implementation in Finite Element Method (FEM)

The finite element method (FEM) is a numerical technique widely used for solving complex engineering problems, including the analysis of soil behavior. This implementation enables the analysis of large-scale systems and the prediction of the response of soil under various loading and environmental conditions.

In the context of thermo-elastoplastic behaviors of saturated clayey soils, the FEM plays a crucial role in solving the governing equations derived from the thermodynamic-based model. The FEM discretizes the soil domain into finite elements, where the constitutive equations are applied to each element to calculate the stress and strain fields. By considering the effects of temperature, degree of saturation, and stress, the FEM can provide valuable insights into the soil's behavior and its response to different environmental conditions.

Temperature fluctuations have a profound influence on the poromechanical characteristics of geomaterials. In the realm of non-isothermal geotechnical projects such as geothermal energy storage and carbon neutrality-focused storage, comprehending the intricate thermo-hydromechanical (THM) processes is paramount [44, 49]. Nonetheless, accurately describing the interplay between thermal, hydraulic, and mechanical factors in clay soils remains a subject of contention within the geotechnical engineering community [50–52].

The poromechanical behaviors of clay soils are heavily influenced by their saturation state. Even in the case of water-saturated clay soils, the intricate interaction between clay minerals and water introduces complexities in terms of temperature dependency. Thus, a multidisciplinary approach

becomes imperative in fully comprehending and precisely modeling THM behavior. Extensive prior experimental data suggests that heating tends to induce irreversible contraction deformations in clay soils under drained stress conditions, particularly for unconsolidated geomaterials [5–7].

A series of theoretical investigations were conducted to explore the plastic behavior induced by temperature in clay soils [37]. These models primarily describe the thermo-mechanical behaviors by utilizing yield surfaces that are dependent on temperature [6, 21, 32, 38, 53]. A comprehensive review of these advanced thermo-mechanical models for saturated clays can be found in [40, 54]. However, limited attention has been given to the consideration of the impact arising from clay bound water dehydration, which should be treated as a distinct deformation mechanism [12, 13].

The increase in temperature within a water-saturated clay-rich geomaterial can result in the transformation of clay bound water into free water, leading to dehydration-induced changes in pore structure and deformation [14–16]. Geologists studying abnormal pore water pressure generation in basin modeling [14, 47, 48, 55] and pore water geochemistry in smectite-rich geological formations [56], have predominantly investigated clay bound water dehydration. Hueckel, a pioneer in geotechnical engineering, extensively explored thermally driven dehydration in clay soils and its associated elastic and reactive plastic deformations [41, 42, 57].

It is important to note that different types of clay bound water adhere to the external surface of clay particles or the interlayer nanoscale pore space [58]. The dehydration processes of these different types of clay bound water are dependent on temperature and pressure conditions; however, previous studies often did not differentiate between them. Recent advancements in the geotechnical community have primarily focused on the dehydration of bound water adhered to the external surface of clay particles [43, 44, 59, 60], which occurs within a relatively lower temperature range (20°C to 90°C) and is more relevant to shallow geothermal energy engineering projects. These derivations are mainly based on the energy concept and necessitate a complex procedure to obtain related parameters for numerical modeling. Therefore, there is still a need for a versatile, straightforward, and comprehensive model for practical engineering applications.

In the modeling of thermal-hydro-mechanical coupled processes in clay soils, considering bound water dehydration, the convection term in the energy balance, which was previously neglected, becomes significant. The numerical implementation of the unsteady advection-diffusion equation requires stabilization [61]. In this study, the streamline upwind Petro-Galerkin (SUPG)

stabilization method, which was proposed by Brooks and Hughes [62] is employed for achieving stability.

2.4 Advancements in Modeling Thermo-Hydro-Mechanical Behaviors

The literature within the realm of energy systems and thermal storage has witnessed significant developments in response to the ever-increasing demand for sustainable energy solutions. In 2017, a substantial 75% of the world's electricity was derived from thermal power sources, relying on fuel-driven heat for turbine operation [63]. However, as the global commitment to decarbonization intensifies, the transition from fossil fuels to renewable heat sources like geothermal energy, hydrogen fuel, and solar thermal energy has emerged as a crucial paradigm shift [64]. This shift bears the promise of not only meeting energy demands but also fostering a more environmentally friendly and sustainable energy landscape.

This transition towards renewable thermal sources has catalyzed the rise of Thermal Energy Storage (TES) systems in modern energy infrastructure [1, 2, 65]. The integration of intermittent renewable sources such as wind and solar power has propelled TES into a pivotal role, ensuring the efficient management of energy supply and demand. Among various TES variants, Borehole Thermal Energy Storage (BTES) systems have gained prominence [66]. BTES leverages shallow Borehole Heat Exchangers (BHE) to store and release thermal energy, using soil and rock as effective mediums [67–69]. BTES's adaptability across geological formations and cost-effectiveness in installation compared to alternative TES systems position it as an ideal choice for seasonal storage [70–73].

However, the construction costs associated with BTES underscore the necessity for rigorous numerical simulations to ensure both economic viability and thermodynamic efficiency. Computational methods that analyze the thermal, hydraulic, and mechanical behavior of boreholes within BTES systems are vital in this context. Notably, a multiphysics approach that considers ground heat transfer, pore water pressure variations, and mechanical changes stands out for its enhanced accuracy compared to the commonly used parameter fitting models [68]. Extensive research has been devoted to optimizing BTES modeling, often relying on Ingersoll's infinite-line source model for heat transfer within BHEs.

Numerous scholars have contributed to the optimization of BTES modeling in recent decades. Zeng et al. (2002) [74], introduced a quasi-three-dimensional framework for representing the thermal network within a borehole field, emphasizing the significance of axial heat transfer in varying heat exchanger configurations. De Paly et al. (2012) [75], introduced an innovative optimization approach for energy extraction from enclosed shallow geothermal systems, focusing on workload optimization as a proxy for flow rate optimization. Bayer et al. (2014) [76], extended mathematical optimization techniques to enhance ground elements in shallow geothermal energy systems, encompassing both heating and cooling applications.

While research has illuminated heat and fluid flow in soil, robust property models for assessing soil behavior under heat transfer and pore water pressure variation remain underdeveloped. Changes in temperature significantly impact the poromechanical characteristics of geological materials, particularly clay soils, prompting further investigation [50–52].

Researchers such as Cekerevac and Laloui (2004) [6] and Abuel-Naga et al. (2007) [32] have examined thermal effects in clay soils behavior. However, the influence of dehydration of bound water and the conversion of clay-bound water to free water upon temperature increase [13–16, 58] [23–27] on soil deformation have not been well addressed in their research.

Li and Wong (2017) [12], have performed a series of experimental tests to highlight the effects of dehydration strains. They found that distinct types of clay-bound water cause different deformations, which make the soil behavior more complicated. They also mentioned that the dehydration of the outer layer of bound water in clay minerals can occur at relatively low temperatures, starting from 30 °C. However, it necessitates a substantial amount of time for excess pore pressure induced by this process to dissipate in low-permeability soil formations. In theory, thermal disturbances tend to cause short-term ground heave as a response, particularly if there is no significant plastic deformation involved.

Currently, there is a lack of research addressing the impact of such thermal-mechanical disturbances on soil behavior. The role of bound water dehydration in the overall ground deformation remains unexplored. This is especially relevant in Canadian subarctic regions where the soil has undergone significant consolidation during the glacial period, leading to uncertainties

regarding the potential magnitude of deformation during BETS operations in off-grid communities.

Recently Sojoudi and Li (2023) [59] have attempted to address these gaps. They introduced a thermodynamic-based model for the dehydration of bound water on clay particle surfaces but have not yet incorporated this model into the FEM for comprehensive analysis.

In Chapter 4 of this thesis, we presented a FEM-based numerical platform for simulating soil behavior while considering the effect of bound water dehydration. The results have been compared with experimental data, and a reasonable agreement has been achieved. Consequently, in Chapter 5, we used the proposed numerical model to simulate a borehole in a BTES system in the Canadian subarctic region. The results provide significant information for the execution and design of BTES projects in subarctic areas, as well as for further research in these systems.

Preface to Chapter 3

Over the past decades, articulating the accurate thermo-hydro-mechanical behavior of clay soils has presented a formidable challenge. Due to its intricate character, the formulation of an encompassing framework has remained elusive. In this chapter, we undertake the task of not only reviewing antecedent research endeavors but also introducing a more pragmatic and comprehensive poro-elastic-plastic model rooted in the foundational principles of thermodynamics. This model demonstrates the capability to account for the influence of bound water dehydration on soil's thermal strain. The comparative analysis between the results obtained from the model simulations and empirical observations yields commendable outcomes. These achievements substantiate the robustness of the model's formulation, underscore its potential for further refinement, and highlight its capacity for progressive advancement.

Chapter 3

3 A thermodynamic-based model for modeling thermo-elastoplastic behaviors of saturated clayey soils considering bound water dehydration¹

3.1 Abstract

The non-isothermal deformation of soft mudrocks or clay soils is one of the most critical issues in energy and environmental related geotechnics. Clay-related geomaterials hold complex microstructure and mineral composition, which brings difficulty in investigating their thermo-mechanical behaviors. Previous studies pay little attention to the difference between a thermal plastic strain and the strain from clay dehydration. In this study, a new constitutive model is proposed for describing the thermo-elastoplastic behaviors of clayey soils under water-saturated condition. The effect of temperature variation and mechanical loading on elastoplastic strains and dehydration are investigated. The thermodynamics laws and the unconventional plasticity are applied to quantify the thermo-mechanical behavior. The irreversible strain is captured by using Cam-Clay plasticity and subloading yield surface concept. The dehydration strain is described by utilizing a novel method based on generalized thermodynamics approach and Helmholtz free energy function. The internal variables, and the first and second laws of thermodynamics are applied in the model. The hardening rule is established by implementing the laws of physical conservation, energy dissipation, and plastic flow. The proposed model is validated using specially designed thermal consolidation tests on laboratory prepared heavily consolidated clayey soils and some published data of clayey soils with different geological origins.

Keywords: Thermo-mechanical process, Subloading yield surface, Energy methods, Clay-bound water Dehydration.

¹ A version of this manuscript has been published in *Journal of Rock Mechanics and Geotechnical Engineering* (2023).

3.2 Introduction

The thermo-elastoplastic behaviors of clay-related geomaterials are critical for energy projects like deep disposal of nuclear waste [18, 39], geothermal energy exploitation and storage [31, 44, 49, 77–79]. Non-isothermal laboratory and field measurements demonstrate that the properties of clayey soils are highly dependent on applied temperatures [31], and thermal disturbance can induce permanent deformations [6, 32–36]. Extensive experimental data reveal that heating tends to result in irrecoverable deformation in clays under a drained stress path, and the effects are pronounced for unconsolidated clayey soils [37]. A series of thermo-mechanical coupled constitutive models has been developed to predict the non-isothermal poro-mechanical behaviors of clayey soils. These models usually describe the thermo-mechanical behaviors using temperature-dependent yield surfaces [5, 7, 21, 32, 38, 39]. A complete review of these types of advanced thermo-mechanical models for saturated clays is presented by Hong et al. (2013) [40]. There are other thermo-elastoplastic models shedding light on thermodynamics laws [8, 9], where a series of thermodynamic restrictions is applied on constitutive model variables, such as stress and strain states, and strain evolution laws [10]. The final framework of most of thermodynamic-based models is same as the classical phenomenon-based elastoplastic models [11]. The advantage of using the phenomenon-based elastoplastic models is that most of the model parameters can be obtained by utilizing temperature-controlled triaxial tests. One of the major limitations of these models is that the dehydration strain (clay-bound water turns to free water) cannot be considered properly. Constitutive modeling of dehydration-induced strain in clayey soils is primarily highlighted in Hueckel (1992) [80] and Hueckel (2002) [42]. Dehydration in saturated clayey soils draws more attention recently [12, 13, 44, 81].

In this sense, Li and Wong (2017) [12] proposed that the thermally induced strain in soft mudrocks or dense clayey soils is due to the expansion of solid minerals combined with interlayer bound water, the dehydration of clay-bound water, and thermal plastic strain. However, the mechanistic model by Li and Wong (2017) cannot be easily implemented in constitutive modeling tools like the phenomenon-based elastoplastic models. The Tsinghua ThermoSoil model provides a novel concept for simulating the coupled thermo-mechanical behavior of clayey soils, where a double-entropy approach capturing effects of energy dissipation at the microscopic level on

continuum behavior is applied [81]. The exchange between the bound and free water is considered in the Tsinghua ThermoSoil model. Compared to the phenomenon-based elastoplastic models, this model also requires a more complicated procedure to obtain related parameters for numerical modeling. In this context, a new thermo-elastoplastic constitutive model is presented using theories from thermodynamics and unconventional plasticity. The dehydration strain is described using a novel method based on generalized thermodynamics approach and Helmholtz free energy function. The irreversible strain is captured using Cam-Clay plasticity and with the subloading yield surface concept. Specially designed thermal consolidation tests on laboratory prepared heavily consolidated clayey soils are designed for model validations. The proposed model is also validated using published data on some natural clayey soils retrieved from different sites.

3.3 Thermodynamic bases for constitutive model

The accuracy and complexity of the thermodynamic-based models are directly related to the chosen internal variables and the definition of free energy functions of the soil. Appropriate description of evolution law, flow rule and yield function for a specific material is considered as a main challenge in proposing a constitutive thermodynamic-based model. This can be achieved through the fundamentals of thermodynamics by using the first and second laws of thermodynamics. The internal energy (e) is linked with the increment of work (W) and heat supplies (Q) by the first law of thermodynamics:

$$de = \delta W + \delta Q \quad (3.1)$$

The thermodynamics work δW done on the system can be mechanical work, fluid flow, or chemical work. The component of heat supply δQ to the system is constrained by the second law of thermodynamics:

$$dS \geq \frac{\delta Q}{T} \quad (3.2)$$

where S is entropy, and T is temperature.

Eq. (3.2) is always true for a reversible process. For an irreversible one, the variation of entropy is larger than the right-hand side of Eq.(3.2). In the case of a small deviation from equilibrium, the irreversible process can be treated as a series of individual equilibrium [82, 83] :

$$\left. \begin{aligned} dS &\geq \frac{\delta Q_{\text{rev}}}{T} + \delta S^i \\ \delta S^i &\geq 0 \end{aligned} \right\} \quad (3.3)$$

where the $\frac{\delta Q_{\text{rev}}}{T}$ describes the entropy exchange of the system and the δS^i is the variation of entropy due to dissipation with the interior of the system. Substituting Eq.(3.3) into Eq.(3.1) will generate the following relation:

$$\delta W \geq de - TdS + T\delta S^i \quad (3.4)$$

The thermodynamic state of material can be defined in alternative ways through different conjugate variables and related to different energy functions (e.g. internal energy, Helmholtz free energy, enthalpy, and Gibbs free energy). These four different energy functions are related to each other by Legendre transformations [84]. The Helmholtz free energy is a thermodynamic potential of non-thermal work and is given by $\Psi = e - TS$. By using the Legendre transformation of internal energy and using the definition of Helmholtz free energy, the Clausius-Duhem inequality in terms of heat flux (q) can be expressed as

$$\sigma_{ij} \dot{\epsilon}_{ij} - \rho(\dot{\Psi} + S\dot{T}) - \frac{1}{T} q_i \nabla_i T \geq 0 \quad (3.5)$$

where σ_{ij} is the total stress tensor, $\dot{\epsilon}_{ij}$ is the rate of the strain tensor, and ρ is total density.

Clausius-Duhem inequality is particularly significant in determining whether the constitutive relation of a material is thermodynamically allowable or not. Moreover, this inequality links the Helmholtz free energy to the rate of strain $\dot{\epsilon}_{ij}$.

As is shown by Voyiadjis and Abu Al-Rub (2003) [85], the Helmholtz free energy Ψ can be expressed as a function of the thermo elastic strain $\epsilon_{ij}^{\text{Te}}$, temperature (T), and internal state variable for accumulative plastic strain (H). In this study, we added an extra internal variable named dehydration strain ϵ^{Deh} to the Helmholtz free energy:

$$\Psi = \Psi(\epsilon_{ij}^{\text{Te}}, T, H, \epsilon^{\text{Deh}}) \quad (3.6)$$

We assume that under thermo-mechanical loading, the total thermal strain increment of the soil is decomposed into components of thermo-elastic ($\dot{\epsilon}_{ij}^{\text{Te}}$), thermo-plastic ($\dot{\epsilon}_{ij}^{\text{Tp}}$), and dehydration strain ($\dot{\epsilon}_{ij}^{\text{Deh}}$) increments:

$$\dot{\varepsilon}_{ij} = \dot{\varepsilon}_{ij}^{\text{Te}} + \dot{\varepsilon}_{ij}^{\text{Tp}} + \dot{\varepsilon}_{ij}^{\text{Deh}} \quad (3.7)$$

The dehydration strain (assumed to be isotropic) is induced by the change in amount of clay-bound water during temperature variation. More explanation on dehydration related strains is presented in Section 3.3. By using the chain rule and time derivation of Helmholtz free energy with respect to its state variables, the formula is implied as

$$\dot{\Psi} = \frac{\partial \Psi}{\partial \varepsilon_{ij}^{\text{Te}}} \dot{\varepsilon}_{ij}^{\text{Te}} + \frac{\partial \Psi}{\partial T} \dot{T} + \frac{\partial \Psi}{\partial H} \dot{H} + \frac{\partial \Psi}{\partial \varepsilon^{\text{Deh}}} \dot{\varepsilon}^{\text{Deh}} \quad (3.8)$$

By substituting Eq.(3.8) into Eq.(3.5), and making use of Eq.(3.7), the following thermodynamic inequality is postulated:

$$\left(\sigma_{ij} - \rho \frac{\partial \Psi}{\partial \varepsilon_{ij}^{\text{Te}}} \right) \dot{\varepsilon}_{ij}^{\text{Te}} + \sigma_{ij} \dot{\varepsilon}_{ij}^{\text{Tp}} + \sigma_{ij} \dot{\varepsilon}_{ij}^{\text{Deh}} - \rho \left(\frac{\partial \Psi}{\partial T} + S \right) \dot{T} - \rho \frac{\partial \Psi}{\partial H} \dot{H} - \rho \frac{\partial \Psi}{\partial \varepsilon^{\text{Deh}}} \dot{\varepsilon}^{\text{Deh}} - \frac{1}{T} q_i \nabla_i T \geq 0 \quad (3.9)$$

Based on Eq. (3.9), and according to the validity of Clausius-Duhem inequality for all possible loading histories, the thermodynamics conjugate forces with state laws of the model are given:

$$\sigma_{ij} = \rho \frac{\partial \Psi}{\partial \varepsilon_{ij}^{\text{Te}}}; \quad S = -\frac{\partial \Psi}{\partial T}; \quad F = \rho \frac{\partial \Psi}{\partial H}; \quad P^{\text{Deh}} = \rho \frac{\partial \Psi}{\partial \varepsilon^{\text{Deh}}} \quad (3.10)$$

where F is the conjugate force of the internal state variable for accumulative plastic strain, and P^{Deh} is the conjugate force for the dehydration strain.

With Eqs. (3.9) and (3.10), the total dissipation function can be written as

$$\Pi = \left(\sigma_{ij} - \rho \frac{\partial \Psi}{\partial \varepsilon_{ij}^{\text{Te}}} \right) \dot{\varepsilon}_{ij}^{\text{Te}} + \sigma_{ij} \dot{\varepsilon}_{ij}^{\text{Tp}} - F \dot{H} + \left(\sigma_{ij} - \rho \frac{\partial \Psi}{\partial \varepsilon^{\text{Deh}}} \delta_{ij} \right) \dot{\varepsilon}_{ij}^{\text{Deh}} - \frac{1}{T} q_i \nabla_i T \geq 0 \quad (3.11)$$

where the identity tensor δ_{ij} is used to link the dehydration strain with the strain tensor.

In this paper, it is assumed that clayey soil is involved in thermo-elastic, thermo-plastic and bound water dehydration-induced deformations under a thermo-mechanical loading condition. To describe the energy change and dissipation associated with each process, the Helmholtz free energy is treated as a function of thermo-elastic Ψ^{Te} , thermo-plastic Ψ^{Tp} , and dehydration Ψ^{Deh} parts. It is assumed that each process has a specific and distinct mechanism contributing to the total deformation of the soil:

$$\Psi = \Psi^{\text{Te}}(\varepsilon_{ij}^e, T) + \Psi^{\text{Tp}}(H, T) + \Psi^{\text{Deh}}(\varepsilon^{\text{Deh}}, T) \quad (3.12)$$

where ε_{ij}^e is the elastic strain.

Based on the definition of Helmholtz free energy and according to Eq.(3.4), the thermo-elastic, thermo-plastic, and dehydration components of total Helmholtz free energy can be achieved by taking the integral of the work done by each part:

$$\rho\psi^{Te}(\varepsilon_{ij}^{Te}, T) = \int \sigma_{ij} d\varepsilon_{ij}^{Te} = \left(\frac{E_{ijkl} \varepsilon_{ij}^{Te} \varepsilon_{kl}^{Te}}{2} \right) v^e(T) \quad (3.13)$$

$$\rho\psi^{Tp}(H, T) = \int F dH = \left[F_0(\psi - o) \exp\left(\frac{H}{\psi - o}\right) \right] v^p(T) \quad (3.14)$$

$$\rho\psi^{Deh}(\varepsilon^{Deh}, T) = e_b - TS^b = \int P^{Deh} d\varepsilon^{Deh} \quad (3.15)$$

where $v^e(T)$ and $v^p(T)$ are the Arrhenius-type temperature terms for elastic and plastic components of Helmholtz free energy. Darabi et al. (2012) [86] proposed the following equation to describe $v^e(T)$ and $v^p(T)$:

$$v^e(T) = v^p(T) = \exp\left[-\delta \left(1 - \frac{T}{T_0} \right) \right] \quad (3.16)$$

where δ is a parameter representing the temperature coupling term; E_{ijkl} is the fourth-order stiffness tensor; F is the conjugate force of the internal state variable for accumulative plastic strain with function presented in Section 3.1; F_0 is the initial value of F ; ψ and o are the slope of the normal consolidation line in $\ln v - \ln p$ plane and the slopes of swelling lines in $\ln v - \ln p$ plane, respectively; e_b and s^b stands for the internal energy and the specific entropy of clay bound water, respectively.

Darabi et al. (2012) [86] showed that the energy dissipation rate can be decomposed into thermo-elastic, thermo-plastic, dehydration, and thermal components as

$$\left. \begin{aligned}
\Pi &= \Pi^{\text{Te}} + \Pi^{\text{Tp}} + \Pi^{\text{Deh}} + \Pi^{\text{th}} \geq 0 \\
\Pi^{\text{Te}} &= \left(\sigma_{ij} - \rho \frac{\partial \Psi}{\partial \varepsilon_{ij}^{\text{Te}}} \right) \dot{\varepsilon}_{ij}^{\text{Te}} \geq 0 \\
\Pi^{\text{Tp}} &= \sigma_{ij} \dot{\varepsilon}_{ij}^{\text{Tp}} - F\dot{H} \geq 0 \\
\Pi^{\text{Deh}} &= \left(\sigma_{ij} - \rho \frac{\partial \Psi}{\partial \varepsilon_{ij}^{\text{Deh}}} \delta_{ij} \right) \dot{\varepsilon}_{ij}^{\text{Deh}} \geq 0 \\
\Pi^{\text{th}} &= -\frac{1}{T} q_i \nabla_i T \geq 0
\end{aligned} \right\} \quad (3.17)$$

The Cauchy stress is the conjugate force of the thermo-elastic strain tensor, and the following relation $\sigma_{ij} - \rho \frac{\partial \Psi}{\partial \varepsilon_{ij}^{\text{Te}}} = 0_{ij}$ is supposed to fulfill the non-negative nature Π^{Te} . In this study, since only

reversible dehydration behavior is considered, the amount of $\sigma_{ij} - \rho \frac{\partial \Psi}{\partial \varepsilon_{ij}^{\text{Deh}}} \delta_{ij}$ is also equal to null similar to the thermo-elastic component. The evolution of thermo-plastic strain and accumulative plastic strain rate can be described by the thermo-plastic rate of energy dissipation Π^{Tp} , the Lagrange plastic multiplier $\dot{\lambda}$, as well as the normal yield surface function f [87]:

$$\Pi^{\text{Tp}} = \sigma_{ij} \dot{\varepsilon}_{ij}^{\text{p}} - F\dot{H} \geq 0 \quad (3.18)$$

$$\Omega = \Pi^{\text{Tp}} - \dot{\lambda} f \quad (3.19)$$

$$\frac{\partial \Omega}{\partial \sigma_{ij}} = 0, \quad \frac{\partial \Omega}{\partial F} = 0 \quad (3.20)$$

Accordingly, plastic strain and hardening variables are expressed by

$$\dot{\varepsilon}_{ij}^{\text{Tp}} = \dot{\lambda} \frac{\partial f}{\partial \sigma_{ij}}, \quad \dot{H} = -\dot{\lambda} \frac{\partial f}{\partial F} \quad (3.21)$$

3.4 A new thermo-elastoplastic model

As mentioned above, we assumed that the total thermal strain is equal to the summation of thermo-elastic, thermo-plastic, and dehydration strains. Each of these strain equations and relations will be presented in this section.

3.4.1 Thermo-elastic strain and thermo-plastic strain

The thermo-elastic behavior is obtained based on the hypotheses of elasticity theories and linear relationships between the thermodynamic conjugate forces and the variation of thermo-elastic strains:

$$\varepsilon_{kl}^{\text{Te}} = \frac{\sigma_{ij} v^c(T)}{E_{ijkl}} \quad (3.22)$$

In the proposed model, thermo-plastic deformation is calculated based on the subloading surface concept of the elastoplasticity framework [88]. The normal yield surface and a subloading surface are applied in this framework. The normal yield surface is the same as the conventional yield surface, while the domain inside its interior is not regarded as purely elastic (Figure 3-1).

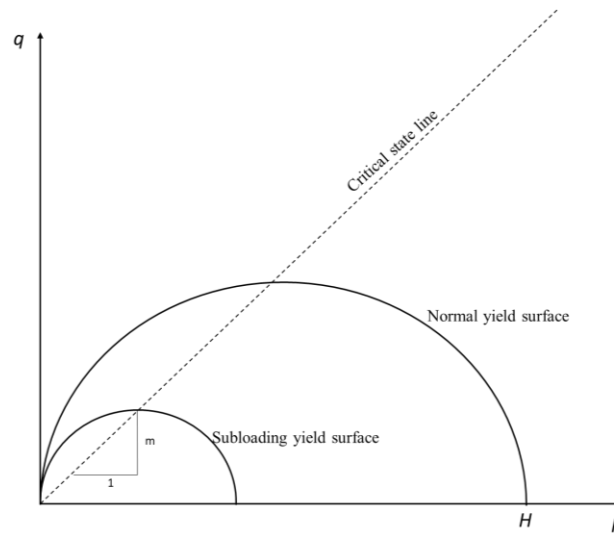


Figure 3-1 Sketch showing normal yield and subloading yield surfaces of the modified Cam-Clay model in p - q plane.

The subloading surface always passes through the current stress point while keeping a similar shape to the normal yield surface. The ratio of the length of an arbitrary line connecting two points on two yield surfaces is called the similarity ratio. The similarity ratio is comparable to the ratio of the sizes of these surfaces. This similarity ratio is also named as normal yield ratio, R . The conditions, $R = 0$, $0 < R < 1$, and $R = 1$, correspond to the null stress state, the sub-yield state, and the normal yield state, respectively. Compared to traditional plasticity models, the use of

subloading yield surface results in smooth and nonlinear stress-strain curves, which describes the behaviors of clayey soils more accurately [88–90]. The function of subloading surface is described as

$$f(\boldsymbol{\sigma}) = RF(H, T) \quad (3.23)$$

Differentiating Eq.(3.23) gives:

$$\left[\frac{\partial f(\boldsymbol{\sigma})}{\partial \sigma_{ij}} \right]^T d\sigma_{ij} = FdR + R \left(\frac{\partial F}{\partial H} \dot{H} + \frac{\partial F}{\partial T} \dot{T} \right) \quad (3.24)$$

The evolution of the normal yield ratio is given by Hashiguchi et al. (2002) [88]:

$$dR = U \left\| \dot{\boldsymbol{\epsilon}}_{ij}^p \right\| \quad (\dot{\boldsymbol{\epsilon}}_{ij}^p \neq 0) \quad (3.25)$$

where U is given by

$$\left. \begin{array}{l} U \rightarrow +\infty \quad (R = 0) \\ U = 0 \quad (R = 1) \\ U < 0 \quad (R > 1) \end{array} \right\} \quad (3.26)$$

These conditions ensure that the subloading surface goes toward the normal yield surface during the loading process. The conditions given in Eq.(3.26) can be expressed as

$$U = -u \ln R \quad (3.27)$$

where u is a material parameter.

According to Eqs. (3.10) and (3.14), the hardening function is introduced as

$$F(H, T) = \rho \frac{\partial \Psi^{Tp}}{\partial H} = \left[F_0 \exp \left(\frac{H}{\psi - o} \right) \right] v^p(T) \quad (3.28)$$

$$\frac{\partial F}{\partial H} = \frac{F}{\psi - o}, \quad \frac{\partial F}{\partial T} = \frac{\delta}{T_0} F \quad (3.29)$$

Substituting Eqs. (3.25) and (3.29) into Eq. (3.24) yields

$$\left[\frac{\partial f(\boldsymbol{\sigma})}{\partial \sigma_{ij}} \right]^T d\sigma_{ij} = U \left\| \dot{\boldsymbol{\epsilon}}_{ij}^{Tp} \right\| F + R \left(\frac{F}{\psi - o} \dot{H} + \frac{\delta}{T_0} F \dot{T} \right) \quad (3.30)$$

According to Eq. (3.21) and the associated flow rule, the plastic strain is given by

$$\dot{\boldsymbol{\epsilon}}_{ij}^{Tp} = \dot{\lambda} \bar{\mathbf{N}} \quad (3.31)$$

where $\bar{\mathbf{N}}$ is the unit normal vector, and it can be written as

$$\bar{\mathbf{N}} = \frac{\partial f(\boldsymbol{\sigma})}{\partial \sigma_{ij}} \bigg/ \left\| \frac{\partial f(\boldsymbol{\sigma})}{\partial \sigma_{ij}} \right\| \quad (3.32)$$

Substitution of Eq. (3.31) into Eq. (3.30) leads to:

$$\dot{\lambda} = \frac{\bar{\mathbf{N}}^T d\boldsymbol{\sigma}}{M^P} - \frac{\delta R F \dot{T}}{M^T} \quad (3.33)$$

where M^P and M^T are expressed as:

$$\mathbf{M}^P = \left(\frac{U}{R} + \frac{\bar{h}}{\psi - o} \right) \text{tr}(\bar{\mathbf{N}}\boldsymbol{\sigma}) \quad (3.34)$$

$$\mathbf{M}^T = \mathbf{T}_0 \left(UF + \frac{RF\bar{h}}{\psi - o} \right) \quad (3.35)$$

$$\bar{h} = \frac{\dot{H}}{\dot{\lambda}} \quad (3.36)$$

According to Hashiguchi et al. (2002) [88], the loading criterion is given by

$$\left. \begin{array}{l} \text{tr}(\bar{\mathbf{N}}\mathbf{E}\dot{\boldsymbol{\epsilon}}) > 0 \rightarrow \dot{\boldsymbol{\epsilon}}^P \neq 0 \\ \text{tr}(\bar{\mathbf{N}}\mathbf{E}\dot{\boldsymbol{\epsilon}}) \leq 0 \rightarrow \dot{\boldsymbol{\epsilon}}^P = 0 \end{array} \right\} \quad (3.37)$$

where \mathbf{E} is the elastic matrix.

3.4.2 Dehydration strain

Water in saturated clayey soils is presented as free water and bound water. The difference is due to the electrochemical interaction between clay particles and water. As shown in Figure 3-2, free water is the amount of water that fills the clay pores and is known as bulk water in the soil skeleton, while bound water is absorbed by the surface of clayey minerals and plays a significant role in the thermo-hydro-mechanical behavior of clayey materials.

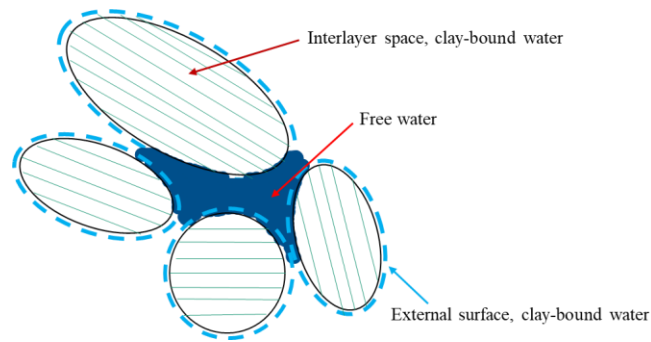


Figure 3-2 Sketch showing free water and bound water in clay-water composites.

When clayey soils are heated, the bonding between water and surface of clayey minerals is weakened, and some of bound water transforms into free water under certain temperature and pressure conditions. This transformation of water composes the deformation in the soil skeleton and produces dehydration strain [12, 15, 16, 48]. This strain naturally develops in a microscopic scale which causes difficulties for an appropriate understanding of dehydration behaviors. Quantitative description of dehydration strain in clayey soils draws considerable attention from geotechnical and geological communities [12, 60, 91]. It should be noted that clay-bounded water sticks to the external and internal surfaces of minerals (Figure 3-2). The dehydration of both types of bound water is reversible if there are no chemical reactions or smectite-illite transformations, but the mechanisms associated with temperature, pressure, and time conditions are different. A general conclusion drawn from the literature shows that the first layer of interlayer-bound water becomes free water at a temperature of about 60 °C [12, 48]. While the dehydration of clay bound water along the external surface can start at $T = 20$ °C [60]. A detailed description of this point is addressed in the discussion section.

In this context, an approach for describing the dehydration strain is presented based on the assumption that some parts of the soil's free energy relate to the variation of bounded water content (ψ^{Deh}). This component of free energy is considered as a function of the volume fraction of bound water n_b , and its value can be altered with the variations in soil temperature and mechanical loading.

Li and Wong (2017) [12] suggested that the dehydration strain can be expressed as a variation of bound water volume over total volume of the soil:

$$\varepsilon^{\text{Deh}} = \frac{dv_b}{v} = dn_b \quad (3.38)$$

where v_b is the volume of bound water, and v is the total volume of the soil.

Accordingly, the dehydration strain can be linearly related with its conjugate force [12, 13]. According to Eqs. (3.10) and (3.38), the following linear relation between the dehydration strain and its conjugate force is postulated:

$$\varepsilon^{\text{Deh}} = \alpha_{\text{bf}} \frac{\partial \Psi^{\text{Deh}}}{\partial n_b} \quad (3.39)$$

where α_{bf} is a coefficient controlling bound water to free water transformation.

According to Eq.(3.15) and Zhang (2017) [13]'s work, the following equations are derived:

$$e_b = T v_b + g_b \quad (3.40)$$

$$v_b = \frac{S^b}{\rho_b n_b} \quad (3.41)$$

$$g_b = \rho_b n_b \frac{\partial (\omega_e^b / (\rho_b n_b))}{\partial (\rho_b n_b)} \quad (3.42)$$

where s^b and ρ_b are the specific entropy and density of bound water, respectively; and ω_e^b is defined as

$$\omega_e^b = f_b(\rho_b n_b) [(E_v^e)^{\beta+2} + \xi (E_v^e)^\beta (\varepsilon_s^e)^2] \quad (3.43)$$

$$f_b(\rho_b n_b) = B_b (\rho_b n_b)^{k_b} \quad (3.44)$$

$$E_v^e = \varepsilon_v^e + \beta_b \dot{T}; \varepsilon_s^e = \sqrt{e_{ij}^e e_{ij}^e}, e_{ij}^e = \varepsilon_{ij}^e - \frac{\varepsilon_v^e}{3} \delta_{ij} \quad (3.45)$$

where β is a power exponent (taken as 1 in this study), β_b is bound water's thermal expansion coefficient. ξ is a material constant; B_b and k_b are parameters governing the effect of bound water on the soil deformation modulus. By using Eqs.(3.40) –(3.45), the derivation of Helmholtz free energy over the changing of bound water density are derived as

$$\frac{\partial \Psi^{\text{Deh}}}{\partial n_b} = B_b (k_b - 1) (\rho_b)^{(k_b-1)} (n_b)^{(k_b-2)} [(E_v^e)^{\beta+2} + \xi (E_v^e)^\beta (\varepsilon_s^e)^2] \quad (3.46)$$

In this study, the dehydration strain is reversible, which is like a nonlinear thermal-elastic behavior. However, dehydration strain may turn out to be irreversible under certain temperature, pressure, and chemical conditions [79]. Treating the dehydration strain separately can provide the opportunity to make such strain components flexible to different environmental conditions.

3.5 Model validations

In the proposed constitutive model for clayey soils, six mechanical parameters (ν , m , F_0 , ψ , o , u) and five dehydration related parameters (α_{bf} , δ , β_b , B_b , K_b , ξ) are required. Values of Poisson's ratio (ν) and the slope of the critical state line (m) can be obtained from traditional drained triaxial tests. Parameter F_0 is the pre-consolidation pressure, which can be obtained from one-dimensional (1D) consolidation tests. ψ and o are the slope of the normal consolidation line and the slope of the rebound curve in the $\ln \nu - \ln p$ plane, respectively. The parameter u is used for adjusting the curvature of the stress–strain diagram.

The value of α_{bf} can be obtained using the following equation proposed by Zymnis et al. (2018) [60]:

$$\alpha_{bf} = - \left(\frac{G_s}{1 - G_s \frac{\rho_f}{\rho_s}} \right) \frac{1}{M_s} \frac{\partial M_w}{\partial T} \quad (3.47)$$

Where G_s is the specific gravity at room temperature (20 °C); ρ_f and ρ_s are the densities of free water and oven-dried solid minerals, respectively; M_s is the mass of solid; and $\frac{\partial M_w}{\partial T}$ is the change of mass of water with temperature.

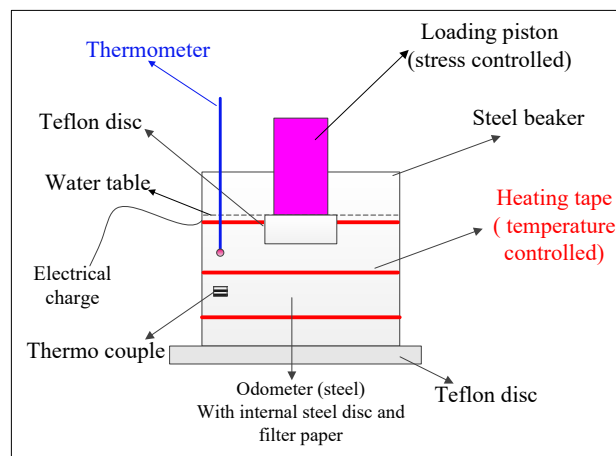
The value of δ can be identified by comparing creep tests at different temperatures. The value of β_b can be estimated based on soils' clay fraction and mineralogical composition [12, 44, 60]. B_b can be obtained by carrying out an isotropic compression test. Values of K_b and ξ can be derived by from critical state parameters [13]. A series of experimental results of smectite-quartz mixtures with different clay fractions, Boom clay, Bangkok clay, and Kaolin clay was applied to validate the proposed model. It should be noted that we have specially designed the thermal

consolidation tests on laboratory using smectite-quartz mixtures to examine the dehydration process in saturated dense clayey soils. Data on other samples were from the literature.

3.5.1 Thermally induced volumetric strain

3.5.1.1 Reconstituted mudrock

We designed high temperature 1D consolidation tests using an oedometer on two dense clayey soil samples to investigate the deformation behaviors. To prepare heavily consolidation clayey soils samples, we poured water-saturated (fluid is brine) smectite-quartz mixtures into an oedometer cell and applied a vertical stress of 10 MPa in a week for consolidation. Two samples with clay fractions of 20% and 45% (by weight; marked as SQ1 and SQ2) were prepared using the above-mentioned approach. The prepared samples showed similar swelling properties with that of natural soft mudrocks [58]. After consolidation, samples were unloaded to a consolidation stress of 3 MPa yielding an overconsolidation ratio (OCR) of 3.3. Figure 3-3 shows the experimental setup of the high temperature 1D consolidation test.



(a)



(b)

Figure 3-3 Experimental details for the high temperature oedometer test: (a) Schematic of setup; and (b) Insulated consolidation cell under a loading frame.

During the test, a heating tape was used to provide heating with thermocouples mounted on the steel beaker for temperature regulation (Figure 3-3a). A thermometer was used to monitor water temperature. To prevent heat loss, we applied insulating material around the beaker. Displacement and loading data were collected by a data acquisition system. During each test, we carried out two heating cycles. In the first cycle, a temperature up to 45 °C at a heating rate of 8 °C/h was applied and the sample was cooled to the room temperature overnight. In the second cycle, the samples were heated to 73 °C at a heating rate of 17 °C/h. A calibration test on a stainless-steel sample (with known thermal properties) was also conducted to determine the thermally induced deformation from the equipment. The present setup does not have a pore pressure monitoring facility; thus, the evaluation of thermally induced pore pressure and dehydration behaviors will be indirectly evaluated based on the deformation behaviors of samples with different clay fractions and different applied temperatures.

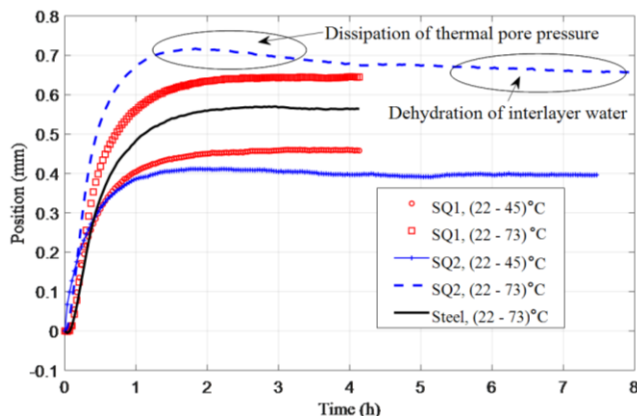


Figure 3-4 Monitored position changes of soil samples' top surface during heating tests.

Measured deformation behavior of samples SQ1 (clay fraction = 20%) and SQ2 (clay fraction = 45%) are displayed in Figure 3-4. It took around 3 h for soil samples to reach the expected temperature. In the heating cycle of $T = 45\text{ }^{\circ}\text{C}$, both samples continuously display expansion behavior, which shows that thermally induced excess pore pressure is easily dissipated at a heating rate of $8\text{ }^{\circ}\text{C/h}$ and no dehydration among the interlayer space of clay particles occurs at temperature of $45\text{ }^{\circ}\text{C}$. In the heating cycle of $73\text{ }^{\circ}\text{C}$, the sample SQ1 still shows a thermal expansion behavior. It is due to the reason that the low clay fraction sample SQ1 has a high permeability and a silt framework-supported structure. Under a water drained condition, thermally induced pore pressure is not easily accumulated in high permeability samples even if there is a high heating rate. For a low clay fraction sample, clay dehydration is not significant because clay-water composites are well protected by surrounding non-clayey minerals. By contrast, sample SQ2 shows significant thermal contraction behavior after 2 h heating (Figure 3-4). There are two mechanisms contributing to the contraction behavior in sample SQ2. In the initial stage from $t = 2\text{ h}$ to 4 h , the observed contraction behavior is mainly from the dissipation of thermal pore pressure since sample SQ2 has a low permeability and a high heating rate ($17\text{ }^{\circ}\text{C/h}$) is applied. In the stage from $t = 4\text{ h}$ to 8 h , there is a slower deformation rate compared with that in the initial stage. This contraction might be due to the dehydration of interlayer bound water. A pore pressure monitoring device should be added to the experimental setup to validate such statement. Figure 3-5 shows a complete heating-cooling cycle of sample SQ2, indicating that the induced deformation due to clay dehydration is reversible. The observation is consistent with the experimental results by Bish

(1988) [92] and Vidal and Dubacq (2009) [16]. The result also confirms that no thermal plastic deformation occurs to the sample with an OCR of 3.3.

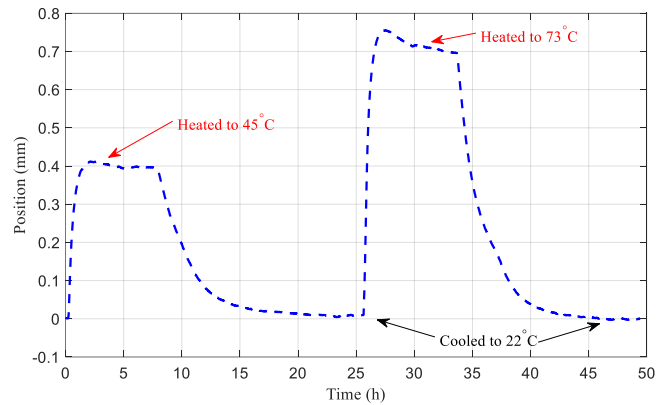


Figure 3-5 Monitored position evolution curve of the top surface of sample SQ2.

Thermally induced deformation from the facility can be estimated based on measured data in Figure 3-4 and the thermal expansion coefficient of stainless steel. A value of $1.5 \times 10^{-5}/^{\circ}\text{C}$ for stainless steel was used herein [93]. The axial thermal strains are calculated and displayed in Figure 3-6 after deformation calibrations. Both samples show nonlinear thermal expansion behavior. The sample SQ2 displays a larger thermal expansion than that from sample SQ1. The main reason is the expansion behavior of interlayer clay-bound water involved in the clay-water composites [12]. For investigating the capability of proposed model, the comparison between experimental data and results for the axial thermal strains of samples versus temperature variation are also included in Figure 3-6. The material parameters listed in Table 3-1 are applied to predict this soil behavior. The measured trend of contraction behavior at temperatures beyond 45°C is well captured.

Table 3-1 Parameters involved in proposed model.

| | | | SQ1 | SQ2 | Boom clay | Bangkok clay | Kaolin clay |
|------------------------|---------------|-----------------------------|---------|---------|--------------|-----------------|----------------|
| Mechanical | ν | (-) | 0.1 | 0.1 | 0.1 | 0.37 | 0.3 |
| | m | (-) | 0.9 | 0.89 | 0.9 | 0.8 | 0.85 |
| | Ψ | (-) | 0.05 | 0.05 | 0.2 | 0.17 | 0.104 |
| | o | (-) | 0.01 | 0.012 | 0.001 | 0.009 | 0.001 |
| | u | (-) | 25 | 25 | 25 | 30 | 40 |
| | σ_0 | (MPa) | 3 | 3 | 1-6 | 0.3 | 0.6 |
| Thermo- dehydration | α_{bf} | ($^{\circ}\text{C}^{-1}$) | 0.03 | 0.035 | 0.05 | 0.01 | 0.0357 |
| | β_b | ($^{\circ}\text{C}^{-1}$) | -0.0008 | -0.0008 | $-2*10^{-5}$ | $-2*10^{-5}$ | $-5*10^{-5}$ |
| | B_b | (Pa) | 0.003 | 0.004 | 0.003 | 0.0009 | 0.0001 |
| | K_b | (m^3/Kg) | 0.045 | 0.06 | 0.4 | 0.02 | 0.01 |
| | ξ | (-) | 0.7 | 0.7 | 0.7 | 0.3 | 0.28 |
| | δ | (-) | 4.5 | 4.2 | 5 | 3 | 3.3 |

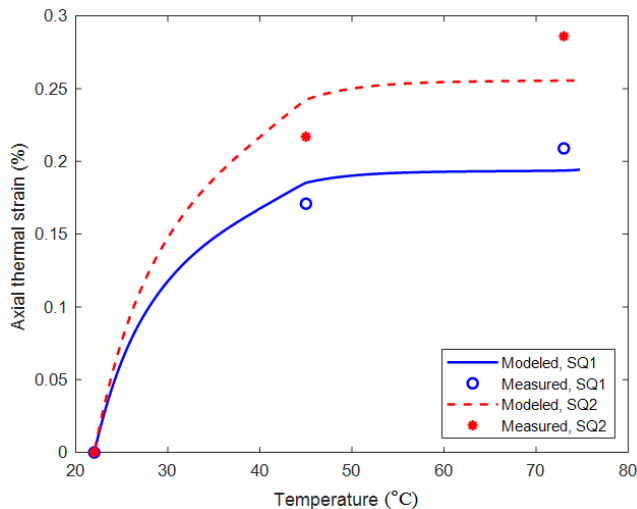


Figure 3-6 Measured and modeled thermal deformation behaviors of smectite-quartz mixtures.

3.5.1.2 Boom clay

Del Olmo et al. (1996) [35] presented the thermal strain measurements of drained heating-cooling tests on Boom clay samples with different OCRs. The volumetric thermal strain was estimated from the volume of expelled water during heating. Boom clay is abundant in the smectite group, and its plasticity index is about 50%. It has a porosity of 40%, and the water content is 24%–30%. The proposed model was applied to simulate this thermal strain behavior. The comparison between measured and modeled results is displayed in Figure 3-7. The thermal contraction behavior for Boom clay at low OCRs (= 1 and 2), and thermal expansion behavior at a high OCR (= 6) are well simulated with the proposed model.

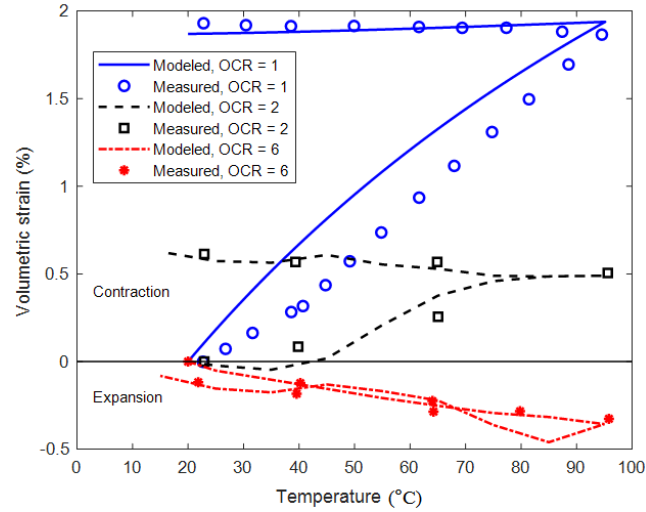
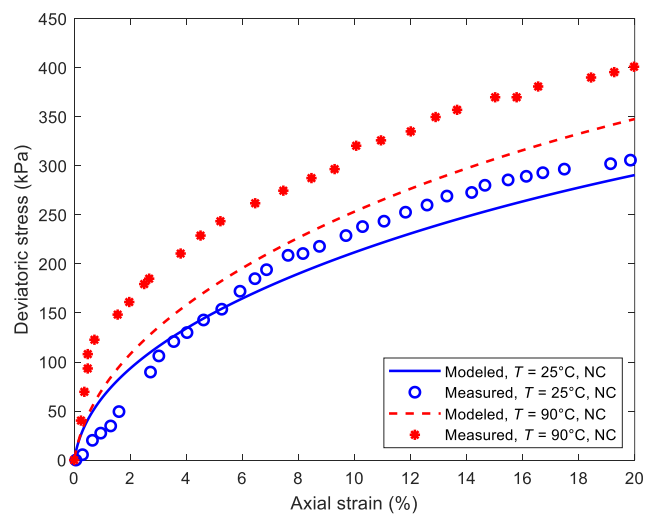


Figure 3-7 The modeled results and measured data for the thermal volumetric behavior of Boom Clay (adopted from Del Olmo et al., 1996 [35]).

3.5.2 Temperature-controlled triaxial compression behavior

3.5.2.1 Bangkok clay

Experimental results on Bangkok clay is also used to validate our proposed model. Abuel-Naga (2006) [94] conducted a series of drained triaxial loading tests on Bangkok clay at different temperatures. Figure 3-8 demonstrates the test results and the model predictions for drained triaxial tests under a confining pressure of 300 kPa at $T = 25\text{ }^{\circ}\text{C}$ and $90\text{ }^{\circ}\text{C}$.



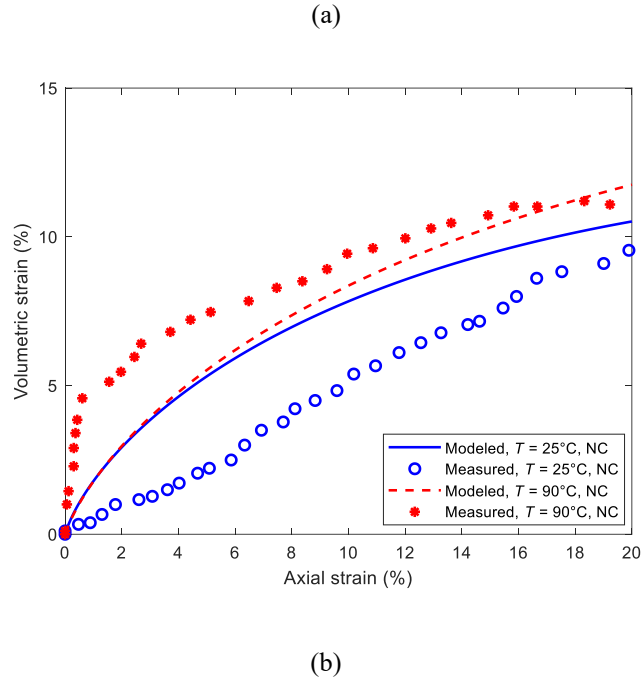
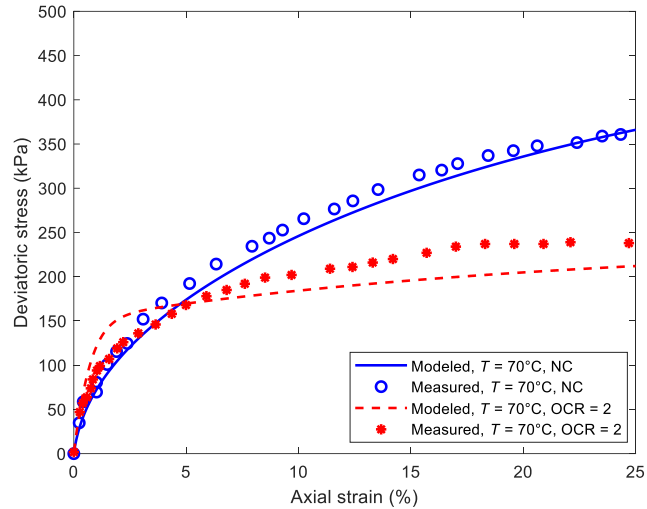
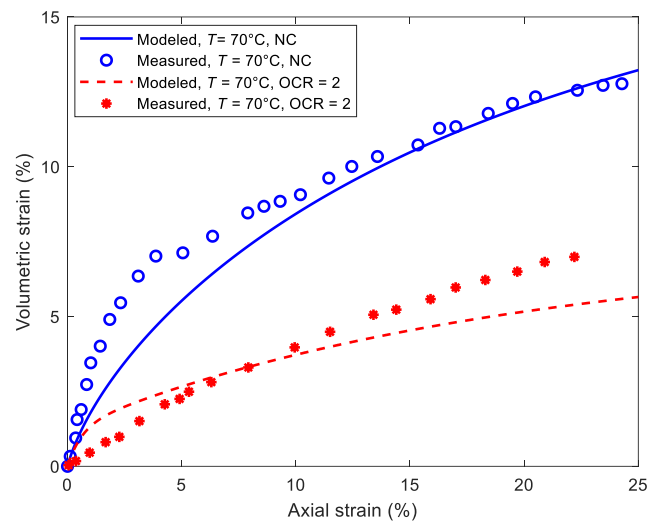


Figure 3-8 Modeled results and measured data of drained triaxial compression tests on normally consolidated (NC) Bangkok Clay at different temperatures: (a) Stress-strain curves; and (b) Axial strain-volumetric strain curves ($P'_0 = 300$ kPa, measured data is from Abuel-Naga, 2006 [94]).

Figure 3-9 exhibits the mechanical behaviors of Bangkok clay during drained triaxial tests under a confining pressure of 300 kPa, temperature of 70 °C, and different consolidation conditions. As shown in Figure 3-8, the model predictions display an appropriate increase of deviatoric stress and volumetric strain with temperature elevation under the NC condition. In Figure 3-8b, although the model prediction cannot completely match with the experimental data, it generally captures the trend of drained behaviors of soft Bangkok clay at different temperatures. In Figure 3-9a and Figure 3-9b, the effect of OCR on the decrease of deviatoric stress and volumetric strain are simulated, and an appropriate match with test data is achieved.



(a)



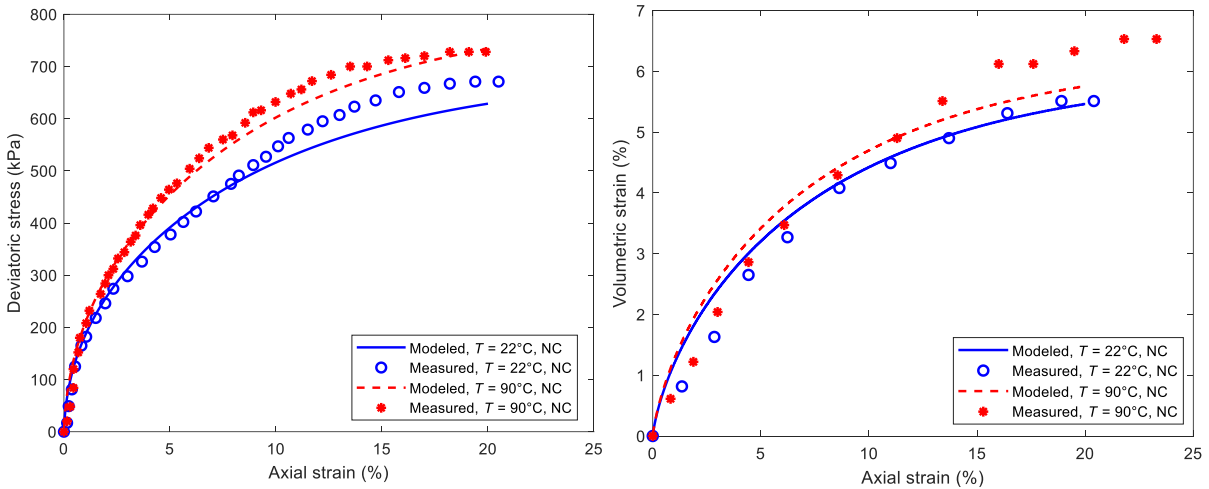
(b)

Figure 3-9 The modeled and measured results of drained triaxial compression tests on NC and OC Bangkok clay at $T = 70^\circ\text{C}$: (a) Stress-strain and (b) Axial strain - volumetric strain (measured data is from Abuel-Naga, 2006 [94]).

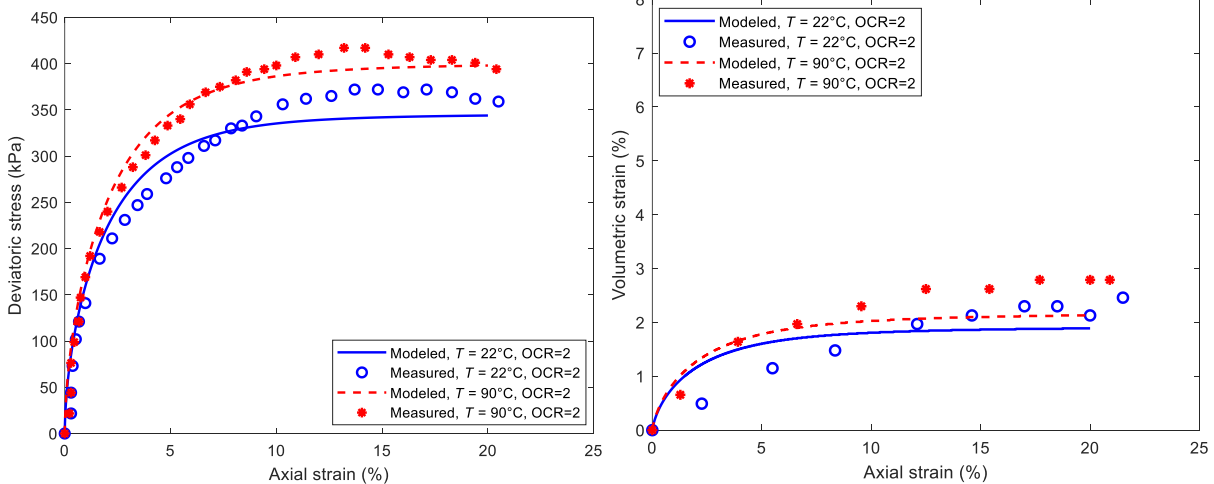
3.5.2.2 Kaolin clay

Cekerevac and Laloui (2004) [6] carried out a series of triaxial compression tests on Kaolin clay under different temperatures and OCRs. In their test, samples are isotropically consolidated to a

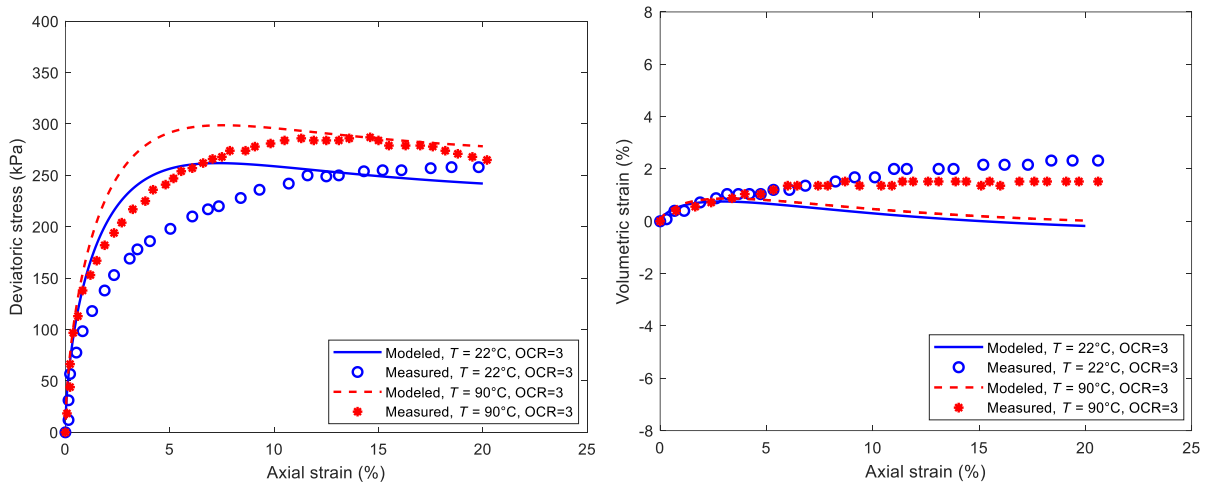
stress of 600 kPa at room temperature firstly, and subsequently unloaded to achieve stress states with different OCRs. Under a drained condition, the temperature of the sample is increased slowly to obtain 22 °C and 90 °C, respectively. Figure 3-10 displays the comparison of measured results and the model. It shows that the model predictions match with the test results. The decrease in the volumetric strain and failure of stress due to the OCR increase are simulated accurately. The thermal hardening phenomenon during temperature variations is another aspect that is appropriately predicted by the model.



(a)



(b)



(c)

Figure 3-10 Plots of modeled results and experimental data of drained triaxial compression tests on NC and OC Kaolin clay: (a) NC; (b) $OCR = 2$ and (c) $OCR = 3$ (measured data is from Cekerevac and Laloui, 2004 [6])

3.6 Discussion

3.6.1 On clay-bound water

Physically bound water due to capillary pressure is not involved in the present study. This study focuses on the chemically bound water, which is tightly bounded. As shown in Figure 3-2, clay-bound water is presented in the external and internal surfaces of clayey mineral platelets. The dehydration of both types of bound water is reversible, but the required pressure and temperature conditions are different. Under the water-saturated condition, the clay-bound water in smectite's interlayer space requires special temperature and pressure conditions to remove [15, 16]. The effects of smectite dehydration are considered in the geopressed development, pore-water freshening, and smectite-to-illite transformation [14, 15, 48]. There are three layers of bound water adhered to the interlayer space of the smectite internal surface, and one layer of bound water is approximately 1.5 Å in its thickness. The temperature required to deplete the bound water is dependent on the applied pressure condition and water activities. A summary of measured results of interlayer bound-water thickness and temperature from the literature value are presented by Li and Wong (2017) [12], in which a stepwise function is needed to quantify the nonlinear relationship. The result also shows that the first layer of interlayer bound water becomes free water at a temperature of about 60 °C. However, it should be noted that the flow rate through nano-pore space of smectite interlayers is much less than that in the micro-pore space. In addition, the bound water in the smectite interlayer has a lower viscosity than that of free water, which also contributes to a lower drainage rate [95]. Thus, the dehydration of interlayer water is mostly related to a long-term time-dependent study on a geological time scale. The quantity of interlayer bound water is usually estimated from the volume content of smectite [55, 96].

Contrastingly, the bound water on the external surface is abundant in all types of clayey minerals. A broken of the equilibrium between the van der Waals attractive forces and the electrostatic repulsive forces is considered responsible for this type of dehydration behavior. This type of bound water is mostly involved in generating the diffusion of double-layer in a clay-water system. Such dehydration should be considered in a quasi-static geomechanical analysis. The experimental data by Zymnis et al. (2018) [60] indicate that the dehydration can start at $T = 20$ °C. At temperatures from 20 °C to 38 °C, the thickness of this type of bound water has a linear relationship with temperature [60].

3.6.2 Dehydration-induced strain

Both dehydration and plastic yielding can induce contraction behavior in clayey soil or soft mudrock. Dehydration and plastic yielding induced contractions were usually merged in previously developed constitutive models. However, it should be noted that dehydration is reversible when there is no chemical reaction induced mineral changes [42, 92]. In order to quantify the contraction part from dehydration, the characteristics of irreversible contraction due to plastic yielding should be focused on. The effect of OCR on thermally induced plastic strains of some fine-grained geomaterials has been highlighted by previous studies (e.g. Del Olmo et al., 1996 [35]; Abuel-Naga et al., 2007 [32]). A summarized relationship between ε^{Tp} and OCR is presented in Figure 3-11. The results of ε^{Tp} are from samples with different clayey minerals and the measurements are under different temperature cycles. Thus, a normalized value $\varepsilon^{Tp} / \varepsilon_{OCR=1}^{Tp}$ is used in Figure 3-11. Adopting strains after heating-cooling cycles can obtain the irreversible plastic strains. Generally, the thermal plastic strain (contractive is treated positive) decreases nonlinearly with OCR and a critical value $OCR \approx 3.3$ is marked. At the NC condition ($OCR = 1$), the samples have the maximum irreversible contraction in the magnitude upon heating. For OC condition, very small irreversible contraction or even dilation can be generated. Upon heating, the anisotropic expansion of clay aggregates will generate local shear stress [12], which brings thermal plastic strains when induced shear stresses touch the yield limit. It is conclusive that thermal tests will not generate significant plastic strains in clays soils at an OCR of 3.3.

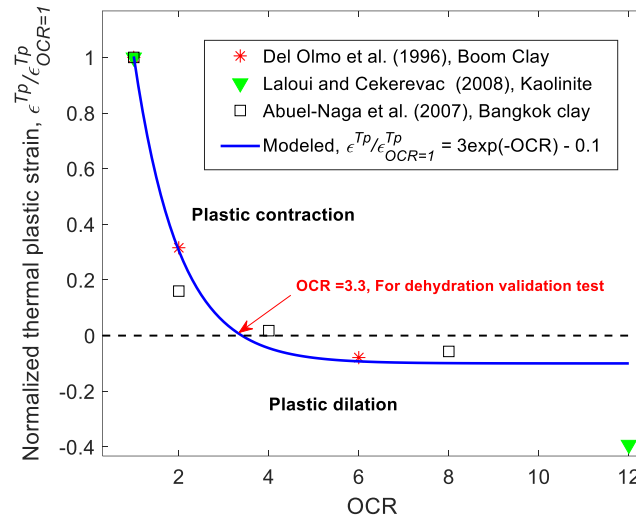


Figure 3-11 Measured relationship between thermal plastic strain and OCR of geomaterials with different geological origins (modified after Li and Wong, 2017 [12]).

Thus, our previous thermal consolidation tests were conducted at an OCR of around 3.3, which can highlight the contractive deformation due to dehydration. Under such condition, plastic strain is negligible. Thus, we were able to notice the reversible deformation behaviours as shown in Figure 3-5.

It should be mentioned that this amount of dehydration-induced strain is only attributed to the removal of bound water adhered to clayey minerals' external surface. A removal of interlayer water results in a major volumetric change; thus, it is necessary to consider the dehydration of interlayer water for a long-term creep analysis. In addition, the relationship drawn in Figure 3-11 is based on tests of fine-grained geomaterials at temperatures below 90 °C. The critical OCR can be different when a higher temperature condition is applied. A different critical OCR value can also be obtained for the geomaterial with a certain degree of cementation that is sensitive to the temperature disturbance.

3.7 Conclusions

We proposed a new thermo-elasto-plastic constitutive model to describe the coupled thermo-mechanical behavior of water-saturated clayey soils under the drained stress-path condition. The main conclusions are as follows:

- (1) Subloading surface plasticity and thermodynamics laws can be employed to describe the nonlinear thermo-mechanical behavior, where the selected mechanical framework considers the elasto-plastic domain inside yield surface. The proposed model well characterizes the smooth elastic-plastic transition behavior of clayey soils.
- (2) The possibility of treating plastic strain and dehydration-induced strain behavior separately is demonstrated, while maintaining the basic thermodynamic laws. The capability of the model is verified using several clayey soils with different geological origins and stress histories. The present model only considers the dehydration of bound water adhered to the external surface of clayey minerals. However, treating the dehydration strain separately provides the opportunity to make such strain component flexible to different environmental conditions.
- (3) The new model has the advantage in phenomenon-based plasticity for the convenience of obtaining model parameters as well as the advantage in mechanism-based thermodynamics for interpretation of different stages of dehydration process. However, the present model is not suitable for characterizing a time-dependent behavior. An investigation of dehydration due to the removal of interlayer bound water on the overall time-dependent response of soil behavior is recommended for a future study.

3.8 List of symbols

| | |
|-------|---|
| B_b | Parameter for clay bound water and soil modulus |
| e | Internal energy |

| | |
|--------------------|--|
| E_{ijkl} | Fourth-order stiffness tensor |
| F | Conjugate force of the internal state variable for accumulative plastic strain |
| F_0 | Initial value of F |
| f | Normal yield surface |
| H | Internal state variable for accumulative plastic strain |
| k_b | Another parameter for clay bound water and soil modulus |
| $\bar{\mathbf{N}}$ | Unit normal vector |
| n_b | Volume fraction of bound water phase. |
| O | Slopes of swelling lines in $\ln v - \ln p$ plane |
| P^{Deh} | Conjugate force for the dehydration strain |
| q_i | Heat flux vector |
| R | Similarity ratio |
| S | Soil entropy |
| s^b | Specific entropy of bound water |
| T | Temperature |
| U | Monotonically decreasing function of R |
| u | Material parameter |
| v | Total volume of the soil |

| | |
|----------------------------|--|
| v_b | Volume of bound water |
| ψ | Helmholtz free energy |
| ψ^{Te} | Thermo-elastic part of Helmholtz free energy |
| ψ^{Tp} | Thermo-plastic part of Helmholtz free energy |
| ψ^{Deh} | Dehydration part of Helmholtz free energy |
| $\dot{\epsilon}_{ij}$ | Total strain rate |
| $\dot{\epsilon}_{ij}^{Te}$ | Thermo-elastic strain rate |
| $\dot{\epsilon}_{ij}^{Tp}$ | Thermo-plastic strain rate |
| ϵ^{Deh} | Dehydration strain |
| ρ | Total density |
| ρ_b | Density of bound water. |
| ρ_s | Density of solid minerals |
| ρ_f | Density of free water |
| ψ | Slope of the normal consolidation line |
| δ | Temperature coupling term |
| Ω | Objective function |
| Π | Rate of energy dissipation |
| $\dot{\lambda}$ | Lagrange plastic multiplier |

| | |
|---------------|---|
| α_{bf} | Coefficient for bound water conversion |
| β | Power exponent |
| β_b | Thermal expansion coefficient of bound water. |
| ξ | Material constant |
| ν | Poisson's ratio |

Preface to Chapter 4.

Implementing a constitutive framework into FEM to characterize the Thermo-Hydro-Mechanical responses of geological materials through coupled simulations remains an essential step in numerical analysis. Proposing appropriate mass, momentum, and energy balance equations, rewriting the equations in weak form, applying discretization methods to the weak form, addressing the challenges of appropriate THM coupling coding, and employing proper stability methods are among the most outstanding challenges when implementing a poro-elastoplastic framework into FEM. Within this chapter, we have integrated our devised numerical model into the FEM to replicate the soil's response when subjected to thermal loading. The validation of the model was carried out by comparing the simulated outcomes against existing empirical data from high-temperature triaxial and high-temperature odometer tests.

Chapter 4

4 Finite element modeling of thermal-hydro-mechanical coupled processes in clay soils considering bound water dehydration.²

4.1 Abstract

This paper presents a new finite element method (FEM) model to simulate the thermo-hydro-mechanical (THM) responses of water saturated clay soils. The model can account for the effects of temperature variation on bound water dehydration and the corresponding thermo-poromechanical strains. The governing equations, including mass balance, momentum balance, and energy balance, are derived based on the principles of continuum mechanics for porous media. The impact of bound water dehydration on THM behavior is incorporated into the coupled THM equations. The model is equipped with an unconventional plasticity for more accurate description of elasto-plastic behavior. To solve the non-linear system of equations, a modified Newton-Raphson method is employed. The model is validated using laboratory tests on various clay soils with different geological origins and reasonable agreement is achieved. The thermally induced contraction behavior of clay soils at a low overconsolidation ratio and thermally induced expansion behavior at a high overconsolidation ratio are well simulated. During heating, the effect of bound water dehydration on the generation of excess pore pressure in clay soils is highlighted in our numerical results.

Keywords: thermo-hydro-mechanical coupling, bound-water dehydration, clay soils, finite element method, unconventional plasticity.

² A version of this manuscript has been submitted to the journal of *Acta Geotechnica* (2023).

4.2 Introduction

Temperature variation has a significant impact on the poromechanical behavior of geomaterials. An understanding of complex thermo-hydromechanical (THM) processes is crucial in non-isothermal geotechnical projects like geothermal energy extraction and storage for carbon neutrality [44, 49]. However, accurately describing the thermal, hydraulic, and mechanical interactions in clay soils is still a topic of debate in the geotechnical engineering community [50–52]. Poromechanical behaviors of clay soils are highly dependent on the saturation state. Even for a water-saturated clay soil, the interaction of clay minerals with water makes the temperature dependency complicated. A multi-disciplinary approach is required to fully understand and accurately model the THM behavior. Extensive previous experimental data indicates that heating tends to result in irrecoverable contraction deformation in clay soils under a drained stress path, in particular for unconsolidated geomaterials [5–7]. A series of theoretical studies were conducted to investigate the thermally induced plastic behavior in clay soils [37]. These models mainly describe the thermo-mechanical behaviors using temperature-dependent yield surfaces [6, 21, 32, 38, 53], and a complete review of these types of advanced thermo-mechanical models for saturated clays is presented in [37, 40]. Nevertheless, little attention was given to consider the impact from clay bound water dehydration, which should be treated as a separate deformation mechanism [12, 13]. The temperature elevation in a water-saturated clay rich geomaterial may transfer the clay bound water to free water and bring dehydration induced pore changes and deformation [14, 16, 47]. Clay bound water dehydration was mostly studied by geologists working on abnormal pore water pressure generation in basin modeling [14, 47, 48, 55] and pore water geochemistry freshening in smectite rich geological formations [56]. Hueckel was one of the pioneers in the domain of geotechnical engineering who investigated thermally driven dehydration in clay soils and related elastic and reactive plastic deformations [41, 42, 57]. It should be noted that there are different types of clay bound water sticking to the external surface of clay particles or to the interlayer nanoscale pore space [58]. The dehydration processes of different type of clay bound water are dependent on the temperature and pressure conditions, however, most previous studies did not treat different types of clay bound water separately. Recent progresses in geotechnical community mainly focus on the dehydration of bound water adhered to the external surface of clay particles [44, 59, 60, 81], which occurs in a relative lower temperature range (20 °C to 90°C) and is more relevant to shallow geothermal energy engineering projects. Their derivations are mainly based on

the energy concept and require a complicated procedure to obtain related parameters for numerical modeling. A versatile, straightforward, and inclusive model is still needed for engineering practice. In the modeling of thermal-hydro-mechanical coupled processes in clay soils with the consideration of bound water dehydration, the convection term in the energy balance, which was usually neglected, turns to be important. The unsteady advection-diffusion equation will require stabilization during numerical implementation.

In this study a coupled thermo-hydro-mechanical (THM) finite element framework for describing clay soil behavior considering bound water dehydration is developed. The proposed model is capable to consider the bound water dehydration and its corresponding strain under temperature variation. The model is equipped with an unconventional plasticity for more accurate description of elasto-plastic behavior. Non-isothermal triaxial test results on Boom clay with different overconsolidation ratios (OCRs) and high-temperature oedometer test results on compacted smectite-quartz mixtures are used to validate the developed finite element package. Role of pore water pressure development due to thermally induced dehydration was investigated.

4.3 Bound water dehydration

Clay-bound water is a prominent feature of clay-water composites, which is aligned in different scales of pore space of clay soils (Figure 4-1). Bound water can be found adhered to the external surface of clay particles or in the interlayer pore space [97, 98]. Dehydration in clay soils can cause a volume loss of geomaterials and the associated thermal strains. The process of dehydrating both types of bound water is reversible and accompanied with different pressure and temperature requirements [12, 16]. The interlayer water is associated with the smectite group containing 2:1 platelet. Li and Wong [12] presented a summary of measured interlayer bound-water thickness and temperature relations, which indicates a minimum temperature of 55 °C for the occurrence. Additionally, the release of interlayer bound water is predominantly associated with a long-term duration and usually accompanied with diagenetic transformation (e.g., smectite-illite transformation) [99].

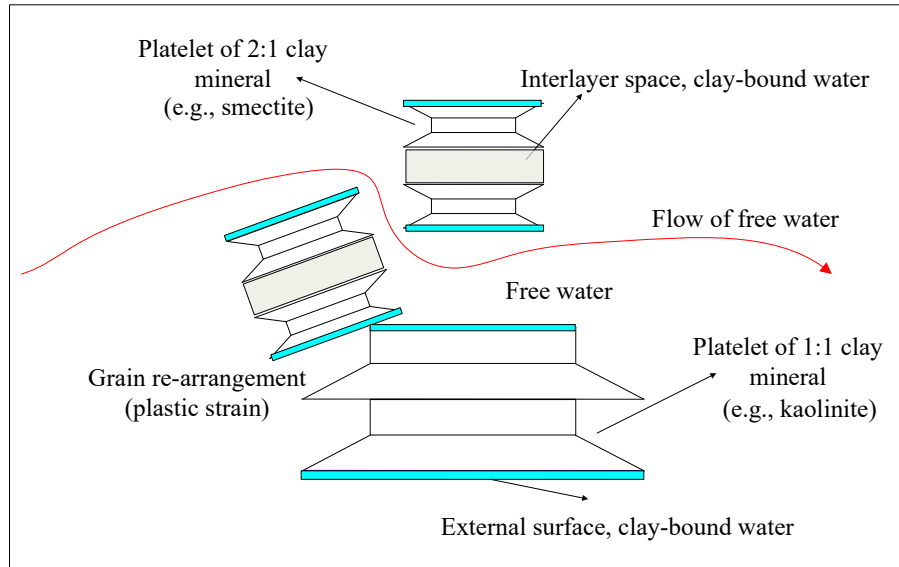


Figure 4-1 Sketch showing free water and bound water in clay-water composites.

In contrast to the interlayer bound water, the bound water adhered to the external surface of clay particles is abundantly present in all types of clayey minerals. This dehydration mechanism occurs due to a disruption in the balance between attractive van der Waals forces and repulsive electrostatic forces. Such dehydration plays a crucial role in generating the diffusion of double-layer in a clay-water system and is highly involved in most non-isothermal geotechnical engineering projects. Experimental findings by Zymnis et al. [60] suggest that this type of external surface bound water starts dehydrating at a temperature below 22°C. Yao et al. [100] applied the nuclear magnetic resonance (NMR) technique to investigate the influence of temperature and pore water concentration on the pore water status in clay soils with temperatures ranging from 0°C to 50°C. They concluded that the bound water (termed adsorptive water) content decreases with an increase in temperature and the decreasing trends for soils with different pore water concentrations are distinct.

Zhang and Cheng [81] have explained that the bound water content of clay soil w_b has an exponential relation with temperature and α_{bf} ($w_b \propto \exp(-\alpha_{bf}T)$). They proposed a simplified function for describing the variation of bound water content with temperature based on the mass balance equation:

$$w_b = w_{b,ini} \exp[-\alpha_{bf}(T - T_{ini})], \quad T[^\circ C] \quad (4.1)$$

where $w_{b,ini}$ is the bound water content at the initial temperature, α_{bf} is a constant that controls the conversion of bound to free water per each unit rise in temperature, T and T_{ini} are the current temperature and initial temperature in Celsius degree respectively. Even though there is only a small amount of bound water adhered to the external surface of clay particles, a thermally driven dehydration can potentially contribute to the mass increase of free water. Thus, an increase in excess pore pressure is expected if the extra amount of free water is not dissipated in time. In addition, dehydration may trigger some sliding among particles and result in grain re-arrangement (plastic strain). The deformations due to the volume loss of bound water and the grain re-arrangement induced plastic strain should be quantified separately.

4.4 Governing equations

In this section, the fundamental partial differential equations that govern the proposed THM (Thermo-Hydro-Mechanical) coupled model for clay soils are presented. Water-saturated soils are made up of solid particles, water films that are bound to solid particles, and fluid that can move through the pore space. To distinguish between these three phases, subscripts "s", "b", and "f" are employed to represent the solid, bound water, and fluid phases, respectively.

4.4.1 THM coupled equations.

The saturated soil system is governed by three primary equations: the linear momentum balance equation, the mass balance equation, and the energy balance equation. In addition, the bound water content variation is taken into consideration, which is related to the degree of water saturation as a function of temperature. The stress-strain behavior of the solid skeleton is also described by a constitutive law, thereby supplementing the governing equations. The mass balance equation for the soil particles, free water, and bound water can be expressed as:

$$\frac{\partial(n_s \rho_s)}{\partial t} + \nabla \cdot (n_s \rho_s v_s) = 0 \quad (4.2)$$

$$\frac{\partial(n_f \rho_f)}{\partial t} + \nabla \cdot (n_f \rho_f v_f) - \rho_b n_b \alpha_{bf} \frac{\partial T}{\partial t} = 0 \quad (4.3)$$

$$\frac{\partial(n_b \rho_b)}{\partial t} + \nabla \cdot (n_b \rho_b v_s) + \rho_b n_b \alpha_{bf} \frac{\partial T}{\partial t} = 0 \quad (4.4)$$

where n_s, n_f and n_b are the volume fractions of the soil, free water and bound water phases respectively; v_s and v_f are soil particles and free water velocity respectively; ρ_s, ρ_f and ρ_b are densities of soil particles, free water and bound water respectively; T is the temperature.

The volume fraction of phases can be written according to the soil porosity n , degree of saturation of free water s_f and bound water s_b :

$$n_f + n_b = n, \quad s_f + s_b = 1 \quad (4.5)$$

$$n_s + n_f + n_b = 1, \quad n_s = 1 - n, \quad n_f = S_f n, \quad n_b = S_b n \quad (4.6)$$

It should be noted that the bound water occupies some pore space but it does not contribute to the fluid flows. Previous studies have indicated the use of a corrected porosity (effective porosity) in quantifying the permeability of clay related geomaterials with the information of total porosity and clay contents [55, 96]. Accordingly, based on Darcy's law, the momentum conservation equation of the fluid phase can be expressed in terms of fluid and solid velocity:

$$\mathbf{q} = n_f (v_f - v_s) = \frac{-\mathbf{k}}{\mu_f} \cdot (\nabla p^f - \rho_f g) \quad (4.7)$$

where \mathbf{q} is the volumetric flow rate per units of surface area; p^f is the pore water pressure, \mathbf{k} is the intrinsic permeability, μ_f is the dynamic viscosity of water and g is the gravity.

Substituting Eqs. (4.7) and (4.6) into Eq. (4.3) yields:

$$\frac{\partial(s_f n \rho_f)}{\partial t} + \nabla \cdot (\rho_f \mathbf{q}) + \nabla \cdot (\rho_f s_f n v_s) - \rho_b n_b \alpha_{bf} \frac{\partial T}{\partial t} = 0 \quad (4.8)$$

Accordingly, the summation of Eqs. (4.8) and (4.4) provides the mass balance for the fluid and bound water phases as:

$$\frac{\partial(s_f n \rho_f)}{\partial t} + \nabla \cdot (\rho_f \mathbf{q}) + \nabla \cdot (\rho_f s_f n v_s) + \frac{\partial(s_b n \rho_b)}{\partial t} + \nabla \cdot (s_b n \rho_b v_s) = 0 \quad (4.9)$$

By applying the Lagrangian derivation with respect to a moving solid $[\frac{D_s(\bullet)}{Dt} \equiv \frac{\partial(\bullet)}{\partial t} + \nabla(\bullet) \cdot v_s]$, a moving fluid $[\frac{D_f(\bullet)}{Dt} \equiv \frac{\partial(\bullet)}{\partial t} + \nabla(\bullet) \cdot v_f]$, and the moving bound water, $[\frac{D_b(\bullet)}{Dt} \equiv \frac{\partial(\bullet)}{\partial t} + \nabla(\bullet) \cdot v_s]$, respectively, the Eqs.(4.2) and (4.9) can be rewritten as:

$$(1-n) \frac{D_s \rho_s}{D_t} - \rho_s \frac{D_s n}{D_t} + \rho_s (1-n) \nabla \cdot v_s = 0 \quad (4.10)$$

$$s_f n \frac{D_f \rho_f}{D_t} + \rho_f s_f \frac{D_s n}{D_t} + n \rho_f \frac{D_s s_f}{D_t} + \rho_f \nabla \cdot \mathbf{q} + \rho_f s_f n \nabla \cdot v_s + s_b n \frac{D_b \rho_b}{D_t} + \rho_b s_b \frac{D_s n}{D_t} + n \rho_b \frac{D_s s_b}{D_t} + \rho_b s_b n \nabla \cdot v_s = 0 \quad (4.11)$$

By using Eq.(4.10) and assuming the incompressibility of solid grains, the evolution of the porosity with respect to the solid deformation velocity can be described as [101]:

$$(1-n) \frac{D_s \rho_s}{D_t} = -(1-n) \rho_s \beta_s \frac{D_s T}{D_t} \Rightarrow \frac{D_s n}{D_t} = (1-n) \nabla \cdot v_s - (1-n) \beta_s \frac{D_s T}{D_t} \quad (4.12)$$

Similarly, by assuming the incompressibility of the free water and bound water, the variation of their densities over variation of time can be driven as:

$$n \frac{D_f \rho_f}{D_t} = -n \beta_f \rho_f \frac{D_f T}{D_t} \quad (4.13)$$

$$n \frac{D_b \rho_b}{D_t} = -n \beta_b \rho_b \frac{D_b T}{D_t} \quad (4.14)$$

where β_s , β_f and β_b are the thermal expansion coefficient of the soil particles, free water and bound water phases respectively.

Substituting Eqs.(4.12), (4.13) and (4.14) into Eq.(4.11) the following governing equation is obtained as:

$$n(1 - \frac{\rho_b}{\rho_f}) \frac{\partial S_f}{\partial t} + (S_f + \frac{\rho_b S_b}{\rho_f}) \nabla \cdot \mathbf{v}_s - ((S_f + \frac{\rho_b S_b}{\rho_f}) \beta_s (1-n) + \beta_f S_f n + \frac{\rho_b S_b \beta_b n}{\rho_f}) \frac{\partial T}{\partial t} + \nabla \cdot \mathbf{q} = 0 \quad (4.15)$$

Total strain can be decomposed into components of elastic strain, plastic strain, and thermal elastic strain:

$$\dot{\boldsymbol{\epsilon}} = \dot{\boldsymbol{\epsilon}}^e + \dot{\boldsymbol{\epsilon}}^p + \dot{\boldsymbol{\epsilon}}^T \quad (4.16)$$

It should be noted that thermally induced plastic strain can be treated as a part of plastic strain when the temperature aspect is explicitly considered [102].

The thermal elastic strain can be expressed in terms of deformation induced by temperature variation as:

$$\dot{\boldsymbol{\epsilon}}^T = \frac{1}{3} \beta_T \frac{\partial T}{\partial t} \mathbf{I} \quad (4.17)$$

where β_T is the equivalent thermal expansion coefficient of a porous media given by:

$$\beta_T = (1-n)\beta_s + nS_f\beta_f + nS_b\beta_b \quad (4.18)$$

In this study we used the Terzaghi's effective stress principle,

$$\boldsymbol{\sigma} = \boldsymbol{\sigma}' - p^f \mathbf{I} \quad (4.19)$$

where \mathbf{I} is an identity matrix, $\boldsymbol{\sigma}$ and $\boldsymbol{\sigma}'$ are the total Cauchy stress and the effective stress tensors respectively. The linear momentum balance equations of the whole system in the quasi-static condition can be expressed as:

$$\nabla \cdot (\boldsymbol{\sigma}' - p^f \mathbf{I}) + \rho_{\text{eff}} \mathbf{g} = \mathbf{0} \quad (4.20)$$

where ρ_{eff} is the bulk density of the solid-bound water-fluid mixture,

$$\rho_{\text{eff}} = (1-n)\rho_s + nS_f\rho_f + nS_b\rho_b \quad (4.21)$$

The energy balance equation for three phases can be presented as [101]:

$$(\rho c)_{\text{eff}} \frac{\partial T}{\partial t} + \nabla \cdot (\rho_f c_f \mathbf{q} \cdot T - \lambda_{\text{eff}} \nabla T) = 0 \quad (4.22)$$

The effective heat capacity and effective thermal conductivity for multiphase porous can be described as:

$$(\rho c)_{\text{eff}} = (1-n)\rho_s c_s + n s_f \rho_f c_f + n s_b \rho_b c_b \quad (4.23)$$

$$\lambda_{\text{eff}} = \lambda_s^{1-n} \cdot \lambda_f^{n s_f} \cdot \lambda_b^{n s_b} \quad (4.24)$$

where c_s, c_f, c_b and $\lambda_s, \lambda_f, \lambda_b$ are the specific heat capacities and the thermal conductivities for solid, fluid and bound water phases, respectively.

According to the fundamentals of soil mechanics the following equation can be written for the degree of saturation of bound water [103]:

$$s_b = \frac{(1-n)\rho_s w_b}{n\rho_b} \quad (4.25)$$

where w_b is the bound water content by weight calculated by m_b/m_s .

By substituting Eq (4.1) into Eq (4.25) the degree of saturation of bound water s_b can be rewrite as:

$$s_b = \frac{(1-n)\rho_s w_{b,\text{Ini}} \exp[-\alpha_{\text{bf}}(T - T_{\text{Ini}})]}{n\rho_b} \quad (4.26)$$

Accordingly, by using the chain derivation, the variation of s_b over the variation of time can be derived as:

$$\frac{\partial s_b}{\partial t} = \frac{\partial s_b}{\partial T} \frac{\partial T}{\partial t} \quad (4.27)$$

By derivating the Eq. (4.26) and applying the chain derivation, the following can be achieved:

$$\frac{\partial S_b}{\partial t} = \frac{-\alpha_{bf}(1-n)\rho_s w_{b,ini} \exp[-\alpha_{bf}(T-T_{ini})]}{n\rho_b} \frac{\partial T}{\partial t} \quad (4.28)$$

Using Eq. (4), the variation of degree of fluid saturation over time can be expressed by:

$$\frac{\partial S_f}{\partial t} = \frac{\alpha_{bf}(1-n)\rho_s w_{b,ini} \exp[-\alpha_{bf}(T-T_{ini})]}{n\rho_b} \frac{\partial T}{\partial t} \quad (4.29)$$

4.5 Thermo-Plasticity

We use the subloading surface plasticity framework [88] to quantify the thermo-plastic behavior herein. This framework introduces two surfaces, a normal yield surface and a subloading surface (Figure 4-2), to describe the mechanical behavior of geomaterials.

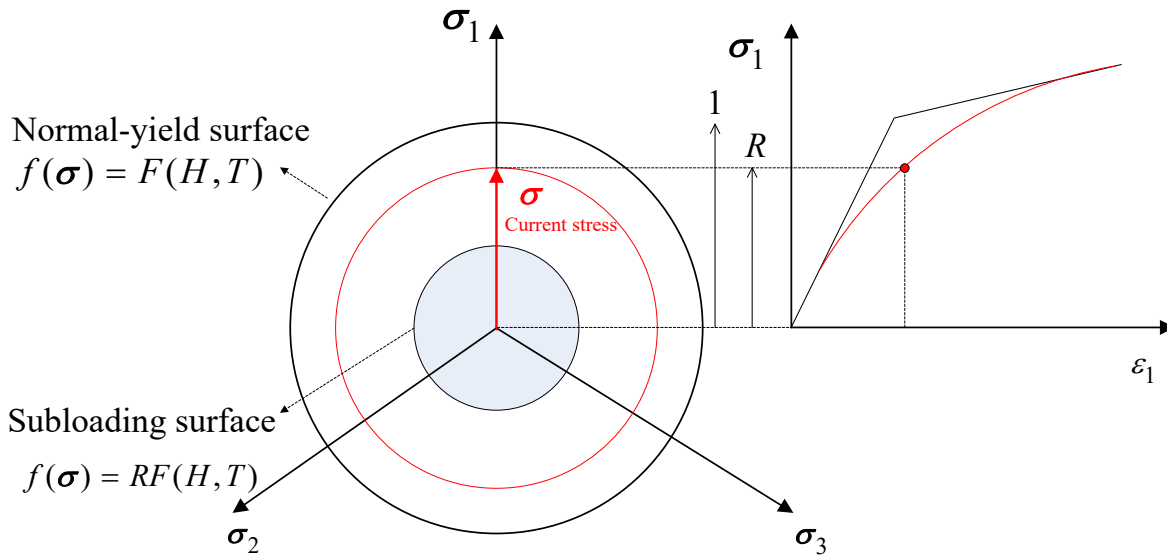


Figure 4-2 Sketch showing normal yield and subloading yield surfaces in a temperature hardening situation, modified after [104].

The normal yield surface is the conventional yield surface, and the subloading surface is movable, which always passes through the current stress point and maintains a similar shape to the normal yield surface. By using two yield surfaces to describe mechanical behavior of clay soils, the interior of the yield surface is not purely elastic, thus provides a more accurate and consistent description of the elastoplastic behavior when compared to the result from a conventional plastic constitutive

model [59, 88–90]. To consider the thermal impact, the normal yield surface function can be written as a function of similarity ratio R , hardening parameter H , and temperature T :

$$f(\boldsymbol{\sigma}) = RF(H, T) \quad (4.30)$$

The similarity ratio R is known as the length of an arbitrary line connecting two points on normal yield surface and subloading surface. Based on the magnitude of R , three conditions will be considered as the following:

$$\left\{ \begin{array}{ll} R = 0 & \text{null stress state} \\ 0 < R < 1 & \text{sub-yield state} \\ R = 1 & \text{normal yield state} \end{array} \right. \quad (4.31)$$

A fully differentiation of Eq. (4.30) gives:

$$\left[\frac{\partial f(\boldsymbol{\sigma})}{\partial \sigma_{ij}} \right]^T d\sigma_{ij} = F.dR + R \left(\frac{\partial F}{\partial H} \dot{H} \right) \quad (4.32)$$

By considering the hardening parameter as a function of the plastic strain rate, the variation of the similarity ratio can be given as [88]:

$$dR = U \left\| \dot{\boldsymbol{\varepsilon}}_y^p \right\| \quad (\dot{\boldsymbol{\varepsilon}}_y^p \neq 0) \quad (4.33)$$

where U has the following indication:

$$\left. \begin{array}{ll} U \rightarrow +\infty & (R = 0) \\ U = 0 & (R = 1) \\ U < 0 & (R > 1) \end{array} \right\} \quad (4.34)$$

The conditions stated in Eq. (4.34) can be taken as requirements that guarantee the subloading surface moves towards the normal yield surface as the loading process occurs. It can be expressed as:

$$U = -u \ln R \quad (4.35)$$

where u is a material parameter.

Applying the modified Cam-Clay model as the normal yield surface [88], the hardening function can be determined using the temperature-dependent isotropic hardening relation proposed by Laloui and Cekerevac [5]:

$$F = F_0 \exp\left(\frac{H}{\lambda - \kappa}\right) \left[1 - \gamma_T \ln\left(1 + \frac{\Delta T}{T_0 - 273}\right) \right] \quad (4.36)$$

where F_0 is the preconsolidation pressure at an initial temperature T_0 , H is the hardening parameter taken as the volumetric plastic strain ε_v^p herein; λ and κ are the slopes of the normal consolidation line and unloading-reloading line, respectively; γ_T is the thermal softening coefficient. When a soil is subjected to a very high OCR, the chance of generating thermal-plastic yielding behavior is still very limited even though the subloading surface plasticity concept has been applied. The use of the similarity ratio R will make the generated plastic strain a negligible amount when the soil is under a very high OCR.

The variation of hardening function over variation of hardening parameter can be derived as:

$$\frac{\partial F}{\partial H} = \frac{F}{\lambda - \kappa} \quad (4.37)$$

Substituting Eqs. (4.33) and (4.37) into Eq. (4.32) yields:

$$\left[\frac{\partial f(\boldsymbol{\sigma})}{\partial \sigma_{ij}} \right]^T d\sigma_{ij} = U \|\dot{\varepsilon}_{ij}^p\| F + R \left(\frac{F}{\lambda - \kappa} \dot{H} \right) \quad (4.38)$$

According to the associated flow rule, the plastic strain is given by.

$$\dot{\varepsilon}_{ij}^p = \bar{\lambda} \bar{N} \quad (4.39)$$

where $\bar{\lambda}$ is the positive proportionality factor, and the \bar{N} is the normalized outward normal of the subloading surface which can be written as:

$$\bar{\mathbf{N}} = \frac{\partial f(\boldsymbol{\sigma})}{\partial \sigma_{ij}} \bigg/ \left\| \frac{\partial f(\boldsymbol{\sigma})}{\partial \sigma_{ij}} \right\| \quad (4.40)$$

Substitution of Eq. (4.39) into Eq. (4.38) leads to:

$$\bar{\lambda} = \frac{\bar{\mathbf{N}}^T d\boldsymbol{\sigma}}{\mathbf{M}^P} \quad (4.41)$$

where \mathbf{M}^P is expressed as:

$$\mathbf{M}^P = \left(\frac{U}{R} + \frac{\bar{h}}{\lambda - \kappa} \right) \text{tr}(\bar{\mathbf{N}}\boldsymbol{\sigma}) \quad (4.42)$$

$$\bar{h} = \frac{\dot{H}}{\bar{\lambda}} \quad (4.43)$$

According to Hashiguchi et al. [88] the loading criterion can be based on:

$$\left. \begin{array}{l} \text{tr}(\bar{\mathbf{N}}\mathbf{E}\dot{\boldsymbol{\varepsilon}}) > 0 \rightarrow \dot{\boldsymbol{\varepsilon}}^P \neq 0 \\ \text{tr}(\bar{\mathbf{N}}\mathbf{E}\dot{\boldsymbol{\varepsilon}}) \leq 0 \rightarrow \dot{\boldsymbol{\varepsilon}}^P = 0 \end{array} \right\} \quad (4.44)$$

where \mathbf{E} represents the tensor matrix of elasticity.

4.6 Finite-element solution

The finite-element discretization approach utilized in this research is created by employing the governing partial differential equation system in an integral context. To reach this objective, it is crucial to establish their weak forms. This can be achieved with the weighted residual method and the Galerkin technique [50, 105].

4.6.1 Initial and boundary conditions

With regards to the problem at hand, where the primary variables or unknowns are the displacements of the soil skeleton (\mathbf{u}), pore water pressure (p^f), and temperature (T), the initial conditions can be specified in the following manner:

$$\mathbf{u} = \mathbf{u}_0 \quad p^f = p_0^f \quad T = T_0 \quad \text{at } t = 0 \text{ in } \Omega \text{ and on } \Gamma \quad (4.45)$$

where Ω is the close domain of volume with the boundary Γ . Accordingly, the boundary conditions could be presented as the following.

Dirichlet boundary condition:

$$\begin{aligned} \mathbf{u} &= \mathbf{u} && \text{on } \Gamma_D^u \\ p^f &= \bar{p}^f && \text{on } \Gamma_D^p \\ T &= \bar{T} && \text{on } \Gamma_D^T \end{aligned} \quad (4.46)$$

Neumann boundary condition:

$$\begin{aligned} \boldsymbol{\sigma} \cdot \mathbf{n} &= \bar{\mathbf{t}} && \text{on } \Gamma_N^u \\ \mathbf{q} \cdot \mathbf{n} &= \bar{q}^f && \text{on } \Gamma_N^p \\ \mathbf{q}^T \cdot \mathbf{n} &= \bar{q}^T + \lambda_e (T - T_e) && \text{on } \Gamma_N^T \end{aligned} \quad (4.47)$$

where $\bar{\mathbf{t}}$ is the traction boundary condition; \mathbf{n} is the outward normal direction; \bar{q}^f and \bar{q}^T are the water and heat fluxes at the boundary, respectively; λ_e and T_e are the thermal conductivity and temperature of the surrounding environment with the following condition:

$$\begin{aligned} \Gamma_D \cup \Gamma_N &= \Gamma \\ \Gamma_D \cap \Gamma_N &= \emptyset \end{aligned} \quad (4.48)$$

where Γ_D and Γ_N represent the Dirichlet and Neumann boundary conditions, respectively.

4.6.2 Variational formulation

By incorporating Equations (4.19) and (4.47) into the equilibrium Equation (4.20), it is possible to derive the constrained Galerkin weak formulation of momentum balance as stated below [101, 105, 106].

$$\int_{\Omega} \nabla^s \boldsymbol{\omega} : \boldsymbol{\sigma} \, d\Omega = \int_{\Omega} \boldsymbol{\omega} \rho_{\text{eff}} \cdot \mathbf{g} \, d\Omega + \int_{\Gamma_N^u} \boldsymbol{\omega} \cdot \bar{\mathbf{t}} \, d\Gamma \quad (4.49)$$

where ω is the weight function. As Lewis and Schrefler [105] have suggested, one approach to computationally incorporate the non-linear behavior into the equilibrium equation is through time differentiation. By taking the arbitrary velocity $\delta \mathbf{v}$ as a weighing function and applying the divergence theorem, the Equation (4.49) can be rewrite as:

$$\int_{\Omega} \dot{\boldsymbol{\sigma}} \cdot \nabla \cdot \delta \mathbf{v} \, d\Omega = \int_{\Omega} \frac{\partial(\rho_{\text{eff}} \mathbf{g})}{\partial t} \cdot \delta \mathbf{v} \, d\Omega + \int_{\Gamma_N^u} \dot{\mathbf{t}} \cdot \delta \mathbf{v} \, d\Gamma \quad (4.50)$$

By substituting Equation (4.29) into Equation (4.15), and then multiplying the resulting equation by an arbitrary pressure δp , the weak form of the mass balance equation can be obtained by integrating over the entire domain Ω as:

$$\begin{aligned} & \int_{\Omega} -\left(\frac{\rho_s (1 - \frac{\rho_b}{\rho_f})(n-1) \alpha_{\text{bf}} w_{\text{b,ini}} \exp[-\alpha_{\text{bf}}(T - T_{\text{ini}})]}{\rho_b} + (s_f + \frac{\rho_b s_b}{\rho_f}) \beta_s (1-n) + \beta_f s_f n + \frac{\rho_b s_b \beta_b n}{\rho_f} \right) \frac{\partial T}{\partial t} \delta p \, d\Omega \\ & + \int_{\Omega} (s_f + \frac{\rho_b s_b}{\rho_f}) \nabla \cdot \mathbf{v}_s \delta p \, d\Omega - \int_{\Omega} \nabla \delta p \cdot \frac{\mathbf{k}}{\mu_f} \cdot \nabla p^f \, d\Omega + \int_{\Omega} \nabla \delta p \cdot \frac{\mathbf{k}}{\mu_f} \cdot \rho_f \mathbf{g} \, d\Omega = - \int_{\Gamma_N^p} \bar{q}^f \delta p \, d\Gamma \end{aligned} \quad (4.51)$$

The energy balance equation, in problems related to heat transport, represents a transient advection-diffusion equation, which may necessitate stabilization during numerical implementation. Diersch and Kolditz [61] suggested that in cases where convection is the primary mechanism of heat transfer, numerical instabilities may arise as spurious oscillations near areas with sharp gradients and boundary layers. To prevent this nonconvergence and instability, it is necessary use a stabilization method. In this study, the streamline upwind Petro-Galerkin (SUPG) stabilization method (proposed by Brooks and Hughes [62]) is applied for stabilization. The method introduces an upwind perturbation along the calculated streamlines to the Galerkin formulation. Accordingly, the energy balance equation of the proposed model can be discretized using the SUPG method by selecting an appropriate arbitrary weighing function δT^* as below:

$$\begin{aligned} \delta T^* &= \delta T + d \\ d &= \tau \rho_f c_f \mathbf{q} \cdot \nabla \delta T \end{aligned} \quad (4.52)$$

where δT is the continuous weighting function, d is a discontinuous streamline upwind correction and τ is an upwind parameter. We used the relation proposed by Galeão et al. [107] to describe this upwind parameter:

$$\tau = \frac{h_e}{2\|\rho_f c_f \mathbf{q}\|} \left(\coth(p_e) - \frac{1}{p_e} \right) \quad (4.53)$$

where h_e is the maximum element length of the mesh, $\|\cdot\|$ is the Euclidean norm, and p_e is the local Peclet number which can be expressed as:

$$p_e = \frac{\|\rho_f c_f \mathbf{q}\| h_e}{2\lambda} \quad (4.54)$$

where λ is the overall thermal conductivity of the media.

By multiplying the weighing function Eq. (4.52) into Eq. (4.22), and integrating it over the domain Ω , the weak form of energy balance equation can be written as:

$$\int_{\Omega} (\rho c)_{\text{eff}} \frac{\partial T}{\partial t} \delta T^* d\Omega + \int_{\Omega} \rho_f c_f \mathbf{q} \cdot \nabla T \delta T^* d\Omega + \int_{\Omega} \nabla \delta T^* \cdot \lambda_{\text{eff}} \nabla T d\Omega = - \int_{\Gamma_N^T} \bar{q}^T \delta T^* dT \quad (4.55)$$

4.6.3 Numerical implementation

The governing equations are to be solved for three field variables: displacements, pore water pressure, and temperature. Choosing basis functions for these variables and applying to the Galerkin formulation, the space-discretized form of the nonlinear coupled system of equations in a compact manner can be expressed as:

$$\mathbf{C} \frac{d\mathbf{X}}{dt} + \mathbf{K}\mathbf{X} = \mathbf{F} \quad (4.56)$$

where \mathbf{C} is the coefficient matrix, \mathbf{K} is the stiffness matrix, \mathbf{F} is the external load vector, and \mathbf{X} is the vector of unknowns.

In order to solve the system of equations, we can utilize the generalized trapezoidal method, also referred to as the generalized midpoint rule, to discretize the equations in time. This involves estimating the rate of change of the unknown vector \mathbf{X} within the time interval of (t_n, t_{n+1}) [105]:

$$\mathbf{X}_{n+\theta} = (1-\theta)\mathbf{X}_n + \theta\mathbf{X}_{n+1} \quad (4.57)$$

$$\left(\frac{d\mathbf{X}}{dt} \right)_{n+\theta} = \frac{\mathbf{X}_{n+1} - \mathbf{X}_n}{\Delta t} \quad (4.58)$$

where θ is a time integration parameter with the variation between 1 (fully implicit) and zero (fully explicit) 0, and Δt is the time step length.

Adopting a fully implicit time integration scheme will yield the final form of the fully coupled thermo-hydro-mechanical discrete equations. This form of Eq. (4.56) can be solved iteratively by the Newton-Raphson method. We implemented the above algorithms into our in-house developed THM coupled 2-D FEM code written in MATLAB.

4.7 Model validations

This section includes numerical examples that aim to confirm and support the proposed THM model's validity. The initial example serves as a validation of the THM model by analyzing high temperature triaxial tests on Boom clay with various OCR values. The subsequent example presents high-temperature oedometer tests on heavily consolidated smectite-quartz mixture samples.

4.7.1 Description of material parameters

Details of the testing conditions and thermo-hydro-mechanical parameters are provided in Table 1, where F_0 is the preconsolidation pressure at an initial temperature T_0 , σ_{con} is the confining pressure; p_{ini}^f is the initial pore water pressure; n_0 is the initial porosity; E is the elastic modulus; ν is the poisson ratio; β_s, β_f and β_b are the thermal expansion coefficient of solid, fluid and bound water respectively; λ_s, λ_f and λ_b are the thermal conductivity of solid, fluid and bound water respectively; c_s, c_f , and c_b are the specific heat capacities of solid, fluid and bound water

respectively; k is the intrinsic permeability; μ_f is the dynamic viscosity of fluid which here is water; $w_{b,Ini}$ is the initial bound water content; γ_T is the thermal softening coefficient; α_{bf} is the constant that describes the mass of free water converted from per unit mass of bound water per each unit rise in temperature. Zymnis et al. [44, 60] proposed a relation for obtaining the value of α_{bf} as below:

$$\alpha_{bf} = -\frac{1}{w_b} \frac{\partial w_b}{\partial T} \quad (4.59)$$

Figure 4-3 demonstrates the nonlinear relations between bound water content and temperature for soils with different values of α_{bf} . As per illustrated, a higher value of α_{bf} ends up with a dehydration at a higher rate.

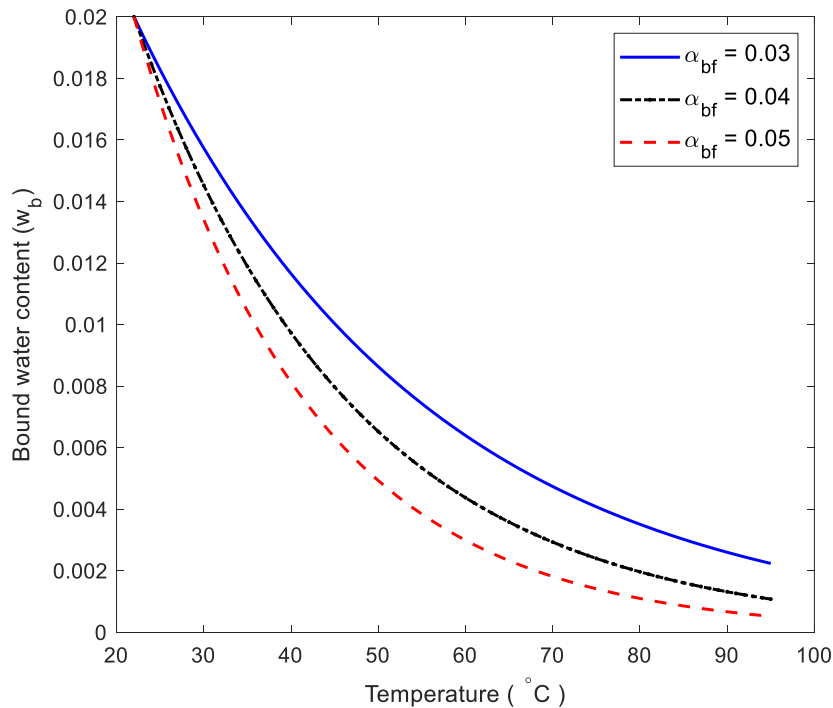


Figure 4-3 Bound water content versus temperature for different value of α_{bf} .

Table 4-1 THM material properties of clay soils for numerical tests (THM parameters of Boom Clay soil samples are from [12, 59, 108]; properties of water-saturated smectite-quartz mixtures (SQ1 and SQ2) are based on [12, 59]; all of the dehydration parameters are according to Zymnis et al. [44, 60]).

| | | | Boom Clay | SQ1 | SQ2 |
|-------------------------------------|------------------------|----------------------|---------------|---------------|----------------|
| Mechanical | F_0 | (MPa) | 6 | 10 | 10 |
| | σ_{con} | (MPa) | 1-6 | 3 | 3 |
| | p_{ini}^f | (MPa) | 0 | 0 | 0 |
| | n_0 | (-) | 0.35 | 0.254 | 0.258 |
| | E | (Pa) | $2*10^7$ | $1*10^6$ | $1.2*10^6$ |
| | ν | (-) | 0.1 | 0.1 | 0.1 |
| Thermal- Hydraulic Properties | β_s | ($^{\circ}C^{-1}$) | $4*10^{-5}$ | $2*10^{-5}$ | $2*10^{-5}$ |
| | β_f, β_b | ($^{\circ}C^{-1}$) | $2.7*10^{-4}$ | $2.7*10^{-4}$ | $2.7*10^{-4}$ |
| | λ_s | (W/m/K) | 0.65 | 0.7 | 0.9 |
| | λ_f, λ_b | (W/m/K) | 0.6 | 0.6 | 0.6 |
| | c_s | (J/kg/K) | 800 | 700 | 700 |
| | c_f, c_b | (J/kg/K) | 4180 | 4180 | 4180 |
| | k | (m^2) | $2*10^{-19}$ | $1*10^{-19}$ | $6.5*10^{-20}$ |
| | μ_f | (Pa.s) | $1*10^{-3}$ | $1*10^{-3}$ | $1*10^{-3}$ |
| | $w_{b,ini}$ | (-) | 0.04 | 0.013 | 0.03 |
| | γ_T | (-) | 0.4 | 0.2 | 0.25 |
| | α_{bf} | ($^{\circ}C^{-1}$) | 0.05 | 0.03 | 0.035 |

4.7.2 High temperature triaxial tests

Del Olmo et al. [35] presented the volumetric thermal strain measurements of heating-cooling tests on Boom Clay samples with different OCRs and under a fully drained stress path condition. All the samples were consolidated to maximum preconsolidation pressure of 6 MPa and unloaded to achieve different OCRs. A heating-cooling cycle was applied subsequent with a temperature range

of 22°C to 95°C. The results of the test have been used for the verification of the proposed THM model. The numerical test is generated by using an axisymmetric simulation with a radius of 25 mm and a height of 100 mm, with 10 elements in the X direction and 40 elements in the Y direction (Figure 4-4). The bottom boundary of the sample was fixed in both vertical and horizontal directions, and the left side lateral boundary was fixed only in the horizontal direction. A FEM mesh sensitivity was conducted to make sure that the select mesh size generates a converged numerical result. A drainage with a constant pore pressure of 0 MPa is provided to both ends. Since the applied heating rate was not provided in Del Olmo et al. [35], we used a low heating rate that no significant thermal pore pressure was built up in the sample. The applied parameters for the numerical tests are included in Table 4-1. Most THM parameters of Boom Clay soil samples can be retrieved from the literature since there were a list of publications working on this set of experimental data [12, 59, 108]. The dehydration parameter is based on the work by Zymnis et al. [1] and the similarity in clay mineral composition and fractions. Figure 4-5 displays a comparison between the modeled results and experimental data at various confining pressure conditions. The thermally induced contraction behavior at low OCRs (= 1 and 2), and thermally induced expansion behavior at OCR of 6 are well simulated with the proposed THM model. For the case with an OCR of 6, there is a slight irreversible plastic expansion behavior shown in Figure 4-5. Even though the sample is simulated to be under an isotropic loading condition, the bottom side is fixed with constraints in all directions. Thus, some local parts of the sample can still be subjected to a thermally induced shear stress state due to the sample end effect. As discussed by Li and Wong [12], a thermally induced shear stress in a sample with an OCR over 3.5 tends to end up with some plastic dilation behavior.

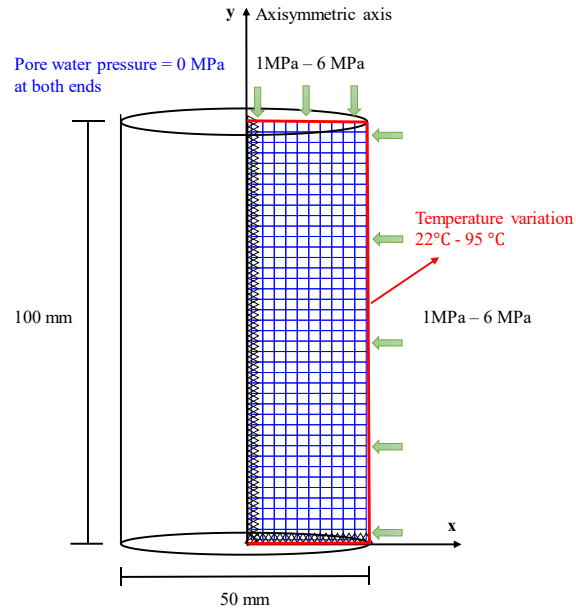


Figure 4-4 Axisymmetric finite element mesh and boundary conditions of numerical tests on Boom Clay soils.

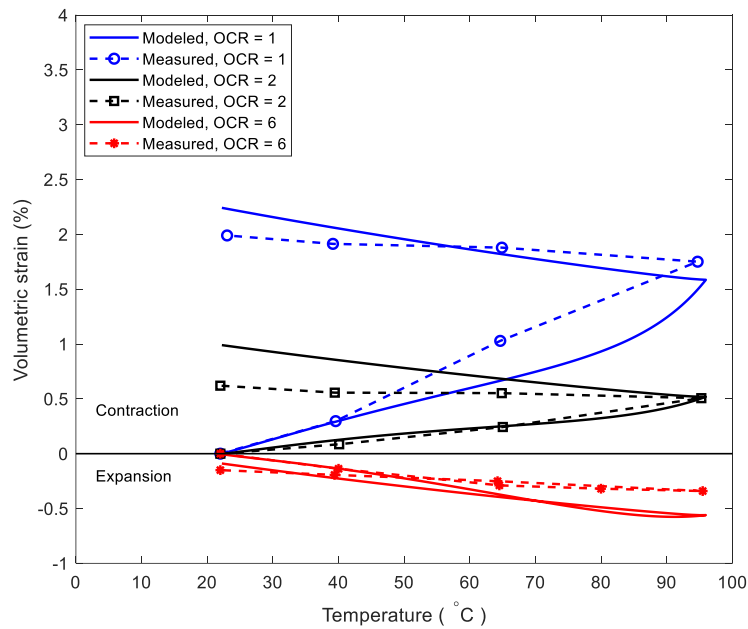


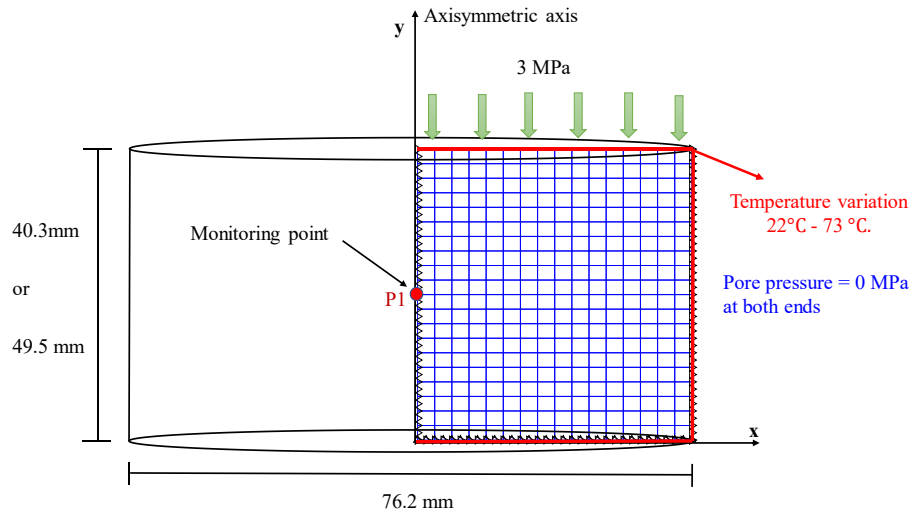
Figure 4-5 Comparison of simulated and measured data for the thermo-mechanical behavior of Boom Clay soils.

4.7.3 High temperature oedometer tests

This section explores the precision of the proposed numerical model by validating with the high temperature oedometer tests on the smectite-quartz mixtures. Water saturated smectite-quartz mixtures with clay fractions of 0.2 and 0.45 (designated as SQ1 and SQ2) were prepared for the tests. The samples were initially consolidated under a vertical stress of 10 MPa and unloaded to a stress level of 3 MPa to create an OCR of 3.3. Upon the completion of mechanical consolidation, two cycles of heating tests were conducted on each sample. During the first cycle, the sample was gradually heated to a temperature of 45°C using a heating rate of 8°C/hr. In the second cycle, the maximum temperature was increased to 73°C and a heating rate of 17°C/hr was applied. The experimental setup is displayed in Fig. 6a, and more detailed description of the experiment can be found in our accompanying published article [59]. The experimental set does not contain a pore pressure monitoring device. Instead, the deformation of samples was monitored by the device equipped in the MTS uniaxial compression system. Nevertheless, some calibration was conducted to accommodate the thermally induced formation for the facility. During the calibration, a stainless-steel sample (with known thermal properties) was used to determine the thermally induced deformation from the equipment. A vertical stress of 3MPa was also applied to the stainless-steel sample and the maximum temperature was increased to 73°C by a heating rate of 17°C/hr. Two cycles of heating-cooling tests were conducted to check the repeatability.



(a)



(b)

Figure 4-6 Plots showing (a) the experimental setup, and (b) axisymmetric finite element mesh and boundary conditions for the numerical test.

We also use our developed FEM code to simulate the thermo-mechanical responses of laboratory prepared smectite-quartz mixture samples. The corresponding THM properties are presented in Table 4-1. Figure 4-6b shows the chosen mesh for SQ1 and SQ2, which are axisymmetric square meshes with dimensions of 1mm x 1mm. According to our experimental data, a height of 49.5mm and diameter of 76.2mm are set for SQ1, and a height of 40.3mm and diameter of 76.2mm for SQ2. The temperature variation is imposed to the surface of model and the top and bottom ends of sample are permeable with a constant pore pressure of 0 MPa. The displacement boundary conditions specify that the vertical and horizontal displacements of the bottom boundary are fixed, while the lateral boundaries are free to move vertically but are fixed horizontally. A monitoring point (P1) is selected to better demonstrate the evolution of bound water saturation and thermally induced pore pressure. Figure 4-7 displays a comparison of the simulated thermo-mechanical responses and experimental data for SQ1 and SQ2 samples. The nonlinear thermal expansion behavior was well simulated using our FEM package. It should be noted that the thermal plastic behavior is significant for the studying smectite-quartz mixture samples since the heating was conducted under a stress condition with OCR of 3.3. Major nonlinearity is a resultant of bound

water dehydration. Figure 4-8 presents the evolution of simulated degree of saturation of bound water (S_b) during the high temperature oedometer tests at the monitoring point P1. When the temperature was raised from 22°C to 73°C during the test, the degree of saturation of bound water (S_b) decreased for both samples. Furthermore, due to a smaller amount of bound water in SQ1 (smaller clay fraction), the degree of saturation of bound water at the start of the test was lower than that of SQ2. A detailed description of bound water evolution and pore pressure development is addressed in the subsequent discussion section.

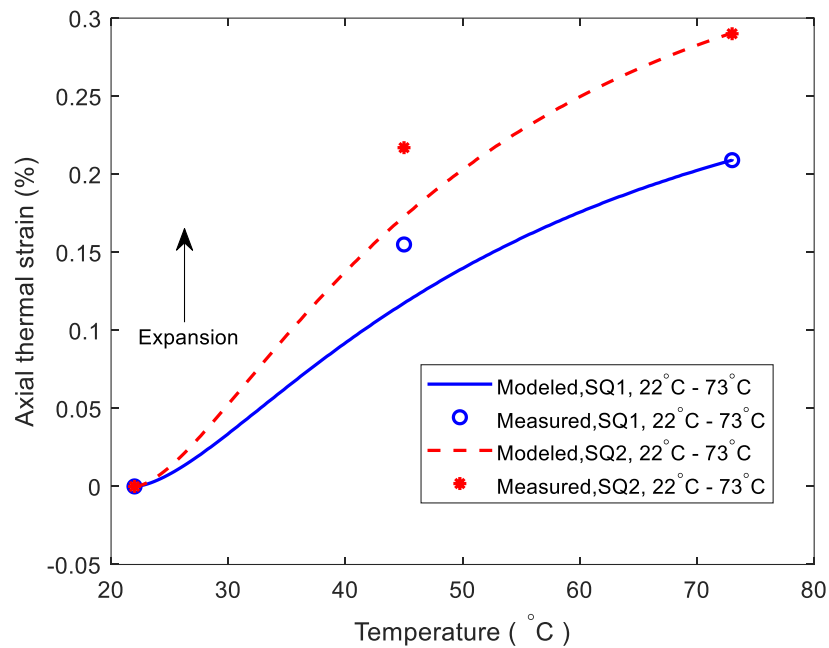


Figure 4-7 Simulated and measured nonlinear thermo-mechanical behaviors of highly compacted smectite-quartz mixture (SQ1, clay fraction = 0.2; SQ2, clay fraction = 0.45), the positive sign is treated as expansion herein.

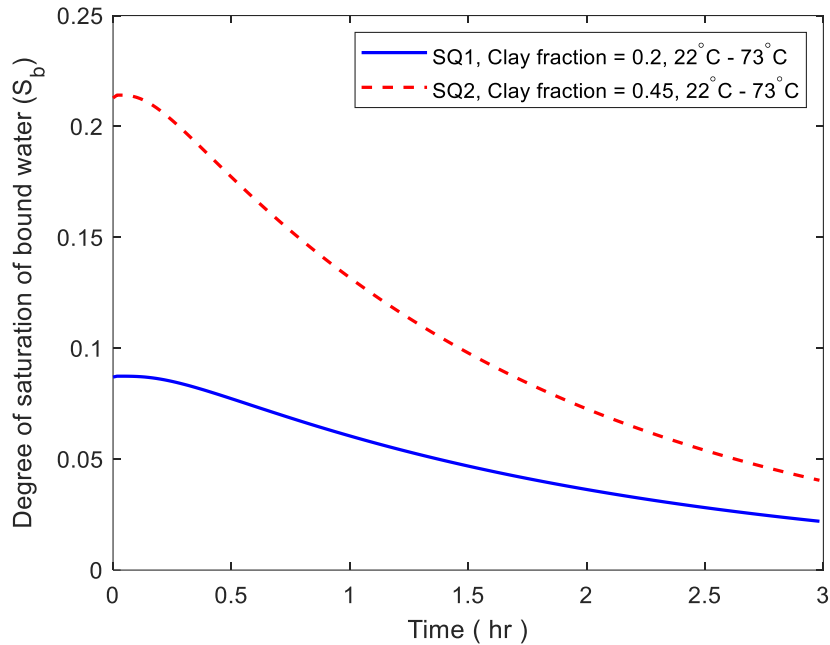


Figure 4-8 Curves showing the variation of degree of saturation of bound water (S_b) with time for samples SQ1 and SQ2 at the monitoring point (P1).

4.8 Discussions

4.8.1 Impact of bound water on deformation behavior

In order to investigate the significance of considering bound water dehydration in characterizing the thermo-mechanical behavior of highly compacted clay soils, we also carried out numerical tests for smectite-quartz samples (SQ1 and SQ2) by neglecting bound water dehydration (setting initial bound water content to 0). The results were summarized and illustrated in Figure 4-9, where the previous numerical results from the section 3.7.3 were also included. The curves indicate that a neglecting of dehydration produces a linear thermal expansion behavior, which is within expectation since we applied a linear elastic law in characterizing the linear thermal expansion behavior of solid minerals. The consideration of bound water dehydration ends up with more precise outcomes. It is also possible to use a nonlinear thermal expansion coefficient to quantify such nonlinear thermal expansion behavior [37, 38]. However, the nonlinear physical mechanism is not as clear as using the concept of bound water dehydration. In addition, bound water dehydration is potentially contributing to water mass balance change and bringing pore pressure

increase. Thus, it is necessary to treat the THM response of bound water separately like in the proposed model.

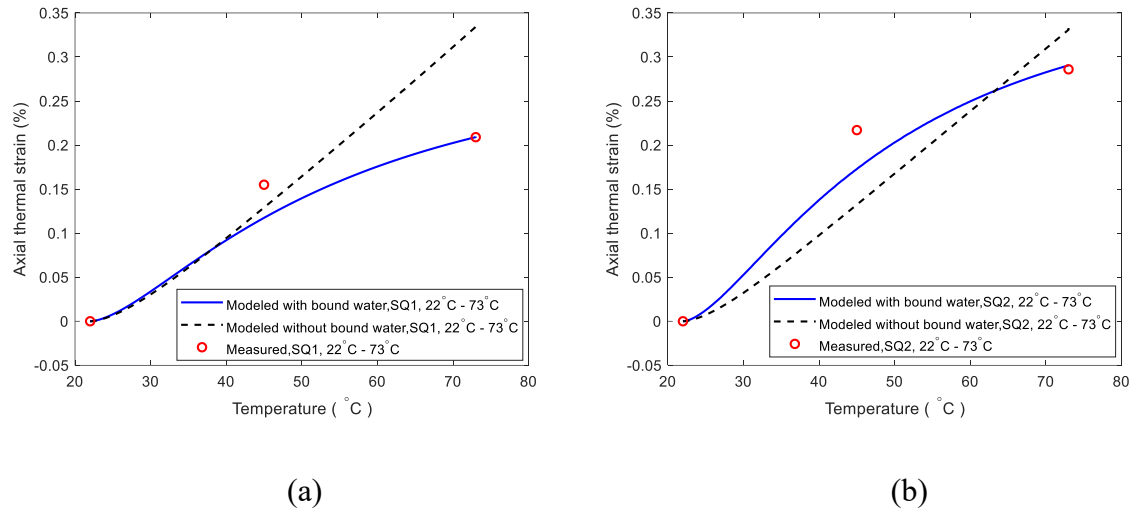


Figure 4-9 Comparison of model simulation with and without bound water for (a) SQ1, and (b) SQ2.

4.8.2 Impact of bound water on pore pressure development

To explore the impact of bound water and applied heating rates on the formation of pore water pressure, we carried out numerical tests on SQ2 under two different heating rates and with different bound water considerations. The results of the monitoring point P1 are summarized and presented in Figure 4-10.

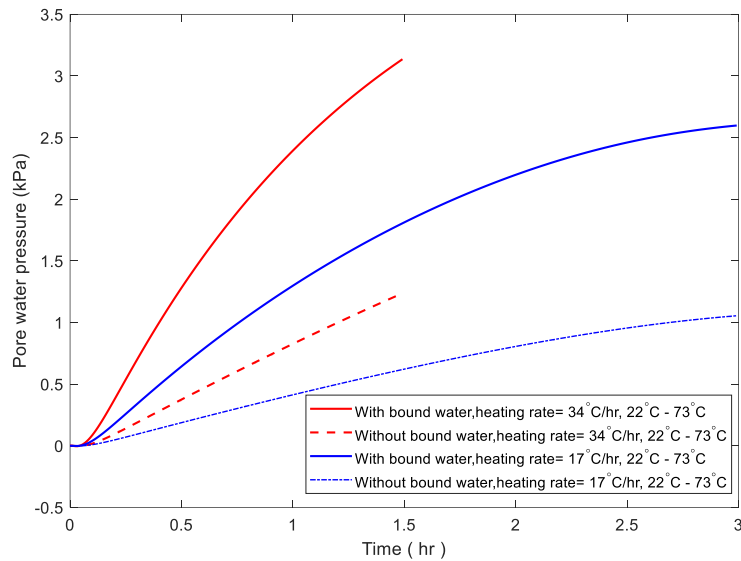


Figure 4-10 Simulated pore pressure generation in monitoring point of SQ2 under different heating rates.

Our results indicate that a heating rate of 17°C/hr produces negligible pore water pressure (less than 1.5 kPa) in the center of the sample (SQ2). It confirms with our previous statement that a fully drained condition was fulfilled for the numerical tests. However, under a higher heating rate (34°C/hr), significant pore pressure was built up in both samples, regardless of whether bound water dehydration was considered. Moreover, the simulation that accounted for bound water dehydration produced a higher pore water pressure, as the conversion of bound water to free water has a significant impact on the formation of pore water pressure during heating. This result is different from the findings presented in Ma and Hueckel [57], which indicates that a consideration of dehydration promotes the pore pressure dissipation in a clay soil. However, it should be noted that the result by Ma and Hueckel [57] is based on an assumption that all of bound water including the interlayer space of smectite minerals is involved in the dehydration process. As is presented in Eq. (4.6) and Figure 4-1, the bound water in a smectite-rich geomaterial can take up a substantial amount of the pore space when the inter-layer bound water is accounted. If all the bound water is involved in the dehydration process, a significant permeability increase will be triggered due to the increase in the hydraulic effective porosity. Thereby, the results by Ma and Hueckel [57] show that the bound water dehydration accelerates the pore pressure dissipation process. In the present study, only the dehydration of bound water adhered to the external surface of clay minerals is

considered, thus the contribution to the hydraulic effective porosity is limited [96]. Nevertheless, an update of permeability with the evolving of time steps is necessary when modeling the pore pressure development for a field scale problem with significant porosity changes in the soil formations.

4.9 Conclusion

In this study a finite element formulation for simulating the fully coupled thermo-hydro-mechanical (THM) responses of clay soils is presented with highlighting the bound water dehydration behavior. Several conclusions are drawn as bellows:

- The theoretical underpinnings of the THM coupled finite element model are rooted in the principles of porous media theory, where the soil is regarded as saturated with free water and bound water. The model incorporates mass balance, momentum balance, and energy balance equations, where the mass balance equation is well adjusted by the consideration of bound water dehydration. The conversion of bound water to free water represents a critical concept that regulates the reversible thermo-mechanical strain that should be handled separately.
- The nonlinear equations that govern the system are formulated and discretized in time and then solved using an in-house developed FEM code. The thermo-plastic behavior of clayey soils can be described by employing the subloading surface plasticity framework. The chosen mechanical framework considers the elasto-plastic domain within the yield surface. The proposed model effectively captures the seamless transition between elastic and plastic behavior. The thermo-plastic constitutive law can be conveniently implemented into our THM coupled FEM framework.
- The proposed THM model simulations have provided a reasonable agreement with experimental data and although there exists limited experimental data on the effect of bound water variation on clay soil behavior under thermal loading, the THM model offers a valuable framework for assessing the thermo-mechanical response of clay. Our numerical results indicate that dehydration will exert a significant impact on the generation of excess pore pressure in clay soils during heating.

4.10 List of symbols

| | |
|--------------|--|
| c_s | Specific heat capacity of solid. |
| c_f | Specific heat capacity of free water. |
| c_b | Specific heat capacity of bound water. |
| F_0 | Preconsolidation pressure. |
| g | Gravity. |
| H | Hardening parameter. |
| h_e | Maximum element length of the mesh. |
| k | Intrinsic permeability. |
| \bar{N} | Normalized outward normal of the subloading surface. |
| n | Soil porosity. |
| n_s | Volume fractions of the solid phase. |
| n_f | Volume fractions of the free water phase. |
| n_b | Volume fractions of the bound water phase. |
| n | Outward normal direction. |
| p^f | Pore water pressure. |
| P_e | Local Peclet number. |
| \mathbf{q} | Volumetric flow rate per unit of surface area. |
| \bar{q}^f | Water flux at the boundary. |

| | |
|--------------------|---|
| \bar{q}^T | Heat flux at the boundary. |
| R | Similarity ratio. |
| s_f | Degree of saturation of free water. |
| s_b | Degree of saturation of bound water. |
| T | Temperature. |
| T_{Ini} | Initial temperature. |
| T_e | Temperature of the surrounding environment. |
| \bar{t} | Traction boundary condition. |
| u | Material parameter. |
| v_s | Soil particles velocity. |
| v_f | Free water velocity. |
| w_b | Bound water content. |
| $w_{b,\text{Ini}}$ | Bound water content at the initial temperature. |
| α_{bf} | Constant that controls the conversion of bound to free water per each unit rise in temperature. |
| β_s | Thermal expansion coefficient of the soil phase. |
| β_f | Thermal expansion coefficient of the free water phase. |
| β_b | Thermal expansion coefficient of the bound water phase. |
| β_T | Equivalent thermal expansion coefficient. |

| | |
|-------------------------|--|
| γ_t | Thermal softening coefficient. |
| ε | Total strain. |
| ε^e | Elastic strain. |
| ε^p | Plastic strain. |
| ε^T | Thermal elastic strain. |
| κ | Slopes of the unloading-reloading line. |
| λ_{eff} | Effective thermal conductivity. |
| λ_s | Thermal conductivity of solid. |
| λ_f | Thermal conductivity of free water. |
| λ_b | Thermal conductivity of bound water. |
| λ | Slopes of the normal consolidation line. |
| $\bar{\lambda}$ | Positive proportionality factor. |
| λ_e | Thermal conductivity of the surrounding environment. |
| μ_f | Dynamic viscosity of water. |
| ρ_s | Density of soil particles. |
| ρ_f | Density of free water. |
| ρ_b | Density of bound water. |
| ρ_{eff} | Bulk density of the solid-bound water-fluid mixture. |
| $(\rho c)_{\text{eff}}$ | Effective heat capacity. |

- σ Total stress tensor.
- σ' Effective stress tensor.

Preface to Chapter 5

Exploring the application of the proposed FEM-based THM model framework constitutes a fundamental phase within numerical simulations. Assessing the stability of the model under thermo-mechanical loading conditions across various time spans and mesh sizes is imperative, as it ensures the dependability and credibility of the suggested THM model. In this chapter, we modeled a borehole in a BTES system and its surrounding soil formations in a Canadian subarctic region. Following model validation, we carried out a series of simulation analyses to investigate the effect of bound water dehydration on soil behavior, the influence of temperature variation ranges on the deformation of the surrounding soil, and the repercussions of different time spans on model performance.

Chapter 5

5 Thermal-hydro-mechanical modeling of short-term ground responses due to the borehole thermal energy storage operations in a Canadian subarctic region³

5.1 Abstract

Seasonal borehole thermal energy storage (BTES) has been recommended as a strategic technology to make an energy transition in the off-grid communities of circum-arctic countries. However, the running of BTES can create thermal disturbance to the surrounding soil formation and bring a thermal-hydro-mechanical coupled process in the ground, potentially triggering geohazards. This thermal-hydro-mechanical coupled process is particularly significant in less permeable formations, where the clay bound water is abundant. The role of clay bound water on the poromechanical responses of soil ground during BTES operation have not been investigated previously. This study aims to numerically assess the short-term impact of poromechanical response of a ground soil due to the thermal disturbance during BTES operations in a Canadian subarctic region. The research entails the creation of a two-dimensional finite element model (FEM) for a BTES well embedded in a clay soil formation and the thermally induced dehydration of bound water on the deformation and pore pressure development of the ground soil is examined. Our numerical results demonstrate the significance of considering bound water dehydration in characterizing the ground heave process during the short-term BTES operation in an over-consolidated soil formation in the subarctic region. The ground expansion behavior is due to the high excess pore pressure generated from thermal disturbance. The surface heave is mainly from a poroelastic impact leveraging the release of some in-situ effective stress during pore pressure

³ A version of this manuscript has been submitted to the journal of *Renewable Energy* (2023).

built up. The neglect of bound water dehydration will underestimate the magnitude of ground heave.

Keywords: THM coupling, borehole thermal energy storage (BTES), FEM, Bound water dehydration, pore pressure, ground heave

5.2 Introduction

During the last decades, Thermal Energy Storage (TES) has gained considerable attention in modern energy systems, aligning with the global transition towards sustainability and renewable energy [1, 2]. In some subarctic regions of Canada, villages rely on fossil fuels to produce both electricity and heat, with production prices several times more than those in the South. Therefore, developing new technologies to meet the energy needs of these communities is of paramount importance to reduce both the high financial costs and environmental impacts of logistically complex fuel shipments [109]. Seasonal borehole thermal energy storage (BTES) has been suggested as a strategic technology to increase energy and food security in the off-grid communities of circum-arctic countries, given that winter season solar energy is insufficient for local needs [3, 4]. BTES is a system that stores and retrieves heat through shallow borehole heat exchangers. It employs soil and rock as a thermal medium for storing thermal energy [67–69]. BTES stands as a widely favored option for seasonal storage due to its versatility, applicability across diverse formations, and its cost-effectiveness in installation compared to other TES systems. The substantial costs linked to BTES construction emphasize the need for numerical simulations to ensure both economic viability and thermodynamic efficiency. Thermal injection in the BTES projects involves a range of temperature variations in the surrounding soil formations, which may affect the stability of the boreholes and the operational life of the projects [110–112]. As is shown in Figure 5-1, a BTES project tends to store heat in low permeable layers that are rich in clay soils to minimize heat loss. The thermal-hydro-mechanical (THM) coupled processes in the surrounding soil formation can significantly influence the stability of the ground and the boreholes in BTES projects. Therefore, it is crucial to have a precise and comprehensive understanding of the geohazard associated with this behavior.

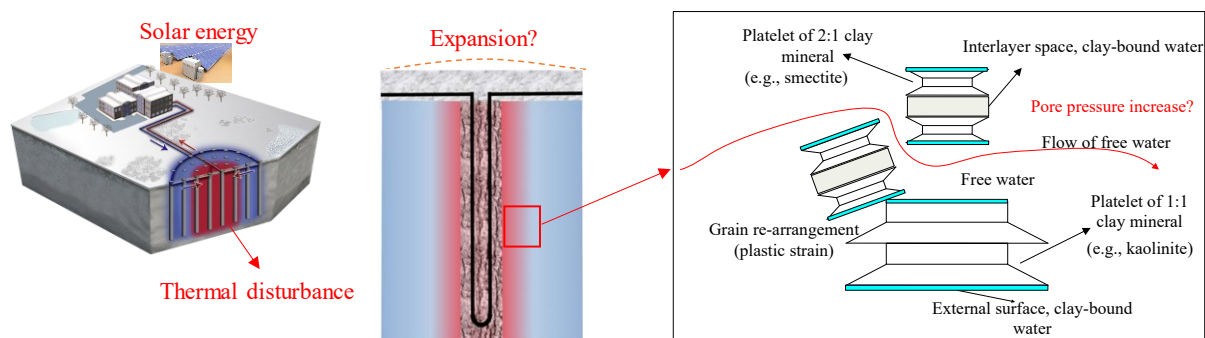


Figure 5-1 Sketch showing the thermal disturbance in soils surrounding a Borehole Thermal Energy Storage (BTES) system.

Extensive theoretical and numerical studies were conducted to investigate the thermal-mechanical responses of clay soils under temperature variations [32, 37, 49]. The developed mechanical models were implemented into numerical programs for carrying out THM analysis for shallow geothermal energy projects [113–116]. However, minimal emphasis was placed on acknowledging the influence arising from the dehydration of bound water in clay minerals, a phenomenon that should be regarded as an independent deformation mechanism [12, 13, 44, 59, 60]. According to Li and Wong [12] the dehydration of the external layer of bound water in clay minerals can happen under a relatively low temperature (starting from 30 °C). However, it requires a considerable drainage time to dissipate the induced excess pore pressure for a low permeable soil formation. Theoretically, the thermal disturbance tends to contribute to a ground heave as a short-term response if there is no significant plastic deformation involved (Figure 5-1). Currently, there is a lack of studies to explore the impact of such thermal-mechanical disturbance on the ground soil. The role of bound water dehydration on the overall ground deformation behavior has not been investigated. In particular, for a Canadian subarctic region, soils are mostly heavily consolidated during the glacial period, and there is a lot of uncertainty about the possible deformation magnitude during BETS operations in such off-grid communities.

In this study, we carried out a numerical study to examine the performance of a potential BTES borehole located in a Canadian subarctic region. To achieve this, a novel fully THM-coupled finite element framework, built upon prior research by Sojoudi and Li (2023) [59] and Norouzi et al. (2019) [36], has been employed. The proposed model can consider the effect of bound water

dehydration on ground deformation and quantify possible plasticity behavior based on a subloading yield surface framework.

5.3 Governing equations

In BTES projects, an accurate description of THM-coupled behavior in the involved soil formation is an essential step. In this study, we propose a comprehensive thermo-hydro-mechanical framework based on the fundamentals of continuum mechanics. In the proposed formulation, the effect of bound water dehydration on the overall THM-coupled responses is considered. With clay bound water content and its degree of saturation, the mass balance equation of a water-saturated soil can be written as:

$$\frac{\partial(n_s \rho_s)}{\partial t} + \nabla \cdot (n_s \rho_s v_s) = 0 \quad (5.1)$$

$$\frac{\partial(n_f \rho_f)}{\partial t} + \nabla \cdot (n_f \rho_f v_f) - \rho_b n_b \alpha_{bf} \frac{\partial T}{\partial t} = 0 \quad (5.2)$$

$$\frac{\partial(n_b \rho_b)}{\partial t} + \nabla \cdot (n_b \rho_b v_s) + \rho_b n_b \alpha_{bf} \frac{\partial T}{\partial t} = 0 \quad (5.3)$$

where ρ_s, ρ_f and ρ_b are densities of soil particles, free water and bound water respectively; n_s, n_f and n_b are the volume fractions of the soil, free water and bounding water phases; v_s and v_f are soil particles and free water velocity; α_{bf} is a coefficient controlling the conversion of bound to free water per each unit rise in temperature, and T is the temperature.

By combining Eqs.(5.2) and (5.3) and substituting Eq.(5.1) into the resulting equation, the following governing equation is derived:

$$n \left(1 - \frac{\rho_b}{\rho_f} \right) \frac{\partial S_f}{\partial t} + \left(S_f + \frac{\rho_b S_b}{\rho_f} \right) \nabla \cdot v_s - \left(\left(S_f + \frac{\rho_b S_b}{\rho_f} \right) \beta_s (1-n) + \beta_f S_f n + \frac{\rho_b S_b \beta_b n}{\rho_f} \right) \frac{\partial T}{\partial t} + \nabla \cdot \mathbf{q} = 0 \quad (5.4)$$

where n is porosity, β_s , β_f and β_b are the thermal expansion coefficients of the soil particles, free water and bound water respectively; s_f and s_b are degree of saturation of free water and bound water respectively; \mathbf{q} is the volumetric flow rate per unit of surface area.

According to the fundamentals of soil mechanics the following relation can be achieved which relates the degree of saturation of bond water to the soil porosity, densities of soil particles, densities of bound water, and bound water content.

$$s_b = \frac{(1-n)\rho_s w_b}{n\rho_b} \quad (5.5)$$

where

$$n = n_f + n_b \quad (5.6)$$

The bound water content value w_b can be obtained from the relation proposed by Zemnis et al. 2019 [44] as below,

$$w_b = w_{b,ini} \exp[-\alpha_{bf}(T - T_{ini})], \quad T[^\circ C] \quad (5.7)$$

where $w_{b,ini}$ is the bound water content at the initial temperature, T and T_{ini} are the current temperature and initial temperature in Celsius degrees respectively.

By taking time derivation of Eq. (5.5), substituting Eq.(5.7) and according to the water-saturated condition ($s_f + s_b = 1$), the variation of degree of fluid saturation over time can be expressed as,

$$\frac{\partial s_f}{\partial t} = \frac{\alpha_{bf}(1-n)\rho_s w_{b,ini} \exp[-\alpha_{bf}(T - T_{ini})]}{n\rho_b} \frac{\partial T}{\partial t} \quad (5.8)$$

The linear momentum balance equation of the whole system in terms of Terzaghi's effective stress principle can be expressed as:

$$\nabla \cdot (\boldsymbol{\sigma}' - p^f \mathbf{I}) + \rho_{\text{eff}} \mathbf{g} = \mathbf{0} \quad (5.9)$$

where $\boldsymbol{\sigma}'$ is the effective stress tensor, p^f is the pore water pressure, \mathbf{I} is the unit tensor, ρ_{eff} is the bulk density of the solid-bound water-fluid mixture and \mathbf{g} is the gravity vector.

The total strain are given as components of elastic strain, plastic strain, and thermal elastic strain:

$$\dot{\boldsymbol{\epsilon}} = \dot{\boldsymbol{\epsilon}}^e + \dot{\boldsymbol{\epsilon}}^p + \dot{\boldsymbol{\epsilon}}^T \quad (5.10)$$

It should be noted that thermally induced plastic strain can be treated as a part of plastic strain when the temperature aspect is explicitly considered [102].

The thermal elastic strain rate can be quantified by:

$$\dot{\boldsymbol{\epsilon}}^T = \frac{1}{3} \beta_T \frac{\partial T}{\partial t} \mathbf{I} \quad (5.11)$$

where β_T is the equivalent thermal expansion coefficient of a porous media given by:

$$\beta_T = (1-n)\beta_s + nS_f\beta_f + nS_b\beta_b \quad (5.12)$$

To describe the plastic behavior, the subloading surface plasticity framework proposed by Hashiguchi et al.[28, 29] is applied therein. This plasticity model is built on the concept that the interior of the yield surface consists of an elastoplastic domain. To effectively describe this elastoplastic interior, the model incorporates two yield surfaces: the normal-yield surface and the subloading surface. Notably, the subloading surface always passes through the current stress points, offering a comprehensive characterization of the material's behavior.

The differentiation form of subloading surface can be write as,

$$\left[\frac{\partial f(\boldsymbol{\sigma})}{\partial \sigma_{ij}} \right]^T d\sigma_{ij} = F \cdot dR + R \left(\frac{\partial F}{\partial H} \dot{H} \right) \quad (5.13)$$

where σ_{ij} is the stress tensor, R is the similarity ratio, which corresponds to the length of an arbitrary line that connects two points on the normal yield surface and the subloading surface and H is the hardening parameter. As is validated by Sojoudi and Li [59], the subloading surface based

plasticity model can better characterize the nonlinear deformation behavior of overconsolidated soils, which is involved in the present study site. A detailed formulation of the plastic model is included in our previous publication [59].

According to Cacace and Jacquey [101], the energy balance equations of the system can be presented as,

$$(\rho c)_{\text{eff}} \frac{\partial T}{\partial t} + \nabla \cdot (\rho_f c_f \mathbf{q} \cdot T - \lambda_{\text{eff}} \nabla T) = 0 \quad (5.14)$$

where $(\rho c)_{\text{eff}}$ and λ_{eff} are the effective heat capacity and effective thermal conductivity, respectively. c_f is the specific heat capacity of the fluid phase.

The implementation of the proposed THM model into FEM is performed based on the work of Norouzi et al. [36]. To incorporate the model into FEM, the aforementioned equations were first reformulated in the weak form. Subsequently, the Galerkin method was applied to discretize them. Following the discretization process, the equations were implemented into our in-house developed MATLAB code.

5.4 Simulation of BTES systems in a Canadian subarctic region

This study aims to evaluate the effectiveness of the suggested numerical model by simulating a BTES system under conditions resembling those found in the Canadian subarctic region. One of the subarctic regions in the need of providing sustainable energy for life and development is Kuujjuaq, the regional capital of Nunavik which is in the Inuit territory of Quebec, Canada. For such off-grid communities, all the villages in Kuujjuaq rely on fossil fuels to produce both electricity and heat, and the provision of a sustainable alternative source of renewable energy plays a significant role. Relevant studies have shown the validity of using BETS as an alternative and sustainable heat production approach for drinking water needs [4]. However, the geomechanical aspect of examining the ground response has never been studied. We used our in-house developed FEM package to carry out a THM-coupled analysis for the studying site.

5.4.1 Material properties

In the target BETS site, most soil formations are formed as marine sediments and glacial tills, which were deposited during the glacial period [3, 117]. A series of hydro-thermal characterizations were conducted previously to explore the geothermal potential [4, 109, 118]. However, there is a lack of geomechanical database so far. The soils can have a wide range of geotechnical characteristics due to their variable composition and deposition process. In addition to compositions, the stress history is also crucial to analyzing geomechanical properties. The stress history of such marine sediment is complex and is closely related to the glacial process. Previous studies indicate that soils in the study area are over-consolidated due to the large pre-consolidation pressure during the glacial period [119]. Related thermo-hydro-mechanical properties of the studying soil are summarized by Ren [119] and are presented in Table 5-1. The material properties result is not aligned with a BETS site in running. Instead, it can be treated as a possible case study for a potential BETS project.

Table 5-1 Related THM properties of the studying soil formation for numerical modeling.

| | Property | Unit | Value |
|------------------------------|------------------------|-----------------------------|-----------------------|
| Mechanical | F_0 | (Pa) | 500×10^3 |
| | ν | (-) | 0.1 |
| | M | (-) | 1.2 |
| | κ | (-) | 0.017 |
| | λ | (-) | 0.155 |
| Thermal-Hydraulic Properties | β_s | ($^{\circ}\text{C}^{-1}$) | 3×10^{-5} |
| | β_f, β_b | ($^{\circ}\text{C}^{-1}$) | 27×10^{-5} |
| | λ_s | (W/m/K) | 1.57 |
| | λ_f, λ_b | (W/m/K) | 0.6 |
| | c_s | (J/kg/K) | 1359 |
| | c_f, c_b | (J/kg/K) | 4180 |
| | k | (m^2) | 3.5×10^{-18} |
| | μ_f | (Pa.s) | 1×10^{-3} |

| | | |
|---------------|-----------------------------|------|
| $w_{b,Ini}$ | (-) | 0.01 |
| γ_T | (-) | 0.2 |
| α_{bf} | ($^{\circ}\text{C}^{-1}$) | 0.02 |

In Table 5-1, F_0 is the pre-consolidation pressure at an initial temperature T_0 ; ν is the poisson ratio; M is the slope of the critical state line; κ and λ are the slope of swelling and compression lines for elastoplasticity, respectively; λ_s, λ_f and λ_b are the thermal conductivities of solid, fluid and bound water respectively; c_s, c_f , and c_b are the specific heat capacities of solid, fluid and bound water, respectively; \mathbf{k} is the intrinsic permeability; μ_f is the dynamic viscosity of water; $w_{b,Ini}$ is the initial bound water content; γ_T is the thermal softening coefficient. The parameters for bound water related properties are retrieved from Sojoudi and Li [59]. The value of α_{bf} is based on common values applicable to clay soils as suggested by Zymnis et al. [44, 60].

5.4.2 FEM modeling

We carry out a FEM modeling to examine the short-term response (3.5 years) of a potential borehole thermal energy storage system. The borehole is subjected to two different temperature variations, one is in the cyclic range of 1°C to 60°C , and the other one is in the temperature range of 1°C to 30°C . The impact of temperature changes in the borehole on the THM responses of the surrounding soil is analyzed. As a preliminary study, a single borehole is simulated. The dimensions of the soil were set at a radius of 20 m and a height of 40 m. The sketch of the modeled BTES is shown in Figure 5-2.

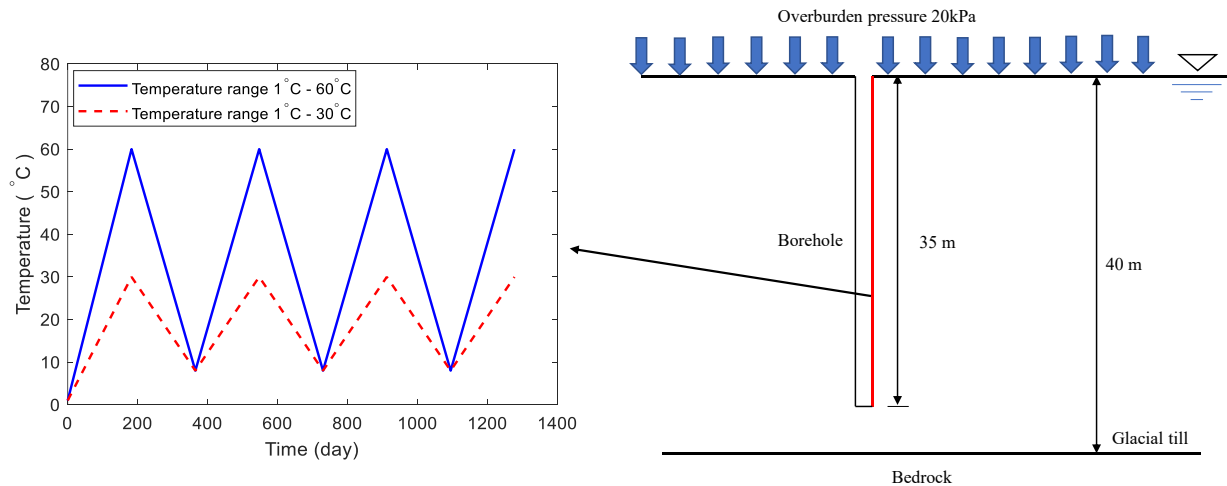


Figure 5-2 Sketch showing the geometry of the modeled BTES well and the applied temperature cycles.

As depicted in the figure, on top of the ground, the active layer that is sensitive to seasonal temperature variations is removed. Instead, a surcharge of 20 kPa is applied on the soil surface. An insulation layer is usually applied to prevent heat exchange between the storage medium and the active layer. The rest studying depth interval holds a stable ground temperature over the years. According to the investigation by Miranda et al. [118], an initial temperature of 1°C is applied to the studying site. Additionally, it should be noted that the soil formation being modeled is significantly over-consolidated and is assumed to have a pre-consolidation pressure of 500 kPa generated during the glacial period [119]. Since the soil formation has a buried depth of up to 40 meters, the overconsolidation ratio (OCR) values vary along the buried depth.

In numerical modeling, the selection of an appropriate meshing technique greatly influences the accuracy of the results. In this study, a non-uniform meshing technique has been adopted to enhance the precision of the model outcomes while reducing computational costs. The mesh has been designed with a finer resolution near the borehole and a coarser resolution for regions farther away from it (Figure 5-3). We have carried out a mesh sensitivity study to make sure the applied mesh size generates a stable result. The model is generated while considering that the bottom boundary is prevented from any horizontal or vertical movements, and the horizontal displacement is fixed at the side boundaries. Additionally, the bottom and surface edges are permeable, while the side edges act as impermeable boundaries to represent the possible drainage impact from a borehole nearby.

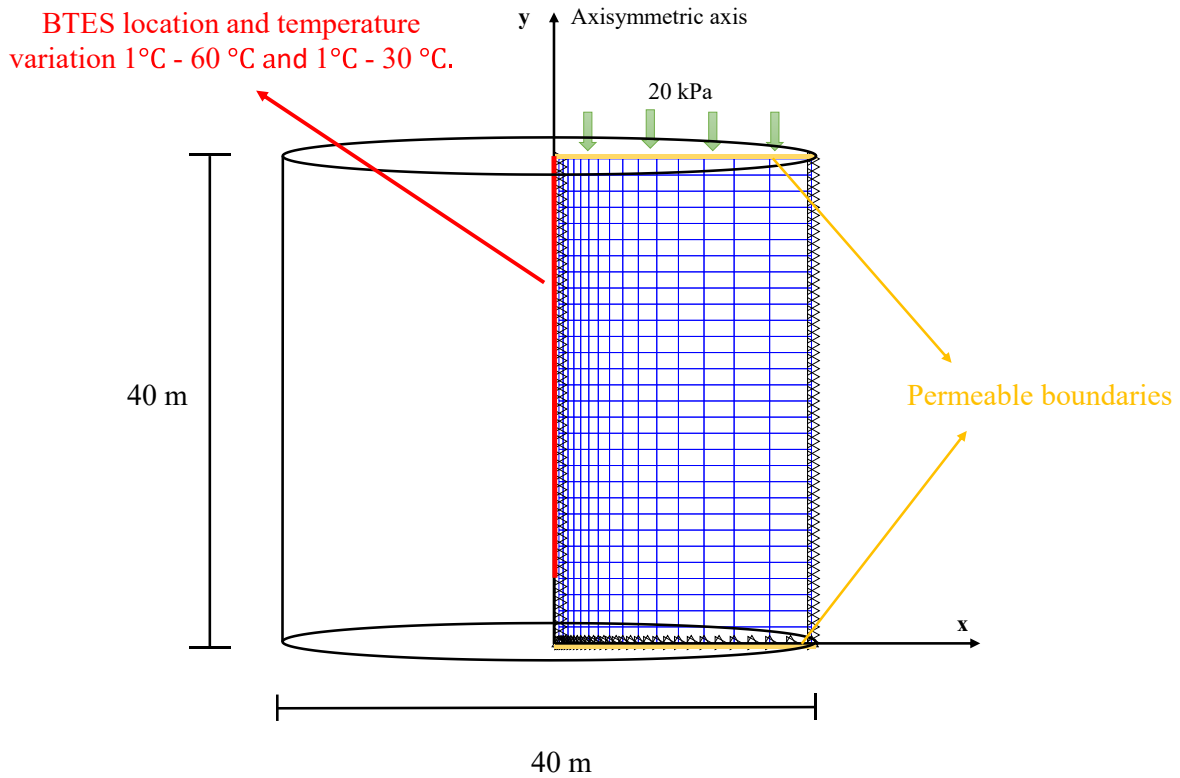


Figure 5-3 Boundary conditions and meshes used for the THM coupled FEM analysis.

To examine the impact of temperature fluctuations on the response of the soil surrounding the BTES, a cyclic temperature load, resembling the one depicted in Figure 5-2, is applied to a soil profile. To depict the effect of thermal loading on temperature distributions, displacements, pore pressures, and stresses within the soil profile, six monitoring points are selected to demonstrate the results (Figure 5-4).

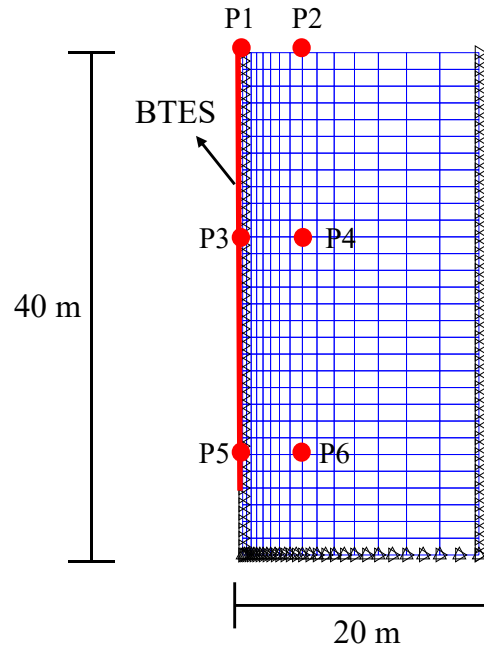
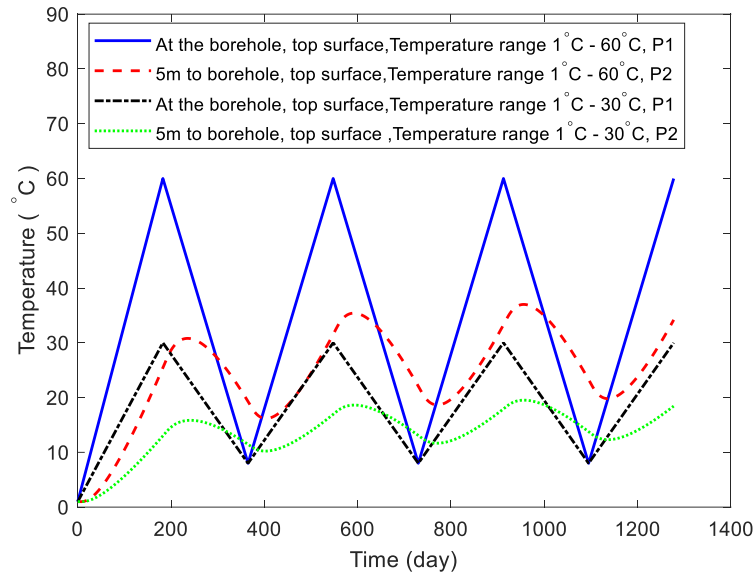


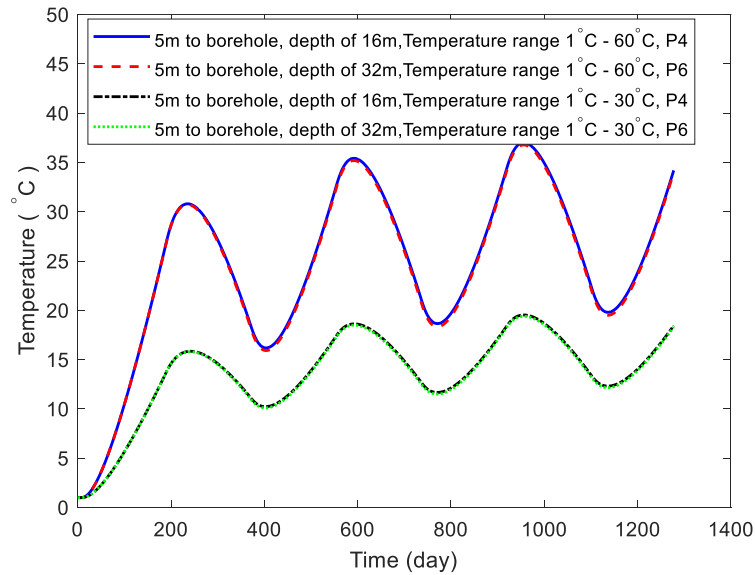
Figure 5-4 Selected six key monitoring points for analyzing the simulation results.

5.4.3 Results and analysis

Figure 5-5 illustrates the temperature development of areas located at varying distances from the borehole with three distinct buried depths. We have considered monitoring points P1, P2, P4, and P6 for a better demonstration. The results indicate that as the distance from the borehole increases, the soil experiences lower temperature levels (Figure 5-5a). Since we keep a uniform temperature variation along the borehole, the depth does not have an impact on temperature distribution (Figure 5-5b). As is shown in Figure 5-6, the influence of temperature variation on the soil profile quickly diminishes as the distance to the borehole increases.



(a)



(b)

Figure 5-5 Simulated temperature development at different monitoring points: (a) P1 and P2, (b) P4 and P6.

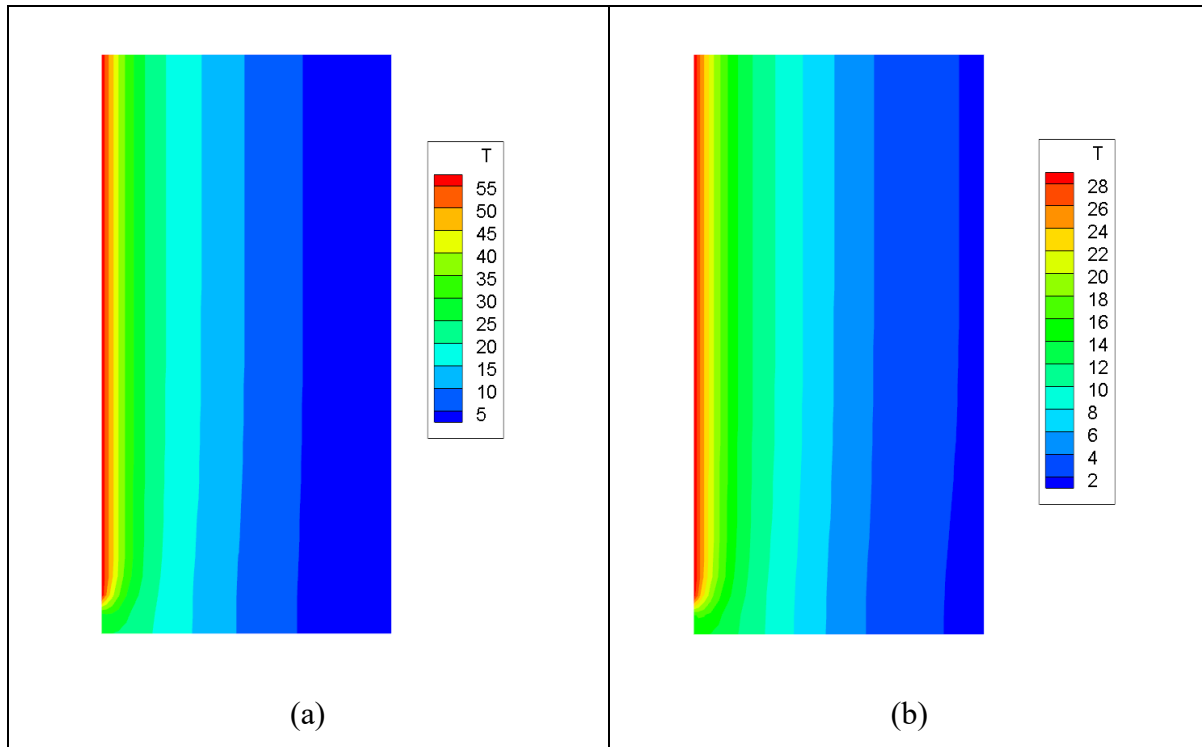


Figure 5-6 Simulated temperature (unit of °C) distribution profiles by the end of 3.5 years: a) Maximum $T = 60^{\circ}\text{C}$, b) Maximum $T = 30^{\circ}\text{C}$.

In Figure 5-7 and Figure 5-8, the vertical displacement versus time at the monitoring points of P1, P2, and P5 for two different temperature ranges are presented. These figures illustrate that a higher storage temperature leads to a much larger vertical displacement (expansion). Furthermore, the result from the first heating cycle reveals that the soil at the surface with an over-consolidation ratio (OCR) around 25 demonstrates a significant expansion behavior (Figure 5-7). By contrast, the soil at a depth of 32m (with an OCR around 2) exhibits small contraction behavior during the initial stage (Figure 5-8). This is due to the considering of thermal-plastic strain in our modeling, which is similar to some previous studies highlighting that thermally induced plastic strain can happen to a slightly consolidated soil [12, 22]. Nevertheless, the ground is experiencing a general trend of expansion behavior. A maximum ground heave of 35 mm is expected for the case with a maximum operation temperature of 60°C .

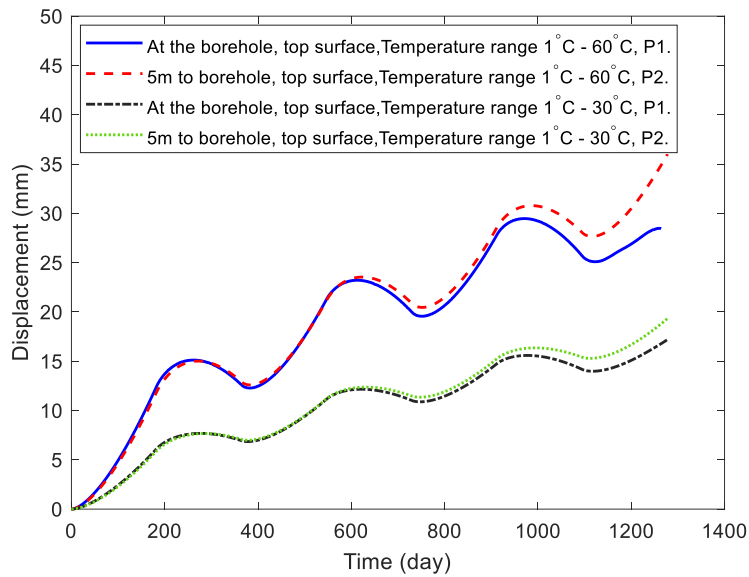


Figure 5-7 Simulated vertical displacements (positive indicates expansion) at the top surface of the soil (monitoring points P1 and P2) under two different temperature ranges (1°C to 60°C and 1°C to 30°C).

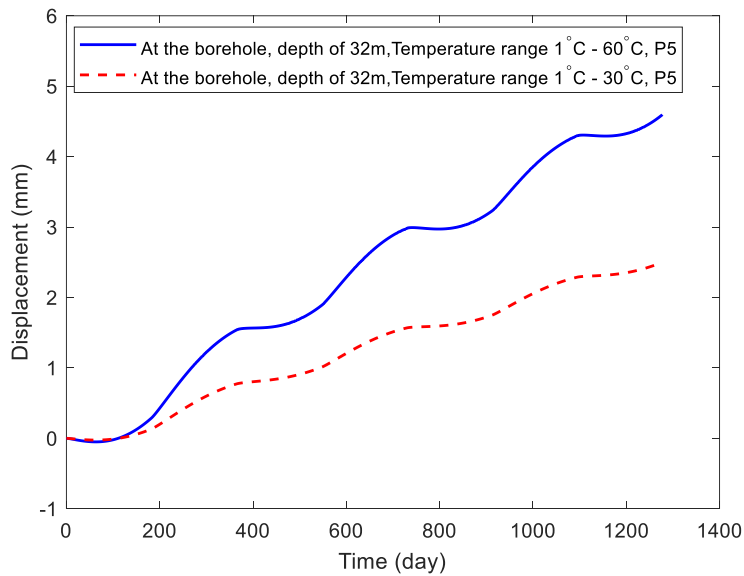
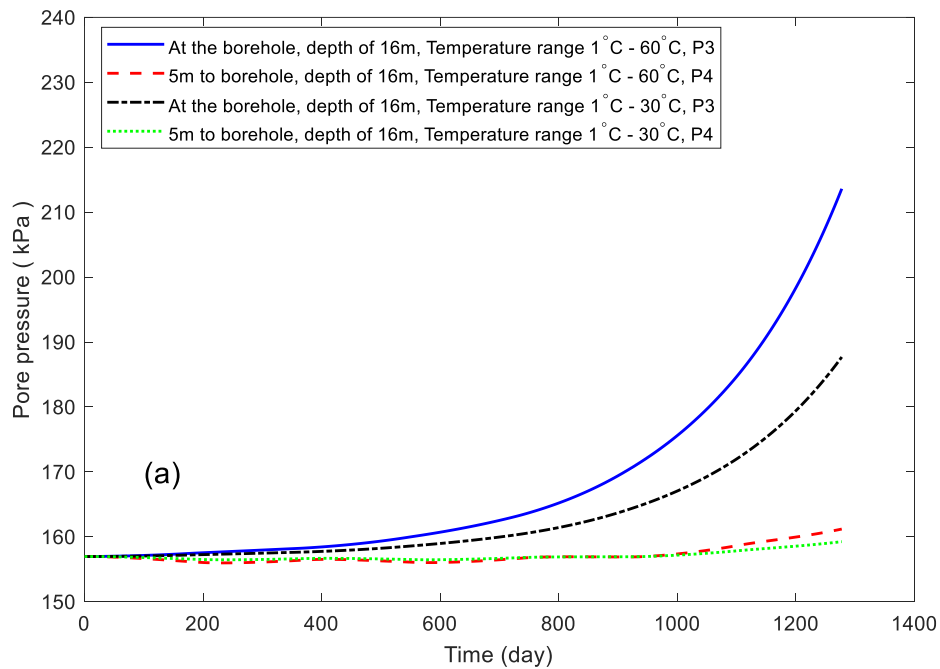


Figure 5-8 Curves showing simulated displacements at P5 for two different temperature ranges.

Figure 5-9 presents the comparison of pore water pressure change at the borehole and within a 5-meter distance from the borehole for points at the depths of 16 meters and 32 meters, respectively.

The monitoring points of P3, P4, P5, and P6 are considered to show the variations. Figure 5-9 provides further evidence, showing that a wider temperature range results in increased creation of pore water pressure, with one possible outcome being attributed to the dehydration of bound water. The curves also demonstrate a continuous increase in pore water pressure over time. An increase in pore water pressure is accompanied by a reduction of effective stress. Thereby, the overall thermal expansion behavior of the ground presented in Figure 5-7 should be mainly from the development of excess pore water pressure due to thermal disturbance.



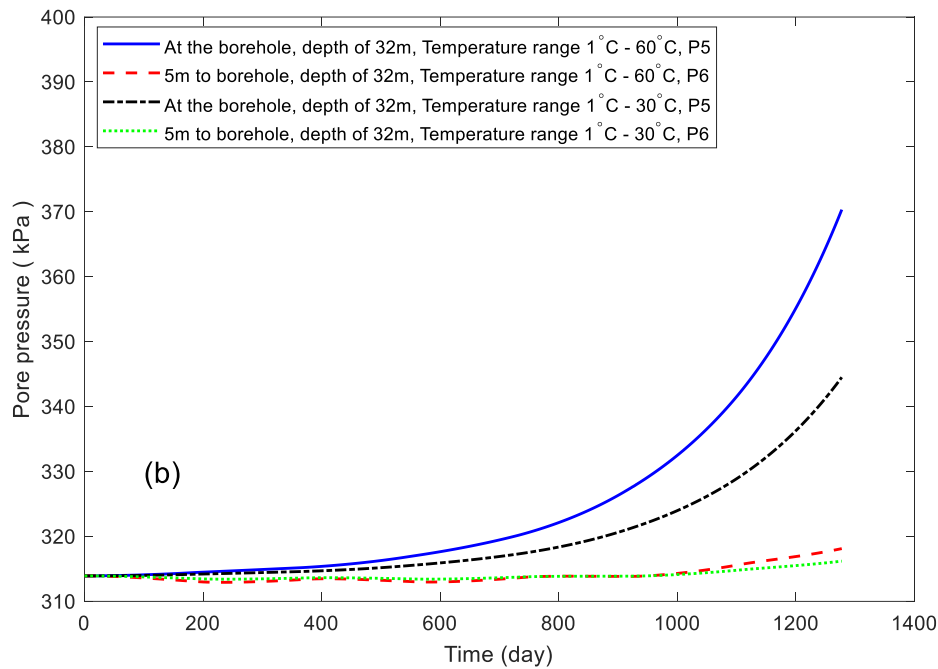


Figure 5-9 Simulated pore pressure development at different monitoring points: (a) P3 and P4, (b) P5 and P6.

5.5 Discussions

5.5.1 Impact of bound water dehydration on displacement and pore water pressure

As is shown in the governing equation, Eq.(5.4), bound water dehydration is likely to contribute to pressure generation and bring changes in the effective stress. To investigate the effect of bound water dehydration on pore water pressure development and ground deformation, we also conducted short-term modeling of the borehole without considering the bound water dehydration process for the case with a temperature range from 1°C to 60°C. The obtained results were then compared with the case that considers bound water dehydration (Figure 5-10).

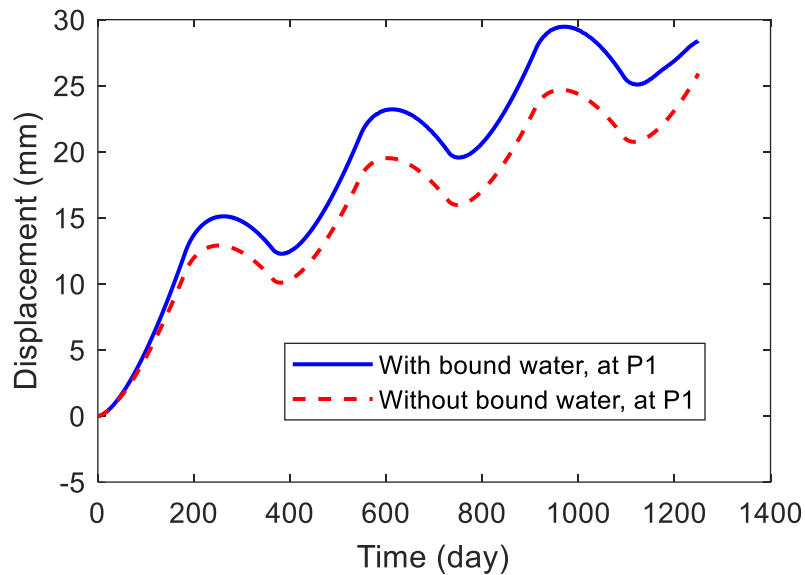


Figure 5-10 Comparison of simulated vertical displacement at P1 for cases with and without considering bound water dehydration, maximum $T = 60^{\circ}\text{C}$.

As is demonstrated in Figure 5-10, the consideration of bound water dehydration has resulted in a higher magnitude of displacement (about 5 mm) at P1. The deformation of the surface reflects the total ground response to the thermal disturbance. As mentioned previously, the induced pore pressure changes should be the major reason for having ground expansion behavior. We also focus on two monitoring points at different depths (P3 and P5) to identify the difference in generated pore pressures for cases with and without considering bound water dehydration. Figure 5-11 illustrates the impact of bound water dehydration on thermal pore pressure development, which demonstrates that the bound water dehydration is potentially exerting a very significant impact on pore pressure elevation during the BETS running process.

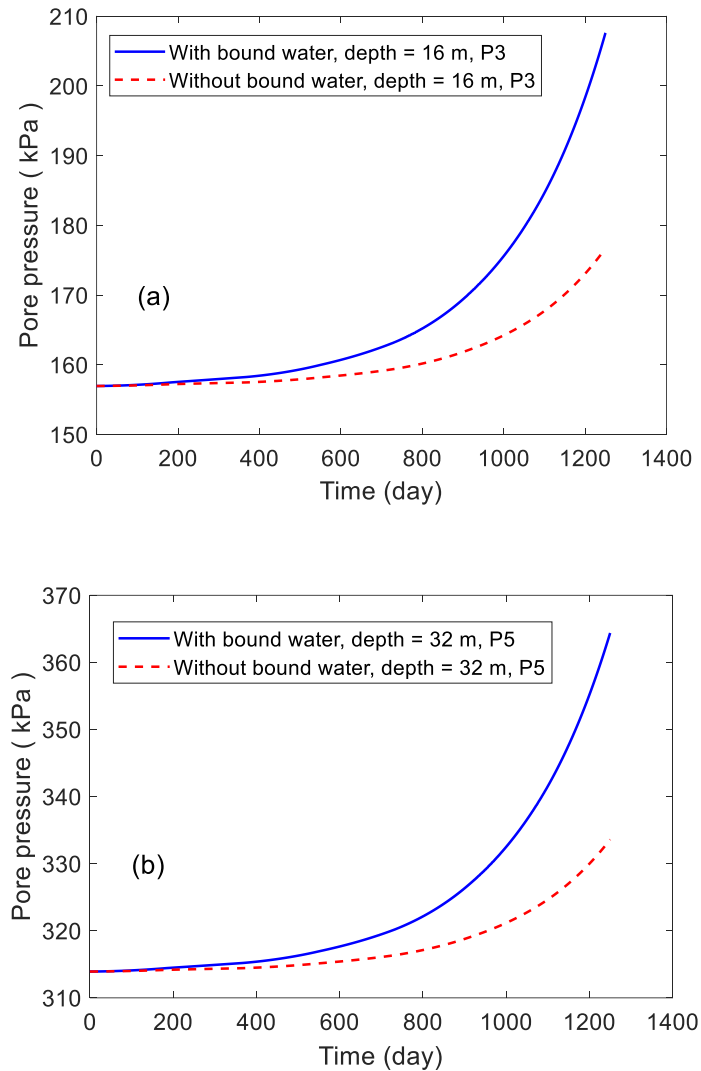


Figure 5-11 Comparison of simulated pore water pressures for cases with and without considering bound water dehydration, maximum $T = 60^{\circ}\text{C}$: (a) at point P3, (b) at point P5.

5.5.2 Effective stress path analysis and the role of plastic strain

The effective stress path can be used to examine the possibility of generating plastic yielding during thermal storage in the ground. We retrieved the simulated total stress and pore pressure data at key monitoring points (P3 and P5) and calculated the effective stresses. The effective stress path curves were plotted in the deviatoric-mean effective stress plane for the case with a maximum temperature of 60°C and were shown in Figure 5-12. Since P3 and P5 are located at two different depths, they have distinct initial stress states. During the thermal storage, shear stresses are

developed due to the thermal disturbance. A reduction of mean effective stress is an indication of an increase in pore pressure. The results also reveal that the stress variations are comparable for these two distinct depths. To examine the possibility of generating plastic deformation in these points, we also include the initial yield surface of the plastic model. As is shown in Figure 5-12, the stress paths are far from any yielding point based on a traditional plasticity framework. However, we've applied a subloading yield surface framework, thus the point with a higher initial stress is still possible to generate some plastic strain as was indicated in Figure 5-8.

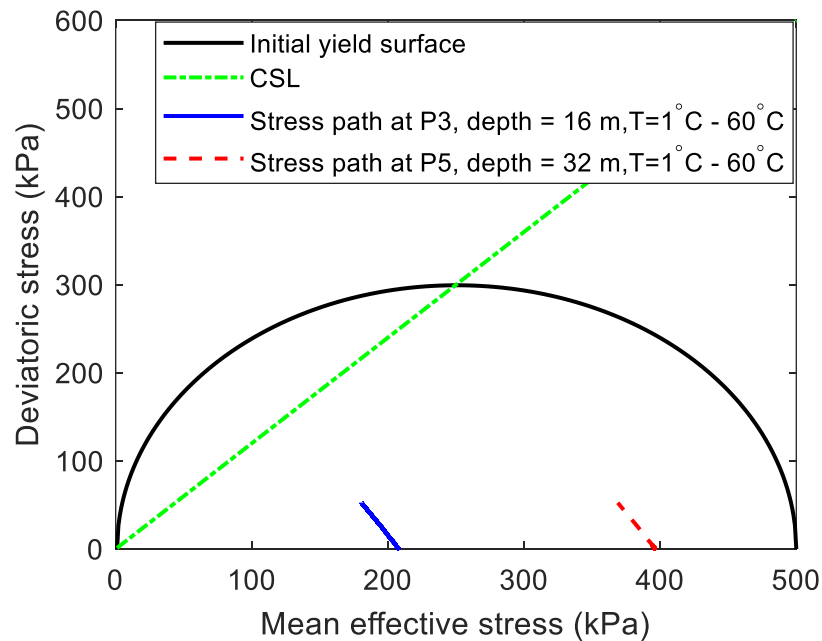


Figure 5-12 Curves showing the effective stress paths at key monitoring points, *CLS* = critical state line.

In order to demonstrate the role of plastic strain on the overall ground response, we also carried out numerical modeling without adopting the plastic model. The result of vertical displacement on the topic surface at P1 is displayed along with the previous result in Figure 5-13. The curves indicate that plastic strain exerts a very limited impact on the ground deformation for a short-term analysis (within 3 years). As time goes longer, the plastic strain tends to contribute to a consolidation settlement. Thereby, the plasticity should be included for a long-term analysis to examine the risk ground settlement due to BETS operations.

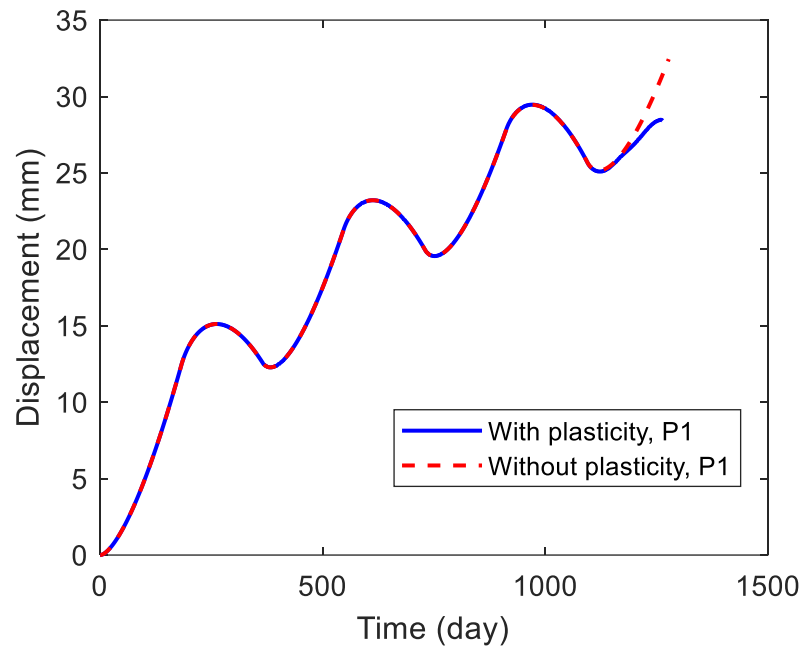


Figure 5-13 Simulated vertical displacements at P1 for cases with and without considering plasticity.

In this study, we don't have laboratory data on the thermo-poromechanical behavior of soil samples from the study site. We just carried out a preliminary THM analysis to highlight the importance of considering bound water dehydration while evaluating the potential of ground heaving during BETS operations in a highly consolidated soil formation. The laboratory characterization of the thermo-elastic-plastic deformation behavior of soil samples from the studying site is our ongoing work.

5.6 Conclusions

This study provides some preliminary numerical analysis on the short-term THM responses of an over-consolidated marine sediment ground due to BTES operations in Kuujjuaq, Quebec, Canada. The aim is to demonstrate the way of considering bound water dehydration in clay soil formation during thermal storage. Several conclusions are drawn as the following:

- Based on the FEM modeling results of cases with two different maximum storage temperatures, we notice that a maximum storage temperature of 60°C tends to yield a considerable vertical displacement (a ground heave up to 35 mm). By contrast, the vertical displacement for the case with a Maximum T of 30°C is much less. The difference in two cases with different storage temperatures is resembled by the results on simulated pore pressures at key monitoring points. Even though the borehole is subjected to a cyclic temperature variation boundary, a continuous pore pressure increase in the ground is expected.
- Our simulations highlight the importance of considering bound water dehydration in characterizing the ground heave process during the short-term BTES operation in an overconsolidated formation in the Canadian subarctic region. The simulated ground expansion behavior is due to the high excess pore pressure generated during thermal storage, which is accompanied by the release of in-situ effective stresses. Neglect of bound water dehydration process will underestimate the amount of ground heave during a short-term BTES operation.
- For such overconsolidated soil formation, the plastic deformation exerts little impact on the short-term poromechanical behavior. However, the plastic deformation should be well considered in a long-term analysis as it may contribute to a ground settlement. Considerable laboratory geotechnical characterizations are needed to quantify the plastic deformation behavior more accurately.

Chapter 6

6 Conclusions, limitations, and recommendations for future work

6.1 Conclusion

In this thesis, a new theoretical framework is proposed to study the interconnected thermo-mechanical responses of clayey soils saturated with water under drained stress-path conditions. The aim is to understand the behavior of these soils in terms of temperature, elasticity, and plasticity.

The proposed framework is then incorporated into a finite element formulation to effectively simulate the fully coupled thermo-hydro-mechanical behaviors of clay soils. The main focus of the research is to gain insight into the complex dynamics of bound water dehydration.

Furthermore, the thesis examines the behavior of borehole thermal energy storage (BTES) systems using a thermal-hydro-mechanical coupled finite element approach. The study specifically investigates the impact of cyclic temperature variations on these systems, which are deployed in glacial till regions of northern Canada and have an operational lifespan of 3.5 years.

Based on the obtained results, several significant conclusions can be drawn from this study.

1- By incorporating subloading surface plasticity and principles of thermodynamics, we can effectively capture the intricate nonlinear thermo-mechanical behavior. This approach adopts a mechanical framework that considers the elasto-plastic domain within the yield surface, providing a comprehensive characterization of the smooth transition between elasticity and plasticity in clayey soils.

2- We have successfully demonstrated the feasibility of independently treating plastic strain and dehydration-induced strain, all while adhering to the fundamental laws of thermodynamics. The validity of the proposed model has been verified using diverse clayey soils originating from different geological sources and experiencing distinct stress histories. It is important to note that our current model solely accounts for the dehydration of bound water adhered to the external surface of clayey minerals. However, by treating dehydration-induced strain as a separate component, we open up opportunities for adaptability to varying environmental conditions. The newly introduced model offers notable advantages in terms of phenomenon-based plasticity, facilitating the convenient determination of model parameters. Additionally, it harnesses the power of mechanism-based thermodynamics to interpret the various stages of the dehydration process.

3- The THM coupled finite element model is grounded in the principles of porous media theory, which considers the soil as saturated with both free water and bound water. The model incorporates equations for mass balance, momentum balance, and energy balance. Notably, the mass balance equation is adjusted to account for bound water dehydration. The conversion of bound water to free water plays a crucial role in governing thermo-mechanical strain and is treated as a distinct aspect. The nonlinear equations governing the system are formulated, discretized in time, and solved using our in-house developed FEM code. The thermo-plastic behavior of clayey soils is effectively described by employing the subloading surface plasticity framework. Within this chosen mechanical framework, the elasto-plastic domain is considered within the yield surface. The proposed model adeptly captures the smooth transition from elasticity to plasticity. Implementation of the thermo-plastic constitutive law into our THM coupled FEM framework is straightforward and convenient.

4- The FEM model simulations demonstrate reasonable agreement with experimental data. Although there is limited experimental data on the impact of bound water variation on clay soil behavior under thermal loading, our THM model offers a valuable framework for assessing the thermo-mechanical response of clay. Based on our numerical results, it is evident that dehydration significantly influences the generation of excess pore pressure in clay soils during heating.

5- Some preliminary results for the field application for BETS simulation are obtained. The impact of heating and cooling cycles on pore water pressure varies depending on the location. In close

proximity to the boreholes, the pore pressure increases throughout both heating and cooling cycles. This phenomenon can be attributed to soil deformation near the borehole and the dehydration of bound water caused by temperature elevation. The transformation of bound water into free water leads to increased pore pressure. During the cooling cycle, pore pressure continues to rise due to soil contraction. In areas further away from the boreholes, where temperature fluctuations are minimal, pore water pressure variation is primarily governed by displacement behavior. The slight temperature changes in this region have a lesser impact on pore pressure, with displacement behavior being the primary influencing factor.

6- Elevated operating temperatures exert a more pronounced influence on displacement, thermal strain, and pore water pressure. Regardless of the temperature range considered (1°C - 60°C or 1°C - 30°C), deformations remain within a few tens of millimeters. Thermal expansion, contraction, and consolidation lead to both heave and settlement in the upper layer, resulting in uneven deformation across the entire till layer.

7- In the case of highly consolidated soil formations, plastic deformation has a minimal effect on the immediate poromechanical behavior. Nonetheless, it is essential to account for plastic deformation in long-term analyses, as it can potentially lead to ground settlement. To gain a more precise understanding of plastic deformation behavior, extensive laboratory geotechnical characterizations are required. Based on the preceding information, this thesis offers a comprehensive framework for describing the THM behavior of geomaterials. This framework holds the potential to be applied by consulting firms, engineers, and governmental bodies across projects where soil temperature fluctuations play a pivotal role. This applicability extends over a diverse spectrum of engineering endeavors, spanning from thermal energy storage projects to underground thermal infrastructures.

6.2 Limitations

This study is based on certain assumptions and limitations, with the most significant ones outlined below:

- 1- The analysis focuses on soil under non-isothermal conditions with temperatures above zero and does not account for the presence of ice lenses and their impact on soil behavior.

- 2- The study is specifically designed for 2D finite element methods, and the model is not extended to 3D modeling.
- 3- The model considers the effects of temperature variations on the dehydration of the external surface of bound water in clay soils. However, it does not address the dehydration of interlayer bound water.
- 4- The proposed study is tailored for fully saturated soils, and the model is not equipped to simulate the THM behavior of unsaturated soils.

6.3 Recommendations for future work

The focus of this thesis is a particular aspect of modeling the coupled thermo-hydro-mechanical behavior of clay soils, specifically its application in borehole thermal energy storage (BTES) systems. However, there are extensive opportunities for further investigation in the realms of both experimentation and numerical analysis. To expand the horizons of this research, the following recommendations are proposed:

- The current constitutive model presented in this thesis is specifically designed for fully saturated clay soils. However, enhancing the model to accommodate unsaturated conditions would be valuable.
- In this research, the use of explicit integration for describing plasticity has been adopted due to its simplicity and the progress made in subloading surface plasticity. However, there is an advantage in expanding the model simulation to incorporate implicit integration.
- The existing body of experimental research on the effect of bound water dehydration caused by temperature variation is limited. Conducting precise THM tests to thoroughly investigate the precise impacts of this phenomenon is strongly advised due to the scarcity of such studies.

Bibliography

1. Sovacool BK (2009) The intermittency of wind, solar, and renewable electricity generators: Technical barrier or rhetorical excuse? *Util Policy* 17:288–296
2. Mason IG, Page SC, Williamson AG (2010) A 100% renewable electricity generation system for New Zealand utilising hydro, wind, geothermal and biomass resources. *Energy Policy* 38:3973–3984
3. Giordano N, Comina C, Mandrone G, Cagni A (2016) Borehole thermal energy storage (BTES). First results from the injection phase of a living lab in Torino (NW Italy). *Renew Energy* 86:993–1008
4. Giordano N, Raymond J (2019) Alternative and sustainable heat production for drinking water needs in a subarctic climate (Nunavik, Canada): Borehole thermal energy storage to reduce fossil fuel dependency in off-grid communities. *Appl Energy* 252:113463
5. Laloui L, Cekerevac C (2003) Thermo-plasticity of clays: an isotropic yield mechanism. *Comput Geotech* 30:649–660
6. Cekerevac C, Laloui L (2004) Experimental study of thermal effects on the mechanical behaviour of a clay. *Int J Numer Anal methods Geomech* 28:209–228
7. Hueckel T, Baldi G (1990) Thermoplasticity of Saturated Clays: Experimental Constitutive Study. *J Geotech Eng* 116:1778–1796. [https://doi.org/10.1061/\(ASCE\)0733-9410\(1990\)116:12\(1778\)](https://doi.org/10.1061/(ASCE)0733-9410(1990)116:12(1778))
8. Laloui L (2001) Thermo-mechanical behaviour of soils. *Rev française génie Civ* 5:809–843
9. Zhang S, Leng W, Zhang F, Xiong Y (2012) A simple thermo-elastoplastic model for geomaterials. *Int J Plast* 34:93–113. <https://doi.org/10.1016/j.ijplas.2012.01.011>
10. Abu Al-Rub RK, Darabi MK (2012) A thermodynamic framework for constitutive

- modeling of time- and rate-dependent materials. Part I: Theory. *Int J Plast* 34:61–92.
<https://doi.org/10.1016/j.ijplas.2012.01.002>
11. Zhu C, Arson C (2014) A thermo-mechanical damage model for rock stiffness during anisotropic crack opening and closure. *Acta Geotech* 9:847–867.
<https://doi.org/10.1007/s11440-013-0281-0>
 12. Li B, Wong RCK (2017) A mechanistic model for anisotropic thermal strain behavior of soft mudrocks. *Eng Geol* 228:.. <https://doi.org/10.1016/j.enggeo.2017.08.008>
 13. Zhang Z (2017) A thermodynamics-based theory for the thermo-poro-mechanical modeling of saturated clay. *Int J Plast* 92:164–185.
<https://doi.org/10.1016/j.ijplas.2017.03.007>
 14. Brown KM, Saffer DM, Bekins BA (2001) Smectite diagenesis, pore-water freshening, and fluid flow at the toe of the Nankai wedge. *Earth Planet Sci Lett* 194:97–109
 15. Colten-Bradley VA (1987) Role of Pressure in Smectite Dehydration - Effects on Geopressure and Smectite-To-Illite Transformation. *Am Assoc Pet Geol Bull* 71:1414–1427. <https://doi.org/10.1306/703c8092-1707-11d7-8645000102c1865d>
 16. Vidal O, Dubacq B (2009) Thermodynamic modelling of clay dehydration, stability and compositional evolution with temperature, pressure and H₂O activity. *Geochim Cosmochim Acta* 73:6544–6564. <https://doi.org/10.1016/j.gca.2009.07.035>
 17. Laloui L, Cekerevac C (2008) Numerical simulation of the non-isothermal mechanical behaviour of soils. *Comput Geotech* 35:729–745
 18. Monfared M, Sulem J, Delage P, Mohajerani M (2012) On the THM behaviour of a sheared Boom clay sample: Application to the behaviour and sealing properties of the EDZ. *Eng Geol* 124:47–58. <https://doi.org/https://doi.org/10.1016/j.enggeo.2011.10.002>
 19. Laloui L, Modaressi H (2002) Modelling of the thermo-hydro-plastic behaviour of clays. *Hydromechanical Thermohydromechanical Behav Deep Argillaceous Rock Sous la Dir Hoteit, Su, Tijani Shao* 161–170

20. Akrouch GA, Sánchez M, Briaud J-L (2014) Thermo-mechanical behavior of energy piles in high plasticity clays. *Acta Geotech* 9:399–412
21. Laloui L, François B (2009) ACMEG-T: soil thermoplasticity model. *J Eng Mech* 135:932–944
22. Hueckel T, François B, Laloui L (2009) Explaining thermal failure in saturated clays. *Géotechnique* 59:197–212
23. Kuntiwattanakul P, Towhata I, Ohishi K, Seko I (1995) Temperature effects on undrained shear characteristics of clay. *Soils Found* 35:147–162
24. Okada Y, Sassa K, Fukuoka H (2005) Undrained shear behaviour of sands subjected to large shear displacement and estimation of excess pore-pressure generation from drained ring shear tests. *Can Geotech J* 42:787–803
25. Mašin D, Khalili N (2012) A thermo-mechanical model for variably saturated soils based on hypoplasticity. *Int J Numer Anal methods Geomech* 36:1461–1485
26. Xiao Y, Liu H, Chen Y, Jiang J (2014) Strength and deformation of rockfill material based on large-scale triaxial compression tests. II: Influence of particle breakage. *J Geotech Geoenvironmental Eng* 140:4014071
27. Xiong H, Yin Z, Nicot F (2019) A multiscale work-analysis approach for geotechnical structures. *Int J Numer Anal Methods Geomech* 43:1230–1250
28. Hashiguchi K (1989) Subloading surface model in unconventional plasticity. *Int J Solids Struct* 25:917–945
29. Hashiguchi K (2017) *Foundations of elastoplasticity: subloading surface model*. Springer
30. Houlsby GT, Puzrin A (2000) A thermomechanical framework for constitutive models for rate-independent dissipative materials. *Int J Plast* 16:1017–1047
31. Cao D, Shi B, Zhu H-H, et al (2019) A field study on the application of distributed temperature sensing technology in thermal response tests for borehole heat exchangers.

- Bull Eng Geol Environ 78:3901–3915. <https://doi.org/10.1007/s10064-018-1407-2>
32. Abuel-Naga HM, Bergado DT, Bouazza A (2007) Thermally induced volume change and excess pore water pressure of soft Bangkok clay. *Eng Geol* 89:144–154
 33. Baldi G, Hueckel T, Pellegrini R (1988) Thermal volume changes of the mineral–water system in low-porosity clay soils. *Can Geotech J* 25:807–825
 34. Chen WZ, Ma YS, Yu HD, et al (2017) Effects of temperature and thermally-induced microstructure change on hydraulic conductivity of Boom Clay. *J Rock Mech Geotech Eng* 9:383–395. <https://doi.org/https://doi.org/10.1016/j.jrmge.2017.03.006>
 35. Del Olmo C, Fioravante V, Gera F, et al (1996) Thermomechanical properties of deep argillaceous formations. *Eng Geol* 41:87–102
 36. Norouzi E, Moslemzadeh H, Mohammadi S (2019) Maximum entropy based finite element analysis of porous media. *Front Struct Civ Eng* 13:364–379. <https://doi.org/10.1007/s11709-018-0470-x>
 37. Rotta Loria AF, Coulibaly JB (2021) Thermally induced deformation of soils: A critical overview of phenomena, challenges and opportunities. *Geomech Energy Environ* 25:100193. <https://doi.org/10.1016/j.gete.2020.100193>
 38. Cui YJ, Sultan N, Delage P (2000) A thermomechanical model for saturated clays. *Can Geotech J* 37:607–620. <https://doi.org/10.1139/t99-111>
 39. Hamidi A, Turchi S, Karooni F (2017) A critical state based thermo-elasto-plastic constitutive model for structured clays. *J Rock Mech Geotech Eng* 9:1094–1103. <https://doi.org/10.1016/j.jrmge.2017.09.002>
 40. Hong PY, Pereira JM, Tang AM, Cui YJ (2013) On some advanced thermo-mechanical models for saturated clays. *Int J Numer Anal Methods Geomech* 37:2952–2971. <https://doi.org/https://doi.org/10.1002/nag.2170>
 41. Ma C, Hueckel T (1992) Effects of inter-phase mass transfer in heated clays: a mixture

- theory. *Int J Eng Sci* 30:1567–1582
42. Hueckel T (2002) Reactive plasticity for clays during dehydration and rehydration. Part 1: concepts and options. *Int J Plast* 18:281–312.
[https://doi.org/https://doi.org/10.1016/S0749-6419\(00\)00099-1](https://doi.org/https://doi.org/10.1016/S0749-6419(00)00099-1)
 43. Zhang Z, Cheng X (2017) A fully coupled THM model based on a non-equilibrium thermodynamic approach and its application. *Int J Numer Anal Methods Geomech* 41:527–554
 44. Zymnis DM, Whittle AJ, Cheng X (2019) Simulation of long-term thermo-mechanical response of clay using an advanced constitutive model. *Acta Geotech* 14:295–311.
<https://doi.org/10.1007/s11440-018-0726-6>
 45. Bennett RH, O'Brien NR, Hulbert MH (1991) Determinants of clay and shale microfabric signatures: processes and mechanisms. In: *Microstructure of Fine-Grained Sediments: From Mud to Shale*. Springer, pp 5–32
 46. Stępkowska ET (1990) Aspects of the clay/electrolyte/water system with special reference to the geotechnical properties of clays. *Eng Geol* 28:249–267
 47. Colten-Bradley VA (1987) Role of pressure in smectite dehydration—Effects on geopressure and smectite-to-illite transformation. *Am Assoc Pet Geol Bull* 71:1414–1427
 48. Hüpers A, Kopf AJ (2009) The thermal influence on the consolidation state of underthrust sediments from the Nankai margin and its implications for excess pore pressure. *Earth Planet Sci Lett* 286:324–332. <https://doi.org/10.1016/j.epsl.2009.05.047>
 49. Di Donna A, Laloui L (2015) Response of soil subjected to thermal cyclic loading: Experimental and constitutive study. *Eng Geol* 190:65–76.
<https://doi.org/10.1016/j.enggeo.2015.03.003>
 50. Bekele YW, Kyokawa H, Kvarving AM, et al (2017) Computers and Geotechnics Isogeometric analysis of THM coupled processes in ground freezing. *Comput Geotech* 88:129–145. <https://doi.org/10.1016/j.compgeo.2017.02.020>

51. Gray WG, Miller CT (2005) Thermodynamically constrained averaging theory approach for modeling flow and transport phenomena in porous medium systems: 1. Motivation and overview. *Adv Water Resour* 28:161–180.
<https://doi.org/10.1016/j.advwatres.2004.09.005>
52. Lewis RW, Roberts PJ, Schrefler BA (1989) Finite element modelling of two-phase heat and fluid flow in deforming porous media. *Transp Porous Media* 4:319–334.
<https://doi.org/10.1007/BF00165778>
53. Hueckel T, Peano A, Pellegrini R (1994) A thermo-plastic constitutive law for brittle-plastic behavior of rocks at high temperatures. *Pure Appl Geophys PAGEOPH* 143:483–510. <https://doi.org/10.1007/BF00874339>
54. Loria AFR, Coulibaly JB (2021) Thermally induced deformation of soils: A critical overview of phenomena, challenges and opportunities. *Geomech Energy Environ* 25:100193
55. Brown KM, Ransom B (1996) Porosity corrections for smectite-rich sediments: Impact on studies of compaction, fluid generation, and tectonic history. *Geology* 24:843–846
56. Saffer DM, McKiernan AW (2009) Evaluation of in situ smectite dehydration as a pore water freshening mechanism in the nankai trough, offshore southwest Japan. *Geochemistry, Geophys Geosystems* 10:1–24. <https://doi.org/10.1029/2008GC002226>
57. Ma C, Hueckel T (1993) Thermomechanical effects on adsorbed water in clays around a heat source. *Int J Numer Anal methods Geomech* 17:175–196
58. Li B, Wong RCK (2016) Quantifying structural states of soft mudrocks. *J Geophys Res Solid Earth* 121:. <https://doi.org/10.1002/2015JB012454>
59. Sojoudi M, Li B (2023) A thermodynamic-based model for modeling thermo-elastoplastic behaviors of saturated clayey soils considering bound water dehydration. *J Rock Mech Geotech Eng* 15:1535–1546
60. Zymnis DM, Whittle AJ, Germaine JT (2018) Measurement of temperature-dependent

- bound water in clays. *Geotech Test J* 42:232–244. <https://doi.org/10.1520/GTJ20170012>
61. Diersch H-J, Kolditz O (1998) Coupled groundwater flow and transport: 2. Thermohaline and 3D convection systems. *Adv Water Resour* 21:401–425
 62. Brooks AN, Hughes TJR (1982) Streamline upwind/Petrov-Galerkin formulations for convection dominated flows with particular emphasis on the incompressible Navier-Stokes equations. *Comput Methods Appl Mech Eng* 32:199–259
 63. (2019) Electricity Information 2019. Int. Energy Agency.
 64. Armstrong R, Chiang YM, Gruenspecht H, et al (2022) The Future of Energy Storage—An Interdisciplinary MIT Study
 65. Jacobson MZ, Delucchi MA, Cameron MA, Frew BA (2015) Low-cost solution to the grid reliability problem with 100% penetration of intermittent wind, water, and solar for all purposes. *Proc Natl Acad Sci* 112:15060–15065
 66. Lanahan M, Tabares-Velasco PC (2017) Seasonal thermal-energy storage: A critical review on BTES systems, modeling, and system design for higher system efficiency. *Energies* 10:743
 67. Rad FM, Fung AS (2016) Solar community heating and cooling system with borehole thermal energy storage—Review of systems. *Renew Sustain Energy Rev* 60:1550–1561
 68. Zhang L, Xu P, Mao J, et al (2015) A low cost seasonal solar soil heat storage system for greenhouse heating: Design and pilot study. *Appl Energy* 156:213–222
 69. Sibbitt B, McClenahan D, Djebbar R, et al (2012) The performance of a high solar fraction seasonal storage district heating system—five years of operation. *Energy Procedia* 30:856–865
 70. Dincer I, Rosen MA (2021) Thermal energy storage: systems and applications. John Wiley & Sons
 71. Kalaiselvam S, Parameshwaran R (2014) Thermal energy storage technologies for

sustainability: systems design, assessment and applications. Elsevier

72. Xu J, Wang RZ, Li Y (2014) A review of available technologies for seasonal thermal energy storage. *Sol energy* 103:610–638
73. Rad FM, Fung AS, Leong WH (2013) Feasibility of combined solar thermal and ground source heat pump systems in cold climate, Canada. *Energy Build* 61:224–232
74. Zeng HY, Diao NR, Fang ZH (2002) A finite line-source model for boreholes in geothermal heat exchangers. *Heat Transf Res Co-sponsored by Soc Chem Eng Japan Heat Transf Div ASME* 31:558–567
75. de Paly M, Hecht-Méndez J, Beck M, et al (2012) Optimization of energy extraction for closed shallow geothermal systems using linear programming. *Geothermics* 43:57–65
76. Bayer P, de Paly M, Beck M (2014) Strategic optimization of borehole heat exchanger field for seasonal geothermal heating and cooling. *Appl Energy* 136:445–453
77. Zhang F, An M, Zhang L, et al (2019) The role of mineral composition on the frictional and stability properties of powdered reservoir rocks. *J Geophys Res Solid Earth* 124:1480–1497
78. An M, Zhang F, Elsworth D, et al (2020) Friction of Longmaxi Shale Gouges and Implications for Seismicity During Hydraulic Fracturing. *J Geophys Res Solid Earth* 125:e2020JB019885. <https://doi.org/10.1029/2020JB019885>
79. An M, Zhang F, Min K, et al (2021) The potential for low-grade metamorphism to facilitate fault instability in a geothermal reservoir. *Geophys Res Lett* 48:e2021GL093552
80. Hueckel TA (1992) Water–mineral interaction in hygromechanics of clays exposed to environmental loads: a mixture-theory approach. *Can Geotech J* 29:1071–1086
81. Zhang Z, Cheng X (2017) A fully coupled THM model based on a non-equilibrium thermodynamic approach and its application. *Int J Numer Anal Methods Geomech* 41:527–554. <https://doi.org/10.1002/nag.2569>

82. Tolman RC, Fine PC (1948) On the irreversible production of entropy. *Rev Mod Phys* 20:51
83. Jacquey AB, Regenauer-Lieb K (2021) Thermomechanics for geological, civil engineering and geodynamic applications: rate-dependent critical state line models. *Rock Mech Rock Eng* 54:5355–5373
84. Houlsby GT, Puzrin AM (2006) *Thermodynamics of porous continua*. Springer
85. Voyiadjis GZ, Abu Al-Rub RK (2003) Thermodynamic based model for the evolution equation of the backstress in cyclic plasticity. *Int J Plast* 19:2121–2147. [https://doi.org/10.1016/S0749-6419\(03\)00062-7](https://doi.org/10.1016/S0749-6419(03)00062-7)
86. Darabi MK, Al-rub RKA, Masad EA (2012) Thermodynamic-based model for coupling temperature-dependent viscoelastic , viscoplastic , and viscodamage constitutive behavior of asphalt mixtures. 817–854. <https://doi.org/10.1002/nag>
87. Simo JC (1998) Numerical analysis and simulation of plasticity. *Handb Numer Anal* 6:183–499
88. Hashiguchi K, Saitoh K, Okayasu T, Tsutsumi S (2002) Evaluation of typical conventional and unconventional plasticity models for prediction of softening behaviour of soils. *Géotechnique* 52:561–578. <https://doi.org/10.1680/geot.52.8.561.38829>
89. Ghasemzadeh H, Ghoreishian Amiri SA (2013) A hydro-mechanical elastoplastic model for unsaturated soils under isotropic loading conditions. *Comput Geotech* 51:91–100. <https://doi.org/10.1016/j.compgeo.2013.02.006>
90. Ghasemzadeh H, Sojoudi MH, Ghoreishian Amiri SA, Karami MH (2017) Elastoplastic model for hydro-mechanical behavior of unsaturated soils. *Soils Found* 57:.. <https://doi.org/10.1016/j.sandf.2017.05.005>
91. Samat S, Brochard L, Stefanou I (2020) Magnitude of latent heat in thermally loaded clays. *Int J Numer Anal Methods Geomech* 44:1926–1957. <https://doi.org/10.1002/nag.3114>

92. Bish DL (1988) Smectite dehydration and stability: Applications to radioactive waste isolation at Yucca Mountain, Nevada. Los Alamos National Lab.
93. Lamb S (2002) CASTI handbook of stainless steels and nickel alloys. 2
94. Abuel-Naga HM (2006) Thermo-mechanical behavior of soft Bangkok clay: experimental results and constitutive modeling. D Eng Diss
95. Ichikawa Y, Selvadurai APS (2012) Transport phenomena in porous media: Aspects of micro/macro behaviour. Springer Science & Business Media
96. Li B, Wong RCK, Heidari S (2018) A modified Kozeny-Carman model for estimating anisotropic permeability of soft mudrocks. *Mar Pet Geol*.
<https://doi.org/10.1016/j.marpetgeo.2018.08.034>
97. Di Donna A, Charrier P, Dijkstra J, et al (2022) The contribution of swelling to self-sealing of claystone studied through x-ray tomography. *Phys Chem Earth, Parts A/B/C* 127:103191
98. Cariou S, Dormieux L, Skoczylas F (2013) An original constitutive law for Callovo-Oxfordian argillite, a two-scale double-porosity material. *Appl Clay Sci* 80:18–30
99. Tremosa J, Gailhanou H, Chiaberge C, et al (2020) Effects of smectite dehydration and illitisation on overpressures in sedimentary basins: A coupled chemical and thermo-hydro-mechanical modelling approach. *Mar Pet Geol* 111:166–178
100. Yao C, Wei C, Ma T, et al (2021) Experimental investigation on the influence of thermochemical effect on the pore–water status in expansive soil. *Int J Geomech* 21:4021080
101. Cacace M, Jacquy AB (2017) Flexible parallel implicit modelling of coupled thermal-hydraulic-mechanical processes in fractured rocks. *Solid Earth* 8:921–941.
<https://doi.org/10.5194/se-8-921-2017>
102. Semnani SJ, White JA, Borja RI (2016) Thermoplasticity and strain localization in

- transversely isotropic materials based on anisotropic critical state plasticity. *Int J Numer Anal Methods Geomech* 40:2423–2449
103. Mitchell JK, Soga K (2005) *Fundamentals of soil behavior*. John Wiley & Sons New York
 104. Kawaragi Y, Okamura K (2017) Application of Subloading Surface Model to Heat Treatment Simulation Based on Explicit Finite Element Method. In: *Key Engineering Materials*. Trans Tech Publ, pp 287–292
 105. Lewis and Schrefler (1996) *The Finite Element Method in the Static and Dynamic Deformation and Consolidation of Porous Media*
 106. Samimi S, Pak A (2016) A three-dimensional mesh-free model for analyzing multi-phase flow in deforming porous media. *Meccanica* 51:517–536. <https://doi.org/10.1007/s11012-015-0231-z>
 107. Galeao AC, Almeida RC, Malta SMC, Loula AFD (2004) Finite element analysis of convection dominated reaction–diffusion problems. *Appl Numer Math* 48:205–222
 108. Delage P, Sultan N, Cui YJ (2000) On the thermal consolidation of Boom clay. *Can Geotech J* 37:343–354
 109. Gunawan E, Giordano N, Jensson P, et al (2020) Alternative heating systems for northern remote communities: Techno-economic analysis of ground-coupled heat pumps in Kuujuaq, Nunavik, Canada. *Renew Energy* 147:1540–1553
 110. Wang Y, Liu X, Li C, et al (2021) Experimental study on thermal deformation of ground heat exchanger pipe. *Sustain Energy Technol Assessments* 45:101190. <https://doi.org/https://doi.org/10.1016/j.seta.2021.101190>
 111. Vidal R, Olivella S, Saaltink MW, Diaz-Maurin F (2022) Heat storage efficiency, ground surface uplift and thermo-hydro-mechanical phenomena for high-temperature aquifer thermal energy storage. *Geotherm Energy* 10:23. <https://doi.org/10.1186/s40517-022-00233-3>

112. Gabrielsson A, Bergdahl U, Moritz L (2000) Thermal energy storage in soils at temperatures reaching 90 C. *J Sol Energy Eng* 122:3–8
113. Laloui L, Sutman M (2023) Energy geotechnology: A new era for geotechnical engineering practice. In: *Smart Geotechnics for Smart Societies*. CRC Press, pp 45–61
114. Rotta Loria AF, Ravera E, Laloui L (2023) Thermo-hydro-mechanical behavior of energy barrettes: Field experiments and numerical simulations. *Geomech Energy Environ* 34:100451. <https://doi.org/10.1016/j.gete.2023.100451>
115. Ding X, Zhang D, Bouazza A, et al (2022) Thermo-mechanical behaviour of energy piles in overconsolidated clay under various mechanical loading levels and thermal cycles. *Renew Energy* 201:594–607
116. Faizal M, Bouazza A, Singh RM (2016) An experimental investigation of the influence of intermittent and continuous operating modes on the thermal behaviour of a full scale geothermal energy pile. *Geomech Energy Environ* 8:8–29. <https://doi.org/10.1016/j.gete.2016.08.001>
117. Giordano N, Kanzari I, Miranda MM, et al (2017) Shallow geothermal resource assessments for the northern community of Kuujuaq, Québec, Canada. In: *Proceedings of the IGCP636 Annual Meeting, Santiago de Chile, Chile*. pp 1–3
118. Miranda MM, Velez Márquez MI, Raymond J, Dezayes C (2021) A numerical approach to infer terrestrial heat flux from shallow temperature profiles in remote northern regions. *Geothermics* 93:102064. <https://doi.org/10.1016/j.geothermics.2021.102064>
119. Ren Z (2022) Numerical modeling of thermally induced ground deformations around potential geothermal energy storage wells in northern Quebec